Department of Neuroscience and Biomedical Engineering

Nucleic Acid Nanostructures

Design, Reconfigurability, and Applications

Ashwin Karthick Natarajan

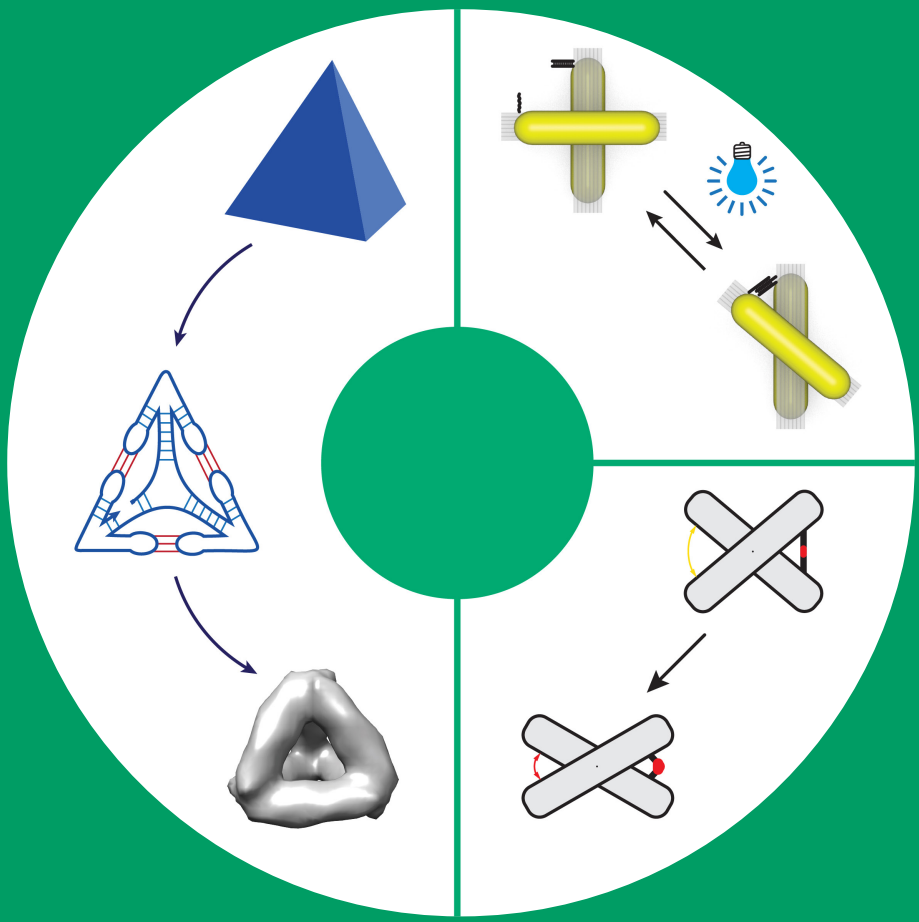

Aalto University

DOCTORAL THESES

Aalto University publication series
DOCTORAL THESES 20/2023

Nucleic Acid Nanostructures

Design, Reconfigurability, and Applications

Ashwin Karthick Natarajan

A doctoral thesis completed for the degree of Doctor of Science (Technology) to be defended, with the permission of the Aalto University School of Science, at a public examination held at the lecture hall F239a of the school (Otakaari 3) on 24 March 2023 at 12 pm.

Aalto University
School of Science
Department of Neuroscience and Biomedical Engineering
Molecular Nanoengineering group

Supervising professor
Professor Anton Kuzyk, Aalto University, Finland.

Thesis advisor
Professor Anton Kuzyk, Aalto University, Finland.

Preliminary examiners
Professor Thorsten-Lars Schmidt, Kent State University, USA.
Professor Cody Geary, Aarhus University, Denmark.

Opponent
Professor Tim Liedl, Ludwig-Maximilians-Universität, Germany.

Aalto University publication series
DOCTORAL THESES 20/2023

ISBN 978-952-64-1152-1 (printed)
ISBN 978-952-64-1153-8 (pdf)
ISSN 1799-4934 (printed)
ISSN 1799-4942 (pdf)
http://urn.fi/URN:ISBN:978-952-64-1153-8

Unigrafia Oy
Helsinki 2023

Finland

NORDIC SWAN ECOLABEL
Printed matter
4041-0619

Author
Ashwin Karthick Natarajan

Name of the doctoral thesis
Nucleic Acid Nanostructures: Design, Reconfigurability, and Applications

Publisher School of Science

Unit Department of Neuroscience and Biomedical Engineering

Series Aalto University publication series DOCTORAL THESES 20/2023

Field of research Biomedical Engineering

Manuscript submitted 15 October 2022 **Date of the defence** 24 March 2023

Permission for public defence granted (date) 27 January 2023 **Language** English

☐ **Monograph** ☒ **Article thesis** ☐ **Essay thesis**

Abstract

Self-assembly with near-atomic precision forms the basis for synthesizing biological structures found in living cells. These self-assembled structures retain the accuracy across sizes ranging from nanometers to macroscopic scale by exploiting the information encoded in the biomolecules. The fabrication of complex 3D synthetic molecular structures with such precision and controllability is cumbersome. Nucleic acid nanotechnology eases this process by enabling bottom-up construction of well-defined nanoscale objects through the predictability and programmability of interactions within DNA and RNA. The design, reconfigurability and a potential application of such nucleic acid nanostructures are presented in this thesis, which is based on three publications.

Publication I presents a highly general and automated approach for the design and assembly of 3D RNA wireframe polyhedral nanostructures. Grounded on the principles of spanning tree-based strand routing, the method renders the target 3D wireframe structure as a single-stranded RNA. The output RNA sequence can be readily transcribed from the corresponding DNA template and assembled into the intended shape. As case examples, the design of three RNA polyhedral models: a tetrahedron, a triangular bipyramid, and a triangular prism were experimentally realized. The developed design pipeline is not restricted to polyhedral models and can be used to render arbitrary straight-line 3D meshes as RNA strands.

Publication II and Publication III focus on the DNA origami approach to fabricate dynamic nanostructures. Publication II presents a reconfigurable chiral plasmonic molecule (CPM) that can be modulated remotely using visible light. The native CPMs are non-responsive to light but can change their spatial configuration by forming DNA triplex locks upon a decrease in the solution pH. To this end, a merocyanine-based photoacid was utilized as a photoresponsive medium that decreases the pH upon exposure to visible light. The chiral response from the CPMs was thus modulated by the intensity of the incident light, which alters the pH. By tuning the intensity, distinct steady out-of-equilibrium states were achieved, both in the pH and in the chiral response.

In Publication III, the precise positioning capability and reconfigurability of the DNA origami technique were exploited. A DNA-origami-based device was fabricated to investigate DNA bending induced by TATA-binding protein. This bending was translated into an angular change in the DNA origami structures directly observable using a transmission electron microscope. Further, the role of transcription factors II A and II B in DNA bending was investigated. Our approach can be readily expanded to other DNA-distorting proteins with careful design considerations.

Overall, this thesis contributes to various facets of nucleic acid nanotechnology from design to reconfigurability to applications. In essence, the findings presented in the individual sections illustrate that nucleic acid nanotechnology still has a large unexplored design space, novel switching mechanisms, and under-explored applications.

Keywords DNA origami, RNA polyhedra, Photoacid, Chiral plasmonics, DNA bending proteins.

ISBN (printed) 978-952-64-1152-1 **ISBN (pdf)** 978-952-64-1153-8

ISSN (printed) 1799-4934 **ISSN (pdf)** 1799-4942

Location of publisher Helsinki **Location of printing** Helsinki **Year** 2023

Pages 208 **urn** http://urn.fi/URN:ISBN:978-952-64-1153-8

Preface

The research presented in this thesis, as like any piece of research, does not belong to the single name stated on the cover, but to numerous people who supported my journey through their encouragement and guidance. I would like to acknowledge all those superb people who showered me with their love and most importantly spent their time and energy to help me achieve my doctorate. While my bad memory might hinder me from individually citing you (please forgive), it doesn't waiver my appreciation for everything you have done.

Of the countless number of people that I should thank, I would like to first and foremost express my sincere gratitude to my supervisor Prof Anton Kuzyk. I still tell people that you gave me the position because I said my favourite football player was Messi (I don't know where I would have been if I had told Ronaldo during the interview). From buying me futsal shoes to getting bruises during futsal and everything in between, you were there for me in your own unique way. I enjoyed working with you for the past five years and I would cherish our numerous discussions and brainstorming sessions. You always lent your ear when I came up with random research questions. I can't emphasize enough how much you have contributed toward my growth as a person and as a researcher. I will forever be indebted for the freedom you gave me during the course of this doctorate, which helped me find my research path and shape my career. I hope you find your cabin by the lake someday.

Dr Jani Seitsonen. You are one of the few people that I know who genuinely wishes well on almost everyone. From frequent calls to ask about the microscope operations to our discussions on the recent microscopy advances, from very competitive pool games to random talks during lunch, I thoroughly cherished all our interactions. I don't think I could have had a better mentor for microscopy. Your patience, support, and infallible teaching style made me a PhD student who can now understand and perform some advanced microscopy techniques without breaking anything (almost). Thank you for everything and especially thank you for being available even during holidays and untimely hours. If I were to perform the same duties as you in the future, I would very much like to replicate you and your solution-oriented attitude.

Joonas Ryssy, probably Dr Joonas Ryssy by the time this thesis is presented to the public. It is always nice to face the challenges in PhD with someone. And in the first years of our PhD, we faced the lows together and held the line. Unfortunately during this time, you had to listen to me (and vice versa)

and share the office space, way too many lunch and coffee breaks, and survive those trips to Bordeaux and Würzburg. Thank you for putting up with me and as I always say, eternal thanks for recommending HIMYM. I would miss singing 'Do You Want to Build a Snowman? ♪' to annoy you.

Dr Sesha Manuguri and Dr Jacky Loo. You guys bought a fresh breath into the group with your ideas and ideologies. It was great to be surrounded by your know-how. I learnt a lot from you both and I will always be amazed by your work ethic and attitude toward Science. Thank you for listening patiently to my complaints and rants, in addition to the occasional scientific discussions.

Throughout my PhD, I was surrounded by hard-working, dedicated and helpful people in the MolEng group. Dr Minh-Kha Nguyen. We started at the same time in the group, and it was a pleasure working with you. I admire your industriousness and your benevolence. Dr Yike Huang. You were one of my first friends in Finland and I relish our interactions during the start of my doctorate. Thank you both. I was also blessed with help from some talented people on different projects. Thank you Arttu Lehtonen, Robin Silva, Kaisu Hiltunen, and Alena Alferova. Mohammed Al-Hussain and Dr Xuan Hung Pham. We only got acquainted toward the end of my PhD, But I wish you guys were there already at the beginning. Thank you for the good company.

I had the chance to work with several people on various projects with some success. The first publication was a result of a wonderful collaboration across various time zones from Japan to the US. I would like to thank everyone involved in that "simple" project, in particular Prof Pekka Orponen, Dr Ibuki Kawamata, Dr Abdul-Melik Mohammed, and Dr Lukas Oesinghaus. Over the years, I have received help from numerous people, who were not directly involved in any of the projects. Especially, Dr Ivan Degtyarenko, Dr Richard Darst, Dr Enrico Glerean, and Simo Tuomisto at Science IT, Prof. Janne Ruokolainen, Dr Hua Jiang, Dr Nonappa, and Dr Ville Liljeström at the nanomicroscopy centre, Elena from Securitas, and Maari, Eva, Noora, Yasmin, and Tiina from the Aalto HR team- who were always there to answer my naive questions and point me in the right direction when I felt lost.

Geet and Anna (I promise I will keep it short). I always come to you guys to whisper about all the drama in my life. Somehow I feel like you enjoyed listening to the drama (hard not to, especially since you ask for new drama every time we meet). Thank you for your friendship and for being a constant since I moved to Finland. Maria (still can't pronounce your last name). I have never met anyone who looks at life the way you do. You have always been a reliable friend and a fellow science enthusiast! Thank you for bestowing me with your warmth, well-thought advice, and positivity even while fighting your own battles. Susanna. I would miss baking cakes together for our birthdays. I learnt a lot from you as a colleague, as a friend, and as a human being. Thank you. Sid. It was great to have shared the apartment with you. You were always a good company whether it be photography or Thai-boxing or just random discussions. I can't thank you enough for all the help.

It is harder to maintain any relationship over a long distance. And I am glad I had a bunch of individuals who were constantly keeping in touch with me, despite being busy with their life and living in different time zones. Thank you Hima, Pavithra, Abdul, Sanjay, Tharangini, Scindia, Jithina, Subha, Varsha, Chris, Rajasekar, and Gokul. Dr Udaya Prakash, Dr Bhuvaneshwari, Mohan, and Mervin. My career could have gone in any trajectory if not for your encouragement and motivation. Thank you for always believing in me, valuing my opinion, and supporting me through this endeavour. The time I spent in Dresden was what served as a primer to this PhD position. Thank you Prof. Thorsten Lars-Schmidt for providing me with the opportunity and still welcoming me to all the lab catch-ups even though I only spent three months in your group. It was a pleasure working with you and everyone in the lab. During my time in Dresden, I was fortunate to meet some fabulous people who have been tremendously supportive of me throughout my PhD. Thank you, Dr Nayan Agrawal, Dr Lara Marrone, and Dr Michael Matthies for all the tips, discussions, and more importantly gossip.

Carina Stiller. Funny how sometimes you just find things in life. From Deutsch or English to Berlin or Bayreuth, we have come a long way. We have shared, among other things, our PhD battles together for the last 3.5 years. While our battle strategies might be different, our goals were similar. We have had so many discussions trying to help each other win, although one can argue about the validity of my "suggestions". I have learnt so many things from you, most importantly the meaning of selfless help. You helped this young padawan in more ways than one, especially in being calma. Thank you for everything and a special thanks to your family for being so warm, welcoming, and helping immensely with my move to Germany.

Amma and Appa. It was at times, a long and difficult road and if not for your trust in me, I might have ended up in a job long ago, doing god knows what. I cannot thank you enough for everything you have given me over the years, be it the education, the independence, or the unerring support and love. Thank you, Amma, for showing me how to look at hard situations through a positive lens. Thank you, Appa, for showing me how to keep going in bad times. Thank you both. Jaichu. I still recall how we managed to book the wrong date for my first international flight and then tried to fix it late at night. Despite that, I come to you to discuss all my big decisions (What am I thinking?). You were there for me at every critical juncture, navigating me toward safety. You took care of everything at home, so I can pursue my dreams. Your sacrifices made me the person I am today. Thank you for being not just a brother, but also one of my best friends. Sarada. I learnt a lot from your optimistic, cheerful, and understanding nature. Thank you. And finally Ansh, thank you for making me realize that I am growing old and should finish my PhD soon.

Berlin, February 08, 2023

Ashwin Karthick Natarajan

Contents

List of Publications

This thesis consists of an overview of the following publications, which are referred to in the text by their Roman numerals.

I Antti Elonen,* **Ashwin Karthick Natarajan**,* Ibuki Kawamata, Lukas Oesinghaus, Abdulmelik Mohammed, Jani Seitsonen, Yuki Suzuki, Friedrich C Simmel, Anton Kuzyk, and Pekka Orponen. Algorithmic design of 3D wireframe RNA polyhedra. *ACS Nano*, 16, 10, 16608–16616, https://doi.org/10.1021/acsnano.2c06035, September 2022.

II Joonas Ryssy, **Ashwin Karthick Natarajan**, Jinhua Wang, Arttu J Lehtonen, Minh-Kha Nguyen, Rafal Klajn, and Anton Kuzyk. Light-Responsive Dynamic DNA-Origami-Based Plasmonic Assemblies. *Angewandte Chemie International Edition*, 60, 11, 5859-5863, https://doi.org/10.1002/anie.202014963, January 2021.

III **Ashwin Karthick Natarajan**, Joonas Ryssy, and Anton Kuzyk. A DNA origami-based device for investigating DNA bending proteins by transmission electron microscopy. Accepted for publication in *Nanoscale*, https://doi.org/10.1039/d2nr05366g, January 2023.

* These authors contributed equally to the work.

Author's Contribution

Publication I: "Algorithmic design of 3D wireframe RNA polyhedra"

PO, IK, and AM initiated the study. PO introduced the basic strand routing scheme, with the use of kissing loops as connector motifs suggested by FCS. IK and LO did the initial strand designs. The Sterna design tool was developed and implemented by AE, with contributions from AM and PO. Later strand designs were done using the Sterna tool, with detailed adjustments by IK. The author performed the amplification of DNA templates in PCR, purification and transcription of DNA templates into RNA, purification of RNA templates, and folding and concentrating of the RNA nanostructures. LO, IK, and YS contributed to the experimental work. Computations for gyration radii of the RNA structures were performed by IK. Cryo-EM grid preparation and imaging were done by the author and JS. AFM sample preparation and imaging were performed by the author, IK, and YS. Numerical simulations and helix-level visualizations were done by AE. The main manuscript was primarily written by the author and PO, with significant contributions from IK, AK, and JS. The descriptions of the strand routing method and the Sterna design tool in Supplement 1 were primarily written by AE, with contributions from PO.

Publication II: "Light-Responsive Dynamic DNA-Origami-Based Plasmonic Assemblies"

AK and RK conceived the research. AK designed the DNA origami structures. JW synthesized the photoacid. JR and AK designed the experiments with contributions from the author. JR, the author, and AJL fabricated DNA origami-based chiral plasmonic assemblies. The author performed the TEM measurements with contributions from JR and AJL. JR and the author performed the TEM data analysis. JR performed the CD characterizations. MKN fabricated gold nanorods. JR, AK, and RK wrote the manuscript.

Publication III: "A DNA origami-based device for investigating DNA bending proteins by transmission electron microscopy"

AK conceived the research. The author folded the DNA origami structures, optimized the concentration of sequences, purified the structures, and optimized the conditions for TBP-binding to the TATA box. The author imaged the samples using TEM with contributions from JR. The author measured the angles, constructed the histograms, and analyzed the data. The author and AK wrote the main manuscript and the supplementary section. The author is a corresponding author in this publication.

Other Publications

The author has contributed to the following list of other publications, that are not included in this thesis.

IV Yike Huang, Minh-Kha Nguyen, **Ashwin Karthick Natarajan**, Vu Hoang Nguyen, and Anton Kuzyk. A DNA Origami-Based Chiral Plasmonic Sensing Device. *ACS Applied Materials & Interfaces*, 10, 51, 44221-44225, https://doi.org/10.1021/acs.chemmater.0c02111, December 2018.

V Minh-Kha Nguyen, Vu Hoang Nguyen, **Ashwin Karthick Natarajan**, Yike Huang, Joonas Ryssy, Boxuan Shen, and Anton Kuzyk. Ultrathin Silica Coating of DNA Origami Nanostructures. *Chemistry of Materials*, 32, 15, 6657-6665, https://doi.org/10.1021/acs.chemmater.0c02111, July 2020.

VI Sesha Manuguri,* Minh-Kha Nguyen,* Jacky Loo,* **Ashwin karthick Natarajan**, and Anton Kuzyk. Advancing the utility of DNA origami technique through enhanced stability of DNA-origami-based assemblies. *Bioconjugate Chemistry*, https://10.1021/acs.bioconjchem.2c00311, August 2022.

* These authors contributed equally to the work.

List of Figures

List of Tables

Abbreviations

2D Two Dimensional

3D Three Dimensional

A Adenine

AdMLP Adenovirus Major Late Promoter

AFM Atomic Force Microscope

APS 3-aminopropyltriethoxy silane

ATP Adenosine Tri-Phosphate

AuNR Gold Nanorod

bp base pair

C Cytosine

CD Circular Dichroism

CPM Chiral Plasmonic Molecules

Cryo-EM Cryogenic Electron Microscope

CTF Contrast Transfer Function

Da Dalton

DNA Deoxyribo Nucleic Acid

DNAzymes DNA enzymes

dsDNA double-stranded DNA

dsRNA double-stranded RNA

DX Double Crossover

EDTA Ethylenediaminetetraacetic acid

EM Electron Microscope

FRET Förster Resonance Energy Transfer

g gram

G Guanine

GDa Giga Dalton

h hour

HB Helix Bundle

kb kilobase

L litre

LH Left-Handed

m meter

M Molar

MCH Merocyanine-based photoacid

MDa Mega Dalton

mg milligram

mRNA messenger RNA

MWCO Molecular Weight Cutoff

N Newton

nm nanometer

nt nucleotide

PAGE Polyacrylamide Gel Electrophoresis

PAINT Points Accumulation for Imaging in Nanoscale Topography

PCR Polymerase Chain Reaction

PDB Protein Data Bank

PEDRIX Programmed Eulerian Routing for DNA Design using X-overs

pN pico-newtons

pRNA promoter-associated RNA

RCF Relative Centrifugal Force

RH Right-Handed

RNA Ribonucleic Acid

rRNA ribosomal RNA

SDS Sodium Dodecyl Sulfate

snac Simple Nucleic Acid Code

ssDNA single-stranded DNA

ssOrigami single-stranded Origami

ssRNA single-stranded RNA

Sterna Spanning Tree Engineered RNA design

T Thymine

TBE Tris(hydroxymethyl)aminomethane Borate Ethylenediaminetetraacetic acid

TBP TATA Binding Protein

TCEP Tris(CarboxyEthyl) Phosphine hydrochloride

TE Tris(hydroxymethyl)aminomethane Ethylenediaminetetraacetic acid

TEM Transmission Electron Microscope

TFIIA Transcription Factor II A

TFIIB Transcription Factor II B

TMSD Toehold-Mediated Strand Displacement reaction

tRNA transfer RNA

U Uracil

UV-Vis Ultraviolet-Visible spectroscopy

Symbols

Å angstrom

μ micro

λ wavelength

1. Introduction

"The nucleic-acid "system" that operates in terrestrial life is optimized (through evolution) chemistry incarnate. Why not use it? Not to make genetic manipulations of human DNA... But to allow human beings to sculpt something new, perhaps beautiful, perhaps useful, certainly unnatural."

-Roald Hoffmann (1)

A repository of molecules performs a plethora of functions in the nanoscale regime in Nature. While the molecular structure dictates the function, the spatial organization of these molecules is also equally relevant (*2*, *3*). Minuscule perturbations in the spatial organization can alter the function entirely (*4*, *5*). On that account, Nature effectively creates complex molecular structures with precise nanoscale accuracy. 'If Nature can build such complex structures in the nanoscale, so can we'- this is the premise upon which this thesis is written.

The technology used to fabricate materials with intricate features at the nanoscale (<100 nanometers (nm)) giving rise to specific functional properties is termed nanotechnology (*6*). Nanotechnology has been around for several centuries, with reports dating back to artisans in ninth-century Mesopotamia using nanoparticles to create a glittering effect in their pots (*7*). In the last 50 years, the finesse to synthesize nanomaterials with high precision and the ability to manipulate the matter at the atomic scale has garnered great interest in fields ranging from drug delivery to photonics. This was first envisioned by Richard Feynman, who in his 1959 lecture suggested that *"there's plenty of room at the bottom"* referring to the possibility of atomic-level control and manipulation of matter at the nanoscale (*8*).

Nanometre scale structures can be fabricated by two different approaches: 'top-down' or 'bottom-up' methods. In the top-down approach, a larger block of matter is etched until the desired nanoscale features are obtained. The top-down approach becomes increasingly difficult to reach molecular-level accuracy through standard manufacturing processes such as lithography, milling, chemical exfoliation, and mechanical cleavage. For example, the resolution in optical nanolithography depends on the wavelength of light used. Whereas in a bottom-up approach, the nanostructures are often built/assembled from

separate or distinct basic units, giving more control at the molecular scale, *e.g.,* atomic layer deposition can precisely control the number of atomic layers being deposited. Among bottom-up methods, self-assembly has become desirable as it can be performed by coding the necessary information in the form of competing molecular interactions with high precision in relatively small sample volumes without the necessity of any complex equipment (*9*). In addition, the small and complex functional nanomachines found in Nature are self-assembled. Molecular self-assembly is mostly employed to generate symmetric or periodic structures with meticulous features in nanoscale regimes from a large diversity of materials. But often, the ability to fabricate complex asymmetric patterns or predict the thermodynamically favoured structural conformation becomes a computationally intensive and experimentally iterative task. Hence, the need for predictable and programmable materials for self-assembly became imperative.

A novel branch of self-assembly called structural DNA nanotechnology, introduced in the 1980s by Nadrian Seeman, exploits the Deoxyribo Nucleic Acid (DNA) programmability to fabricate complex nanostructures (*10*). DNA nanotechnology offers precise control in fabricating nanostructures as DNA hybridization by the Watson-Crick base pairing rule (where adenine forms a double hydrogen bond with thymine and guanine forms a triple hydrogen bond with cytosine) is highly predictable. By exploiting this programmability, various DNA nanostructures were built including a DNA cube (*11*), DNA crystals (*12*), and a DNA octahedron (*13*). DNA nanotechnology was further expanded with the introduction of a more versatile and robust DNA origami technique by Paul Rothemund in 2006 (*14*). With the DNA origami technique introduced by Rothemund, the design and assembly of two-dimensional (2D) shapes with custom patterns became possible.

Custom DNA origami structures are formed by folding a long single-stranded DNA (ssDNA) called a 'scaffold strand' using several short synthetic ssDNA strands called 'staple strands'. The staples are carefully designed such that they hybridize to several parts of the scaffold strand resulting in the formation of the target custom shape. In the 2D DNA origami, the DNA double helices are arranged as an array interconnected by crossovers between the adjacent scaffold strands or staples strands or both. Further advancement of the DNA origami technique came forth with the introduction of a generally applicable three-dimensional (3D) origami technique by Douglas *et al.* in 2009 (*15*), where the DNA helices are constrained in a honeycomb lattice as pleated layers. Since then, the field of DNA nanotechnology has expanded exponentially by further exploiting the ability of DNA to link inorganic nanostructures, fluorophores, lipids, and proteins (*16*). Together with the ability to position these molecules at nanometre accuracy, and the ability to adopt various conformations upon external stimuli (reconfigurability), DNA origami offers solutions to extremely challenging problems facing conventional nanofabrication techniques. Furthermore,

dynamic nanostructures can be exploited for various potential applications including, but not restricted to, characterizing molecular interactions that occur at the nanoscale regime with high spatiotemporal resolution.

With the emergence of DNA nanotechnology, Ribonucleic Acid (RNA) as a building block was often overlooked. RNA performs a plethora of functions in the cell that are essential for transcription and translation. Unlike its DNA counterpart, that typically requires a thermally controlled folding process or downstream purification process, RNA can fold isothermally at room temperature or even co-transcriptionally and can be cloned, genetically expressed in large quantities, and be used for *in-vivo* applications with convenience. Furthermore, RNA offers a range of interactions via secondary motifs (hairpin, bulge, internal loop, and multi-branched junction) and tertiary motifs (pseudo-knots and kissing loops) (*17*), which are often limited or not accessible in DNA. However, RNA typically exists in single-stranded form, and the folding of such single-stranded RNA (ssRNA) into tertiary structures can be quite difficult to predict and control algorithmically. RNA nanotechnology has tried to address this design challenge via several approaches. The earliest approach to assemble 2D and 3D RNA complexes was to link together well-characterised elementary structural modules using connector motifs (*18*). The breakthrough in the RNA origami technique came with the introduction of a *de novo* algorithmic structure design strategy by Geary *et al.*, where "RNA origami tiles" are folded from an ssRNA by utilizing crossovers and kissing-loop motifs (*19*, *20*). The ssRNA folding technique enriched the design space of RNA nanotechnology, and soon wireframe RNA designs from ssRNA were reported (*21*). Wireframe designs allow the fabrication of target shapes with complex boundaries and internal structures using open meshes and can be folded at low magnesium conditions that are relevant for biomedical applications. Combining the wireframe design strategy with the distinct advantages offered by RNA would enrich the available design space of nucleic acid nanostructures and open up a range of potential applications.

1.1 Outline of the thesis

This thesis presents the design and development of nucleic acid nanostructures, their reconfigurability, and their potential application in the biophysical characterization of molecular interactions.

Although DNA origami and DNA wireframe structures can be designed in a fully automated pipeline, the design principles do not completely carry over to RNA, and no software exists for the design of RNA wireframe structures. This is addressed in the first part of the thesis which focuses on the design and characterization of 3D wireframe RNA polyhedra structures (Publication I). As a proof-of-concept of our automated software pipeline, we designed and realized

RNA structures of a tetrahedron, a triangular bipyramid, and a triangular prism.

The second part of the thesis is focused on a strategy to design and fabricate a light-controlled reconfigurable chiral plasmonic molecule (CPM) using DNA origami and gold nanorods (Publication II). Native CPMs are non-photoresponsive, but with the use of a photoresponsive medium, can be spatially reconfigured upon exposure to visible light. Here, modulating the intensity of light alters the pH of the solution, which in turn induces the formation of DNA triplex links. The opening and closing of these DNA triplexes in origami switches the CPMs between open and right-handed conformations, respectively.

And in the final part of the thesis, the utility of DNA origami technique as a device to study DNA bending proteins is presented (Publication III). The extent of DNA distortion by a biologically relevant protein (TATA-binding protein) was evaluated using a DNA origami device. The device can translate the amount of bending caused by the protein into an observable change under a transmission electron microscope (TEM).

The thesis itself is divided into five chapters, detailing the background, methods used, results obtained, and conclusions. Chapter 1 introduced the field of nucleic acid nanotechnology, including both DNA and RNA-based nanostructures. Chapter 2 provides an overview of the physical characteristics of nucleic acids, how these characteristics make them a viable building block for bottom-up self-assembly, and the various design and fabrication techniques that have been introduced in the field. This chapter also gives a prelude to the motivation behind each of the publications. Chapter 3 discusses the methods used in this thesis in detail. Chapter 4, the results and discussion chapter, presents the main findings of Publications I to III. This chapter is divided into three parts (one for each publication) that were discussed earlier. The concluding chapter, Chapter 5, summarizes the major findings and provides some future outlooks and remarks.

2. Nucleic Acid Nanotechnology

Nucleic acids, the large biopolymers that store and express the genomic information in all cells and viruses, are made of nitrogen-containing bases, phosphate groups, and five-carbon sugar molecules. DNA and RNA are nucleic acids that are differentiated based on the type of sugar, a nitrogenous base, and their structure. While nucleic acids are largely known for their role in storing genetic information and enabling protein production, their utility as a programmable biopolymer to construct nanoscale structures has gained traction in the past few decades. This chapter provides a brief overview of the structure of nucleic acids, the properties that make them an exceptional "bottom-up" building material, and the techniques used for the design and fabrication of these nucleic acid nanostructures.

2.1 Structure and composition of Nucleic acids

Johann Friedrich Miescher *circa* 1870, was the first to isolate what we now call DNA (*22*). "Nuclein" as Miescher called it, was first isolated from the nuclei of human white blood cells and was characterized as a weak acidic substance with unknown function (*23*). Miescher, a few years later, went on to separate nuclein into protein and nucleic acid components (*24*). The interest in "Nuclein" grew as researchers understood that it was a novel kind of cellular substance (*25–27*). Upon investigating the composition, Albrecht Kossel between 1895 and 1901 discovered that nuclein was comprised of five nitrogen bases (adenine (A), cytosine (C), guanine (G), thymine (T), and uracil (U)) and a sugar molecule. Further elemental analysis revealed that the nucleic acid component contained phosphorus in large quantities, in addition to carbon, hydrogen, nitrogen, and oxygen (*28*).

With the composition known, Phoebus Levene over several years hydrolyzed the nucleic acids from yeast. In 1919, he proposed that a series of nucleotides, each composed of an inorganic phosphate, a sugar molecule (deoxyribose in DNA and ribose in RNA), and one of four nitrogen-containing bases, comprised the structure of nucleic acid (*29*). The nitrogen-containing bases were characterized

into two monocyclic bases called pyrimidines (C and T in DNA or U in RNA), and two bicyclic bases called purines (A and G). The phosphates in the form of phosphoric acid were attributed to the negative charge of nucleic acids. In the nucleotide (nt), the nitrogenous base is linked to the first carbon of the sugar moiety and the phosphate to the fifth carbon. Nucleotides are linked with each other by a phosphodiester bond between the third carbon atom of one sugar molecule (3′ or 3 prime end) and the fifth carbon atom of another (5′ or 5 prime end). Nucleic acids, a heteropolymer of nucleotides, were postulated to be formed as an alternating co-polymer of phosphoric acid and one of the four nucleosides.

Levene had dismissed DNA as the responsible material for heredity, a view that was challenged by Oswald Awery in 1944 (*30*). Levene also proposed that the four nucleosides were to be found in equal quantities in a tetra-nucleotide sequence that repeats, which was challenged by Erwin Chargaff. Following Awery's footsteps, Chargaff conducted a series of experiments and reported that the amount of A was usually similar to the amount of T, and the amount of G was usually similar to the amount of C, regardless of the source of DNA (*31*). Chargaff's rule, as it would later be known, postulated that the total amount of purines (A + G) was nearly equal to the total amount of pyrimidines (C + T), thus conclusively disproving Levene's theory. He went on to study DNA collected from different sources and found that the composition of nucleotides was species-specific (*32*).

Chargaff's rule (A=T and G=C) together with the X-ray diffraction studies of DNA performed by Rosalind Franklin (*33*) and Maurice Wilkins (*34*) were vital to the discovery of the structure of DNA. Franklin and Wilkins suggested that DNA could have a helical structure with a maximum diameter of 20 Å with phosphates on the outside. The double helical structure of DNA was subsequently proposed in 1953 by James Watson and Francis Crick illustrates DNA as two helical anti-parallel strands coiled around the same axis (*35*). They postulated that each strand followed a right-handed helix and that the phosphates in the nucleotide were on the outside, and the hydrophobic bases were on the inside in an energetically favourable manner. Further, they suggested that a purine in either strand is bound to a pyrimidine on the other strand by hydrogen bonding, *i.e.,* A from either chain is bound to a T in the other chain, and G from either chain is bound to a C in the other chain (following Chargaff's rule). Watson and Crick calculated the helical rise per residue to be 3.4 Å with a pitch of 10 residues (34 Å) and assumed an angle of 36° between adjacent residues in the same chain. With a few minor changes since its inception, the model proposed by Watson and Crick was the first correct 3D model of DNA.

DNA, under physiological conditions, is typically found in the "B-form" configuration that was modelled by Watson and Crick (Figure 2.1 A). Depending on the environment condition (salt concentration, temperature, etc.), the DNA double helix has a diameter between 2.0 and 2.5 nm, a helical pitch (a measure of

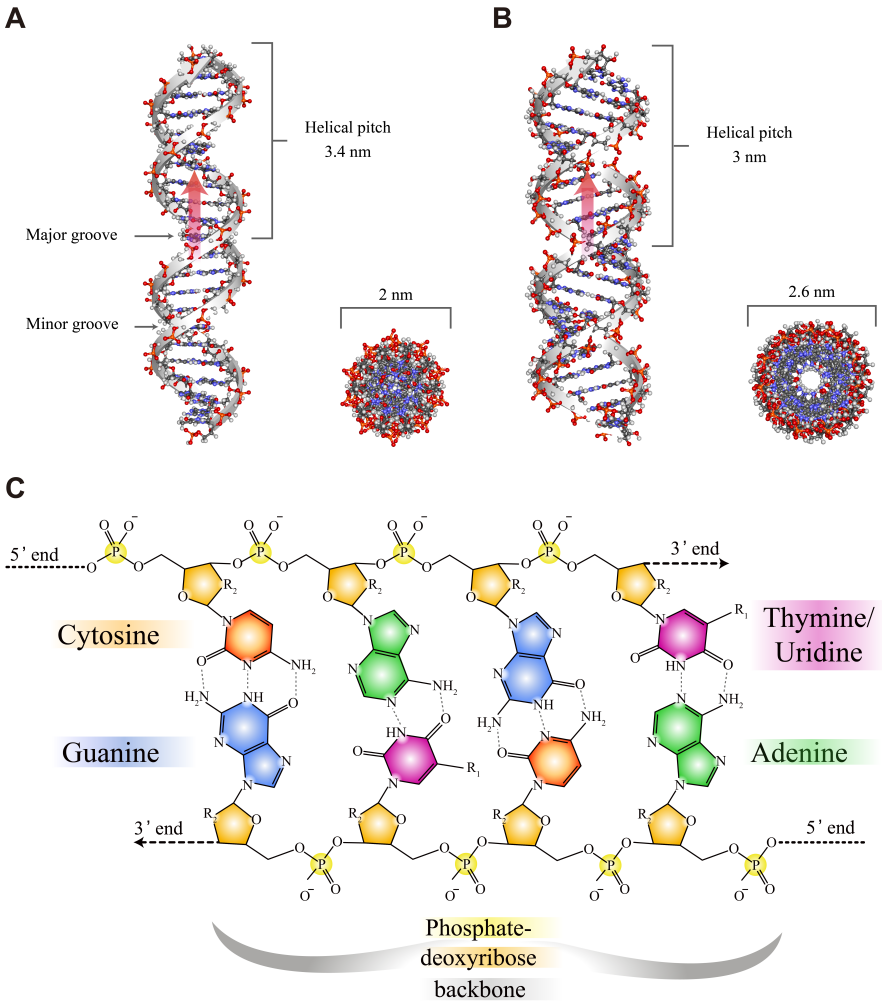

Figure 2.1. Structure and composition of nucleic acids. (A) The double helical structure of B-form DNA; (B) The double helical structure of A-form RNA; (C) Molecular sub-units of nucleic acids. R_1 is CH_3 in DNA and H in RNA and R2 is H in DNA and OH in RNA. Parts A and B were generated in Discovery studio (*36*). Part C is adapted with permission from REF. (*37*).

the shortest structural repeat) between 3.4 and 3.6 nm (≈10.5 base pairs/turn), major groove of 1.7 nm width, minor groove of 1.1 nm width and a persistence length (a measure of stiffness) between 45 and 50 nm (*38–40*). RNA, the close cousin of DNA, can be found in Nature mainly as one of the three different species: messenger RNA (mRNA), transfer RNA (tRNA), or ribosomal RNA (rRNA). The first RNA structure, that was solved by X-ray crystallography, was that of yeast phenylalanine tRNA in 1974 (*41*). RNA predominantly exists as a single-stranded chain, while the double-stranded RNA (dsRNA) exists as an "A-form" following a right-handed helix with an effective hydrodynamic

diameter of ≈2.6 nm, a helical pitch of 3.0 nm (11 base pairs per turn), major groove of 1.0 nm width, minor groove of 1.5 nm width, and persistence length between 45 and 50 nm (*42*, *43*) (Figure 2.1 B). The composition of RNA, however, resembles closely to that of DNA with two main differences. While RNA shares A, C, and G bases with DNA, U is unique to RNA and found in place of T in DNA. And in contrast to the hydrogen atom in DNA, RNA has an OH-group on the ribose sugar which prevents the formation of the "B-form" helix that is found in DNA. Chargaff's rule and Watson and Crick's base pairing rule both apply to dsRNA with a slight modification as A binds to U and G binds to C, which stabilizes the structure.

In addition to hydrogen bonding in base pairs and hydrophobic interactions on the inside of the nucleic acid structure, the stability of the double helical structure is attributed to a significant extent to the π-π stacking interactions that occur between the consecutive aromatic nucleobases on the same strand (*44*–*46*). Both DNA and RNA, are inherently directional as we can define the direction from the first nucleotide to the second as a $5'$ to $3'$ direction. Both the strands run anti-parallel in the $5'$-$3'$ direction. However, if one were to represent a helical rise direction (red arrow in Figure 2.1 A and B) then the forward strand runs in the $5'$-$3'$ sense along this helical direction, while the reverse strand runs in the $3'$-$5'$ sense. The bases in the forward strand along with their complement (A to T or U and G to C) in the reverse strand form base pairs stabilized by hydrogen bonds (*47*): A forms two hydrogen bonds with T in DNA and U in RNA whereas G forms three hydrogen bonds with C (Figure 2.1 C) (*48*, *49*). The process of base-pairing of two complementary nucleic acid sequences to form a double-stranded helix is called hybridization. 'Watson-Crick base pairing rule' or complementary rule governs the hybridization process making it highly specific and laying the foundation for deploying nucleic acids as nanoscale building blocks.

2.2 DNA as nanoscale building blocks

DNA was first envisioned as a nanoscale building block by Nadrian Seeman in the 1980s when he was looking for scaffolds for the 3D organization of biological macromolecules to solve the macromolecular crystallization problem (*10*). Seeman attributes sticky end cohesion/ligation of DNA as the origin of utilizing DNA as a "bottom-up" building block (*39*). Sticky ends are short single-stranded overhangs protruding from the ends of the DNA strand that can be significantly diversified (4^N for N-base sticky ends). The technique serves as an example of programmable molecular recognition, where two DNA strands with complementary sticky ends would hybridize with each other resulting in a classic linear DNA strand.

DNA, explicitly described until now as a linear biomolecule, is found in Nature also in branched forms. The branched DNA occurs as ephemeral intermediates

during cell division when chromosomes exchange information. The aligned DNA strands break and literally cross over to another DNA strand prior to cell division, forming transient branched DNA structures called Holliday junctions. Holliday junction consists of four ssDNA helices with each strand hybridized with two other strands and together forming four double-helical domains that branch off from a point. Holliday junctions exist as extended open-X structures or parallel or anti-parallel stacked-X structures. The open-X structures are seen in complex with proteins, while the anti-parallel stacked-X is observed in DNA and RNA/DNA junctions (Figure 2.2 A). Each strand in a Holliday junction undergoes strand exchange once, a process in which a strand starts on one helix and at the branch point switches over to the next. In Nature, these branch points are mobile and can often slide due to the sequence similarity, or so-called homologous sequences in these junctions. This reaction called branch migration can result in two new linear double-stranded DNA (dsDNA) due to the two-fold symmetry at the branch point.

Seeman realized that by combining these branched structures with the programmable base pairing of sticky ends, one can self-assemble the desired nanostructure such as a 3D crystalline lattice. Thus, DNA was prescribed as a potential material to sculpt complex structures with nanoscale features by Ned Seeman.

2.2.1 Structural DNA nanotechnology

While the foundations were laid, the utility of branched DNA junctions was limited by their geometric flexibility and the instability resulting from branch migration (*50*). Thanks to the pioneering work on solid support-based DNA synthesis (phosphoramidite method) by Marvin Caruthers (*51*), the assembly of junctions with fixed branch points (immobile Holliday junctions) containing between three and at least eight arms from synthetic DNA was made possible experimentally (*10*). The sequence design of these immobile Holliday junctions was further improved (*52*) and subsequently assembled from unique ssDNA sequences, thus bypassing the two-fold symmetry issue (*53*).

Expanding on immobile Holliday junctions, Chen and Seeman used three-arm junctions to construct a 3D cube whose edges were DNA double helices (*11*). Further advancements to tackle the inherent floppiness of Holliday junctions (*59*) were introduced by Fu and Seeman in the form of double-crossovers (DX) molecules (*60*). Unlike the Holliday junction, which has a single exchange of strands for each DNA molecule, DX molecules comprise two DNA double helices linked together with two reciprocal strand exchanges making it geometrically rigid and stable. Figure 2.2 B presents an example DX molecule with anti-parallel-even spacing using five ssDNA. Programmed assembly of these DX molecules along with the specificity provided by sticky-end cohesion helped to overcome the hiatus in the self-assembly of 2D DNA crystals (*12*) (Figure 2.2 C). These DX molecules with sticky ends often called DNA tile motifs,

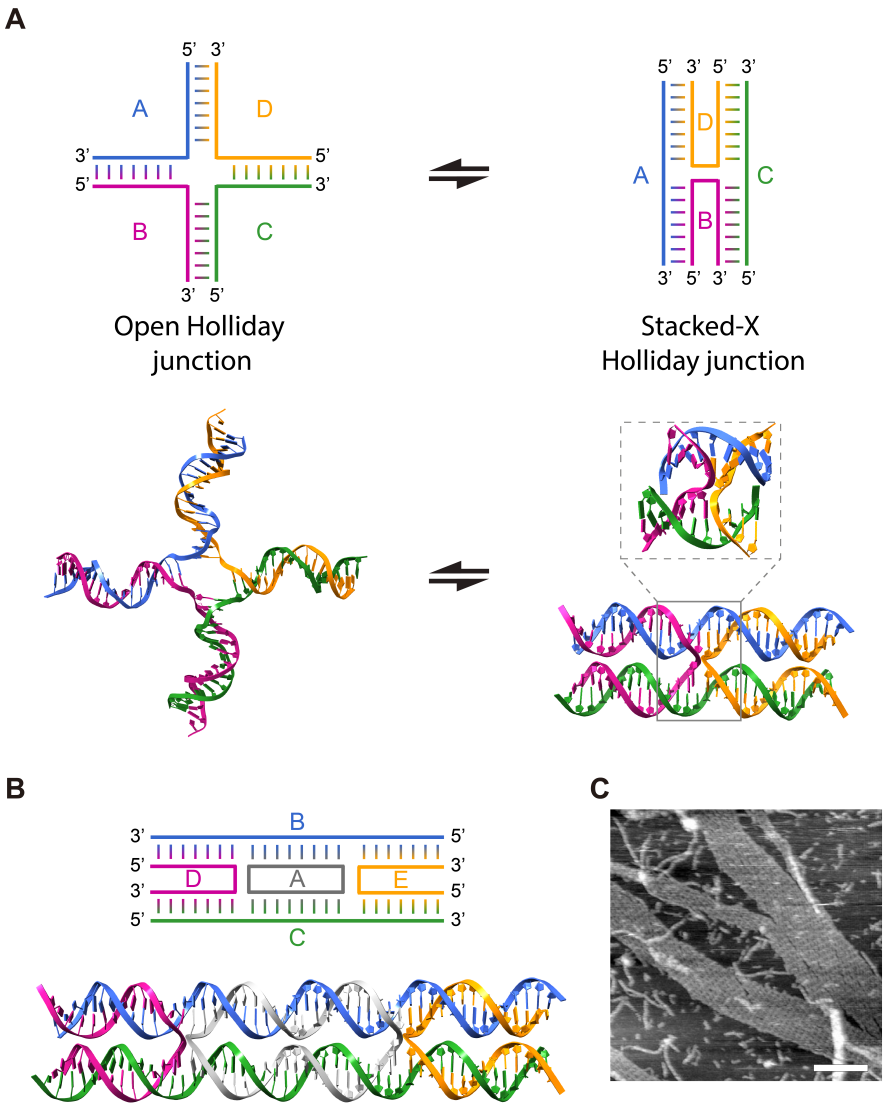

Figure 2.2. Structure of Holliday junction and double crossover tile. (A) Holliday junction in open-X (PDB:3CRX (*54*)) and anti-parallel stacked-X confirmations. The inset in stacked-X confirmation shows a Holliday junction found in Nature (PDB:1DCW (*55*)); (B) Representation of a double crossover tile with anti-parallel-even spacing (DAE tile); (C) AFM image of a DNA crystal grown from DX tiles. The colour codes used in part A are not related to the colour codes in panel B. The 3D representation of stacked-X confirmation of Holliday junction in Part A was made with Nanoengineer-I (*56*). Part C is adapted with permission from REF. (*12*), Springer Nature Limited. All the 3D renderings were made using ChimeraX (*57*, *58*)

expanded the horizons of DNA self-assembly as they provided reliable assembly of stable immobile junctions. Soon, numerous other DNA tile motifs with combinations of multiple-strand exchanges such as cross or X-shaped tiles

(*61*), three-point star or Y-shaped motifs (*62*), five-point-star motifs (*63*), paranemic crossover tiles (PX) (*64*), triple crossover tiles (*65*), Sierpinski triangles (*66*), and tensegrity triangles (*67*) were reported. The latter was used to achieve Seeman's original goal of building 3D lattices using nucleic acids, as Seeman and co-workers assembled 3D crystals using the tensegrity triangle DNA motifs (*68*). In addition to constructing periodic 2D and 3D crystals, it has been shown that aperiodic crystals can be grown from DNA by employing the principles of computer science in algorithmic self-assembly (*66*). These aperiodic crystals were grown using a square tile called 'Wang tile', which has unique sequences on all its four independent sides and assembles into a crystal only if the neighbouring tile had a complementary DNA sequence. However, the assembly of the aperiodic crystals was prone to errors arising from off-template growth and tile misplacement (*50*). While robust molecular algorithms have recently improved the error rates (less than 1 in 3000) (*69*), tile-based assemblies are still controlled by the multiple number of reaction steps and the stoichiometry of the strands that are often required at high purity. Moreover, the limited interaction between a large number of short oligonucleotides restricts the complexity of assembled nanostructures.

2.2.2 DNA origami

DNA tile-based assemblies, despite their limitations, laid the foundations for a groundbreaking technique called 'DNA origami'. More precisely, the assembly of DX tiles into well-defined discrete structures by utilizing ssDNA as a template (*61*) and the construction of a nanoscale wireframe octahedron with five DX and seven PX motifs from a 1.7-kilobase (kb) ssDNA using five synthetic 40-mer oligonucleotide strands (*13*) may have inspired Paul Rothemund to come up with the concept of DNA origami in 2006 (*14*). Rothemund, in his transformative paper, folded a long ssDNA (≈7 kb) called a 'scaffold strand' into the target shape by interactions with hundreds of short synthetic strands called 'staple strands'. The scaffold strand, typically derived from the naturally single-stranded M13mp18 viral genome (7249-nt), was folded with a 100-fold excess of staples (20-80 base pairs (bp) in length) in a 'one-pot' reaction during which the staples bind to the scaffold in prescribed regions. The reaction mixture was annealed from 95 °C to 20 °C at a rate of 1 °C/minute resulting in target 2D shapes with close to 90% yield. The resulting co-planar structures had their helices arranged in an anti-parallel fashion and held together by a periodic array of staple crossovers that occur at every 16 bps or 1.5 helical turns (Figure 2.3 A, marked by blue arrows). The scaffold was folded back and forth in a raster fill pattern by the staples and progressed from one helix to another by 'scaffold crossover' (Figure 2.3 B, marked by red arrows). The strand making the crossover, switches to an adjacent helix, changes the direction by 180° and continues there (Figure 2.3 C). Rothemund demonstrated the fabrication of non-periodic 2D structures of arbitrary complexity such as rectangle, square,

star, smiley face, and triangle with an area of 8000-10000 nm^2 containing approximately 200 addressable points that can be patterned (Figure 2.3 D).

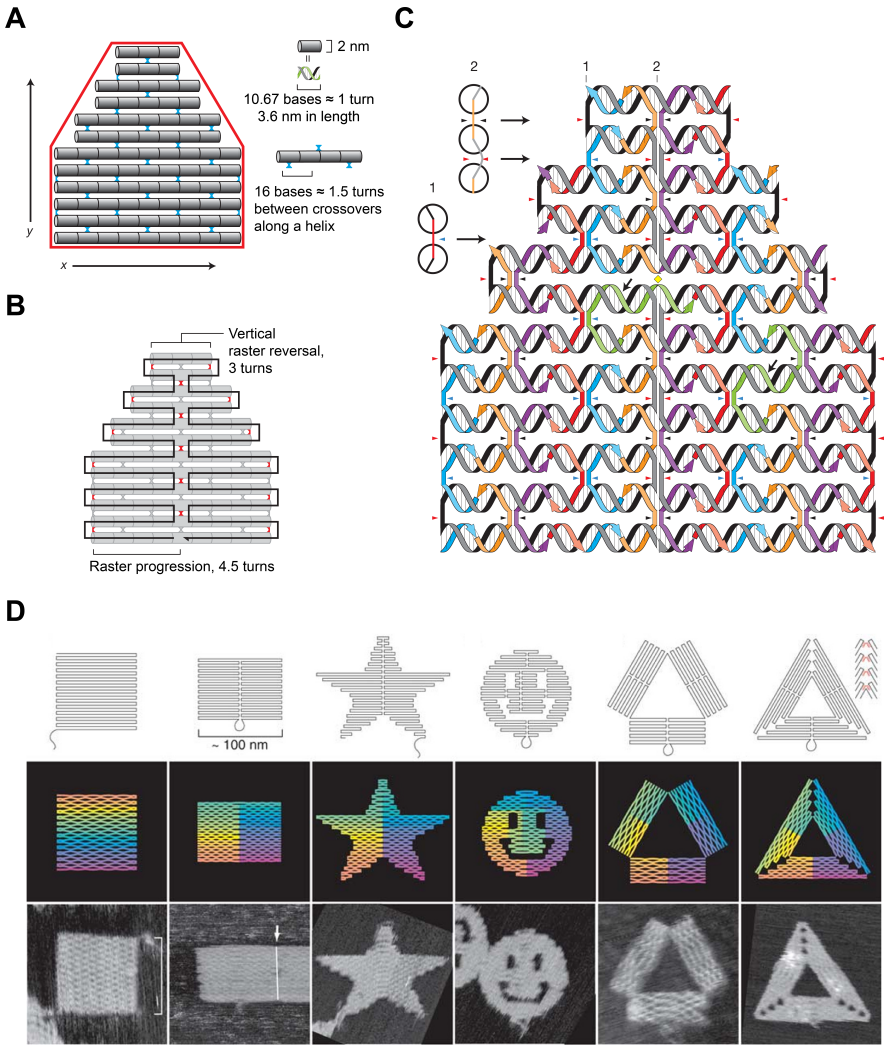

Figure 2.3. Design principles of 2D DNA origami structures. (A) Representation of staple crossover positions (blue arrows); (B) Representation of scaffold crossover positions (red arrows); (C) Design of DNA origami with staples bringing different regions of the scaffold together (blue and black arrows point to the staple crossover positions and red arrows to the scaffold crossover positions); (D) DNA origami shapes and their corresponding Atomic Force Microscopy (AFM) images. The figure is adapted with permission from REF. (*14*), Springer Nature Limited.

DNA origami technique transformed the landscape of nucleic acid nanotechnology in a truly unprecedented way. The beauty of the DNA origami technique is that it alleviated the need for the design and optimization of staple sequences to avoid secondary structures or undesired

binding interactions, the high purity of strands, and the precise control of strand stoichiometries. Further, the robustness of DNA origami can be attributed to the strand invasion by target staples, which through programmed binding displaces unwanted secondary structures, incorrect staples, or grossly truncated staples (*14*).

Soon, the DNA origami technique was expanded for fabricating 3D structures. While earlier approaches connected several planar sub-structures of origami at their edges (*71–73*), the design principles laid by Douglas *et al.* became more generally applicable (*74*, *75*). Douglas *et al.* arranged the helices in a zigzag manner by tuning the distance between the crossovers, which in turn affected the angle between the crossovers. By manipulating the distance to a non-integer value by design, they moved the effected helix out of plane, thereby constructing a six-helix bundle (HB) with a cross-section resembling a honeycomb (*74*). Using this pleated layering design strategy, they further demonstrated the design and assembly of six complex nanostructures – monolith, square nut, railed bridge, genie bottle, stacked cross, and slotted cross (*15*) (Figure 2.4 A). To aid in the design process of 3D origami, Douglas *et al.* released an open-source software package, caDNAno, which simplified an otherwise cumbersome and time-consuming strand-routing process (*75*). For instance, Rothemund took three months to design his structures, while in the same time frame, a cornucopia of arbitrary structures can now be designed with caDNAno. The simple and intuitive graphical user interface and the open-source nature of caDNAno were instrumental in the expansion of the field.

Building upon the design principles of 3D origami, Dietz *et al.* introduced curvature and twists in origami (*70*). By targeted addition and deletion of base pairs, Dietz *et al.* were able to twist the DNA bundles to either handedness or curve (Figure 2.4 B). The curvature was controlled by the use of a balanced gradient of insertions and deletions, resulting in a radius of curvature as tight as 6 nm. The design space of origami was further enriched by utilizing the immanent interactions offered by DNA, *e.g.,* sticky-end cohesion, base pair stacking and blunt-end interactions. Higher-order self-assembly of DNA structures using these interactions helped in scaling up megadalton (MDa) range DNA origami monomers, that was inherently restricted by the length of the scaffold in use (typically ≈7 kb) into the gigadalton (GDa) range. For instance, protruding sticky ends were used by Tikhomirov *et al.* to assemble planar square DNA origami tiles into large 2D structures (*79*). The fractal assembly of several 2D DNA origami tiles using edge loop stacking and two-nucleotide sticky end hybridization created a large canvas. Spanning nearly 1 μm^2 in area, they used these canvases to display patterns such as a portrait of the Mona Lisa with nanometer resolution by adding selected staples to form dsDNA extensions on the surface of the tiles (*76*) (Figure 2.5 A). Large 3D assemblies have also been made possible by harnessing the power of these innate DNA interactions. Blunt end-stacking interactions of DNA-origami-based “tensegrity triangle” structures were exploited to fabricate 3D rhombohedral crystalline

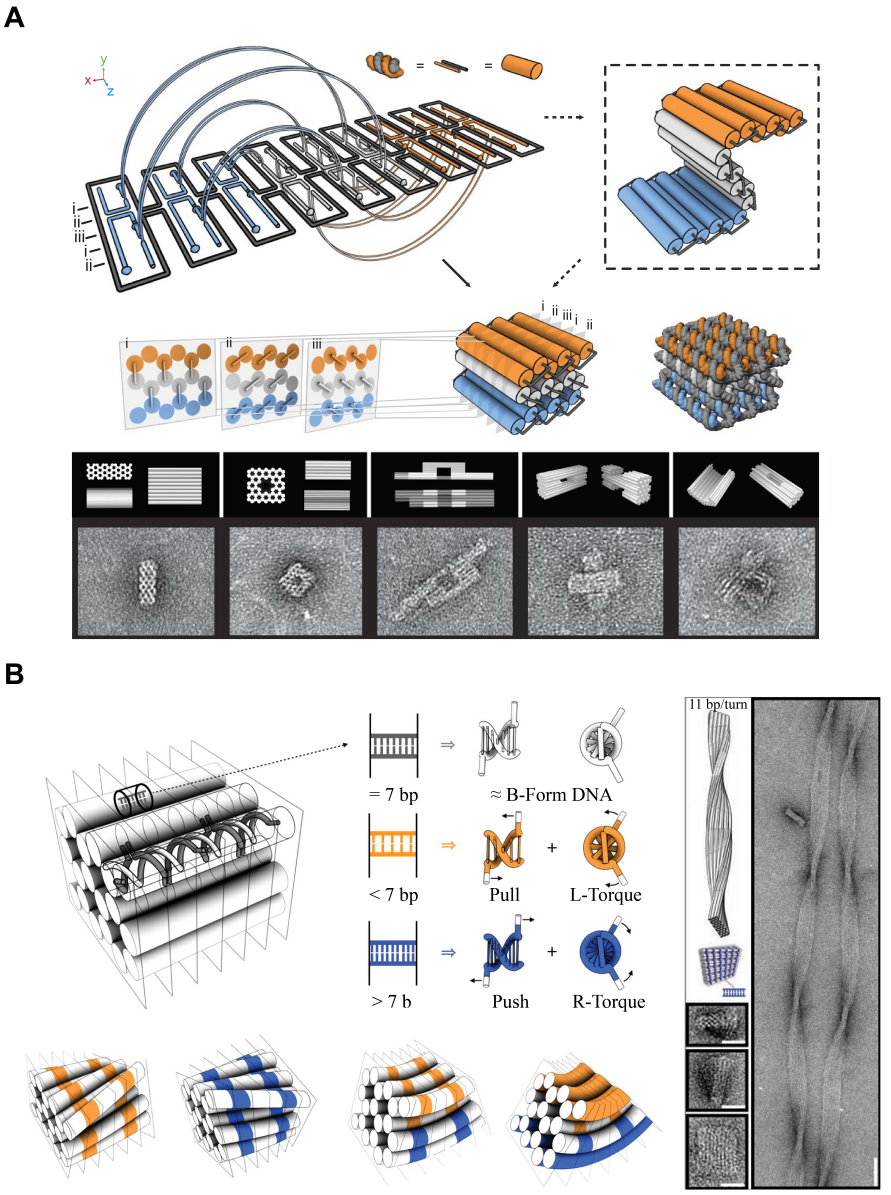

Figure 2.4. Design principles of 3D DNA origami structures. (A) Design principles for rolled 3D DNA origami and representative TEM images of different 3D DNA origami shapes; (B) Design principles for introducing twists and curvature in 3D DNA origami and TEM of a representative twisted structure. Part A is adapted with permission from REF. (*15*), Springer Nature Limited. Part B is adapted with permission from REF. (*70*), AAAS.

lattices (*77*). These 3D crystals had 90% of their volume as empty space and can host a myriad of components including but not restricted to gold nanoparticles (Figure 2.5 B). Gigadalton scale 3D polyhedral DNA assemblies with sizes of up to 1.2 GDa and 450 nm in diameter were demonstrated by

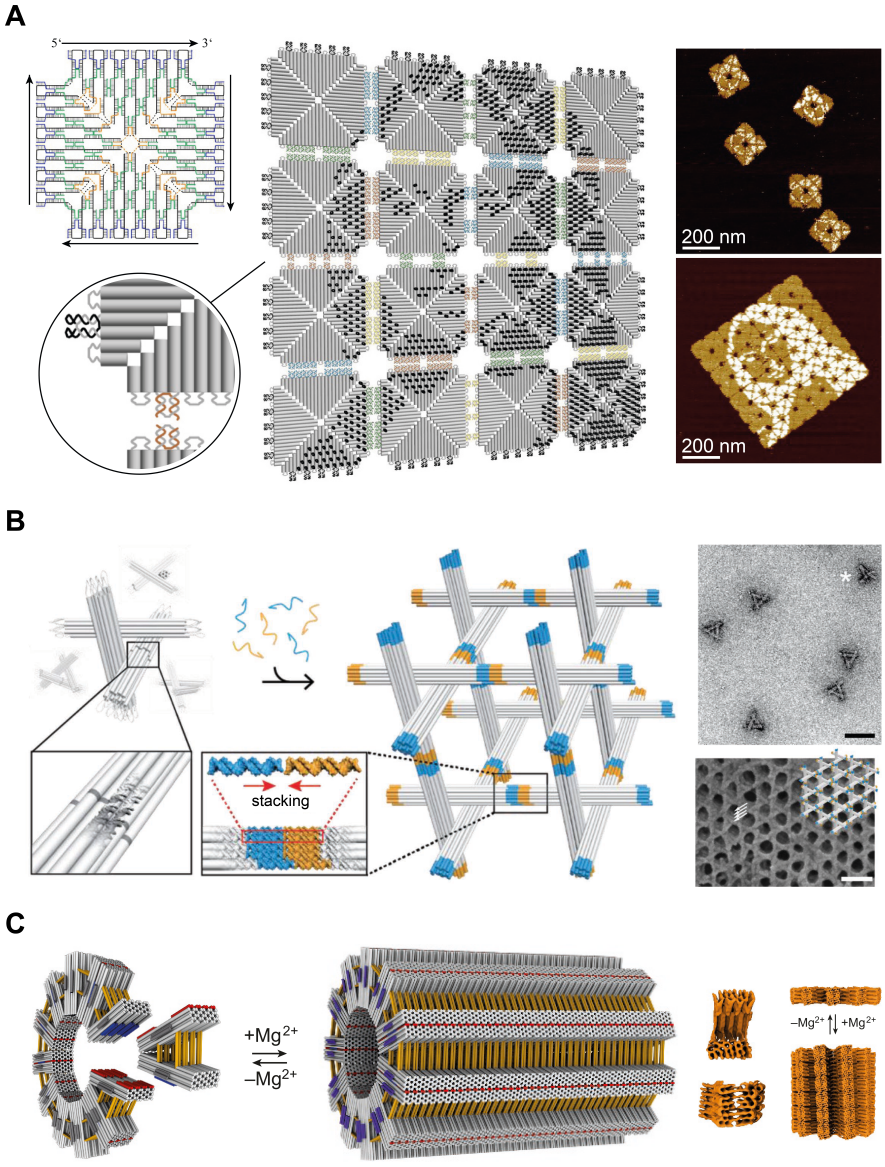

Figure 2.5. Higher-order self-assembly of DNA origami structures. (A) Fractal assembly of DNA origami tiles to large printable canvases;(B) Fabrication of 3D crystals from DNA-origami based tensegrity triangles;(C) Hierarchical assembly of multiple DNA origami structures. Part A is adapted with permission from REF. (*76*), Springer Nature Limited. Part B is adapted with permission from REF. (*77*), Wiley. Part C is adapted with permission from REF. (*78*), Springer Nature Limited.

Wagenbauer *et al.* by utilizing base stacking and shape complementarity in DNA origami (*78*). By manipulating the geometry of the origami and the sequence-based interactions between monomers, they were able to control the copy numbers, positions, and orientations of higher-order assemblies (Figure

2.5 C). Minev *et al.* demonstrated a novel crisscross slat architecture where ssDNA slat monomers polymerize using either DNA-origami or ssDNA seeds into monodisperse ribbons that can further be assembled into tubes of various diameters (*80*). The group later expanded the crisscross polymerization to DNA-origami slats, that can grow into custom multi-micron shapes in a strictly seed-dependent process (*81*). With 1000 uniquely addressable slats and >10000 slats in periodic structures, they were able to show nanoscale patterning in a user-defined fashion in structures as large as 5 GDa.

The gigantic gigadalton nanostructures described above, though mostly assembled from monomers, are still expensive to produce in quantities required for applications such as therapeutics, drug-delivery systems, and nanoelectronic devices. While scaffold strands derived from bacteriophage-based production are amenable to scalable and efficient mass production (*82–84*), the limitations mainly arise from the cost of short-staple strands obtained through solid phase synthesis (*85*) or enzymatic processes (*86*). The cost conundrum was solved using self-excising cassettes comprising two Zn^{2+} dependent DNA-cleaving DNA enzymes (DNAzymes). By interleaving the target strand sequences with these self-cleaving DNAzyme sequences, Praetorius *et al.* demonstrated the production of an ssDNA precursor using bacteriophages that contain hundreds of staple strand sequences (*87*). Upon addition of $ZnCl_2$, DNAzymes cleave themselves to individual staples, that can be of virtually arbitrary lengths and virtually arbitrary sequences, and can self-assemble into DNA origami along with the scaffold. The cost of DNA origami folded by these staples can be reduced to an estimated 18 cents from US $200 per milligram (mg), enabling large-scale applications.

DNA origami, with all its concomitant advantages, faces a major challenge in *in-vitro* and *in-vivo* applications due to the denaturation of DNA structures by the depletion of divalent cations. The denaturation of DNA origami in low cation concentration is caused by the negatively charged backbone of DNA, that when packed tightly like in DNA origami, tends to repel each other through electrostatic interactions. Various approaches have been followed to solve this intricate problem such as i) protecting DNA origami nanostructures using PEGylated lipid bilayers (*88*), polyamine (*89*), polylysine (*90*), block co-polymers (*91*), and inorganic coating (*92*), ii) assembly using monovalent cation (*93*) or buffer exchange to low-Mg buffers after assembly (*94*). While these approaches try to address the denaturation of volume-filled DNA origami assemblies in low cation conditions, others have turned to a design strategy called wireframe origami, which fills only the surface of the 3D nanostructure rendering a hollow interior.

2.2.3 Wireframe origami

Wireframe origami, where the target shape is formed by an open mesh, enables the fabrication of nanostructures with complex boundaries and

internal structures that are challenging to construct with the volume-filling origami technique. Although non-scaffolded wireframe nanostructures ("braided" designs) such as DNA cubes (*11*), octahedron variants (*13*, *95*), and tetrahedron (*96*, *97*) built by entwining together several elementary motifs predate the origami structures, the design principles from origami technique were what ameliorated the possible size and complexity of wireframe structures. Scaffolded origami-based wireframe designs utilize a scaffold strand that either forms a distinct volume-filled origami component first, which links together to form the mesh ("modular" design) or is routed by applying graph theory into a mesh, which is stapled to form the target structure ("global" design) (*98*).

Wireframe origami designed using the modular design approach relies on the interactions between the individual DNA origami components. The strand routing and staple sequence design are rather straightforward as they can be done manually or using open-source tools such as caDNAno. Whereas global origami design is more of a top-down approach, where sequences are designed based on the specification of target geometry. In contrast to the modular approach, the edges of the mesh in global designs are either a single DNA duplex or a DX-type dual-duplex. Han *et al.* were may be the first to introduce a global design approach for 3D wireframe DNA structures (*99*). They routed the scaffold through a mesh framework to create gridiron-like DNA structures, where the vertices of the mesh were formed by self-crossings of the scaffold (Figure 2.6 A). They focus on the design of various 2D and 3D meshes, including meshes with global curvature. However, the approach is not completely general but rather is composed of square motifs. Since designing sequences for most of these structures by hand would be an almost impossible task in practice, a fully automated sequence design pipeline becomes a prerequisite. The first general top-down methodology for designing wireframe DNA origami structures from target polyhedral meshes was presented by Benson *et al.* (*100*). They routed the scaffold strand through the edges of the triangulated mesh by adopting a specific type of Eulerian circuit called A-trial routing theory, where the scaffold traverses each vertex only once. The staple strand sequences were then generated from the strand-level DNA model of the target polyhedron using a semi-automated software called vHelix-BSCOR (Figure 2.6 B). They showcased the versatility of their design approach by constructing several wireframe DNA structures including that of a Stanford bunny (a widely used 3D computer graphics test model). Concurrently, DAEDALUS, another 3D wireframe design tool built on the design principles of Zhang *et al.*, was introduced by Veneziano *et al.* (*101*) (*102*). While vHelix used a single duplex for the edges, DAEDALUS used dual-duplex edges, which visibly increases the rigidity of the edges as seen from their cryo-EM reconstructions (Figure 2.6 C). Moreover, Veneziano *et al.* explicitly utilized spanning-tree-based routing, rendering their method theoretically simpler, computationally more efficient, and applicable as such to general polyhedra compared to the A-trail-based method. The same group

extended their fully autonomous 3D wireframe design approach to 2D DNA origami (*103*) using a Programmed Eulerian Routing for DNA Design using X-overs (PEDRIX) algorithm. PEDRIX fully automated the inverse design of 2D DNA structures by placing multiarm junctions at vertices and utilizing anti-parallel DX crossovers as dual duplex edges. A slightly different approach was introduced by Matthies *et al.* (*104*), where a range of wireframe truss structures such as tetrahedral, octahedral, or irregular dodecahedral trusses were folded by routing the scaffold in the form of equilateral triangles and by connecting the vertices using different connector strands.

These 2D and 3D meshes, designed with single duplex (vHelix-BSCOR) and dual duplexes (DAEDALUS and PERDIX) as edges, are limited by structural fidelity and mechanical stiffness, especially when the edge length approaches the persistence length of DNA (≈50 nm) (*105*, *106*). This was overcome by combining modular and global design approaches for wireframe assemblies, where the mechanical stiffness of wireframe origami was enhanced by exploiting 6-HB as edges in 2D assemblies (METIS) (*107*, *108*), 3D assemblies (TALOS) (*109*), and 2D and 3D assemblies (ATHENA) (*110*). The latter is a unified software environment for fully automated design of arbitrary wireframe origami designs in a top-down fashion. ATHENA and other design tools, together with modelling and visualization software such as Adenita (*111*) make the wireframe origami technique an interesting alternative to volume-filling 3D design approaches.

Other design strategies such as supramolecular DNA assemblies (*112–118*), DNA bricks (*119*, *120*), self-folding ssDNA structures (*121*, *122*), non-scaffolded wireframe assemblies (*63*, *123–125*), and DNA folding using custom protein staples (*126*) have expanded the design space of DNA nanotechnology over the years. Although DNA-based nanostructures exemplify the power of Watson-Crick base pairing and the innate interactions of DNA, the thermal stability and structural and functional diversity offered by RNA cannot be matched by its nucleic acid counterpart, DNA.

2.3 RNA nanotechnology

The functions of RNA have fascinated researchers for years, while their utility as building blocks has gained momentum in recent years (*127–131*). RNA nanostructures, like their DNA counterpart, can be designed and manipulated with simplicity. However, in addition to the orthodox Watson-Crick base pairing, RNA can also form complex quaternary structures (*18*, *132*, *133*), and non-canonical base pairing (G–U, G–A, A–U) (*134–136*) that are often not found or limited in DNA. These interactions along with other secondary (hairpin, bulge, internal loop, and multi-branched junction) and tertiary motifs (co-axial stacking, ribose zipper, tetraloop receptors, pseudo-knots, and kissing loops) (*17*, *137*, *138*) can be found in naturally occurring RNA structures.

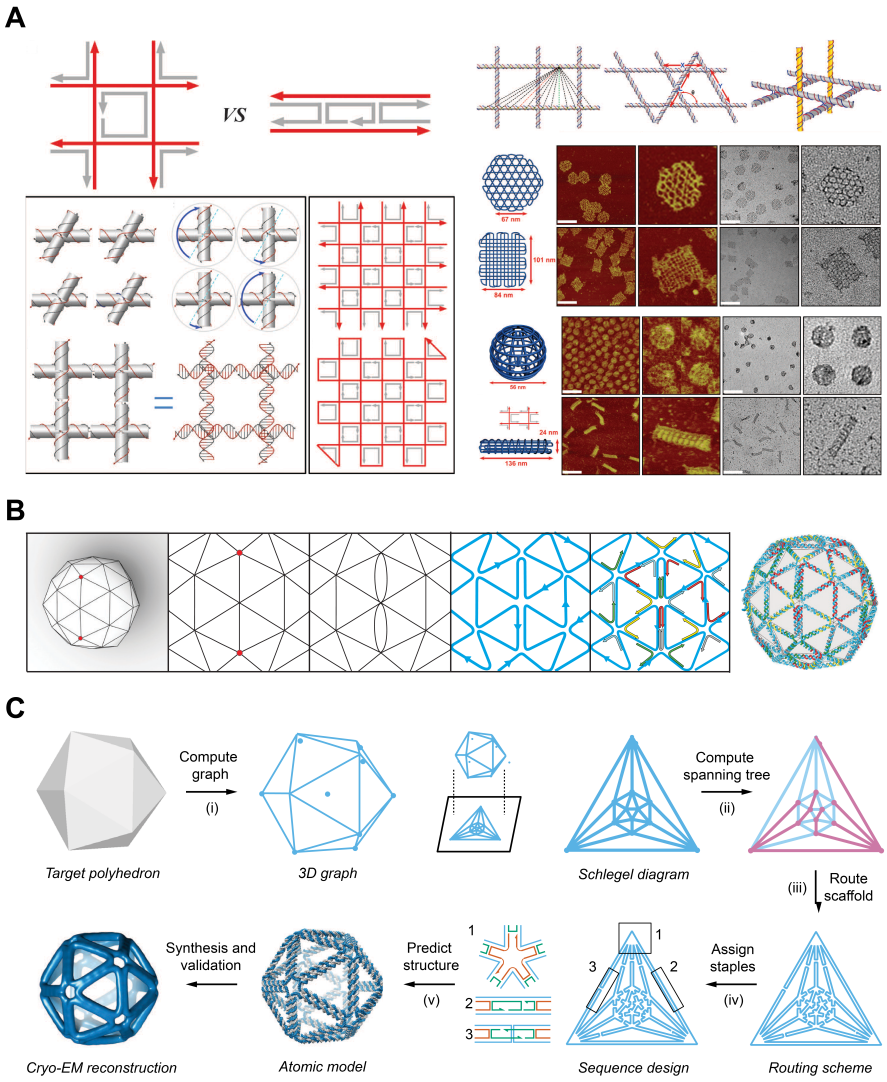

Figure 2.6. Design principles of wireframe DNA nanostructures. (A) Design principles of DNA gridiron nanostructures and representative wireframe designs; (B) A-trial-based scaffold routing of an icosahedron in vHelix-BSCOR; (C) Spanning-tree-based routing of wireframe DNA polyhedra validated using cryo-EM. Part A is adapted with permission from REF. (*99*), AAAS. Part B is adapted with permission from REF. (*100*), Springer Nature Limited. Part C is adapted with permission from REF. (*101*), AAAS.

Figure 2.7 illustrates a few of the structural motifs found in RNA. Besides, among double helices formed by RNA/RNA, RNA/DNA, and DNA/DNA, the RNA/RNA duplex offers the highest thermal stability (*139*, *140*). This stability along with the numerous intra- and inter-molecular interactions offered by RNA make them a unique programmable building block for nanoscale self-assembly.

"RNA tectonics", where natural RNA folds such as tRNA and pRNA

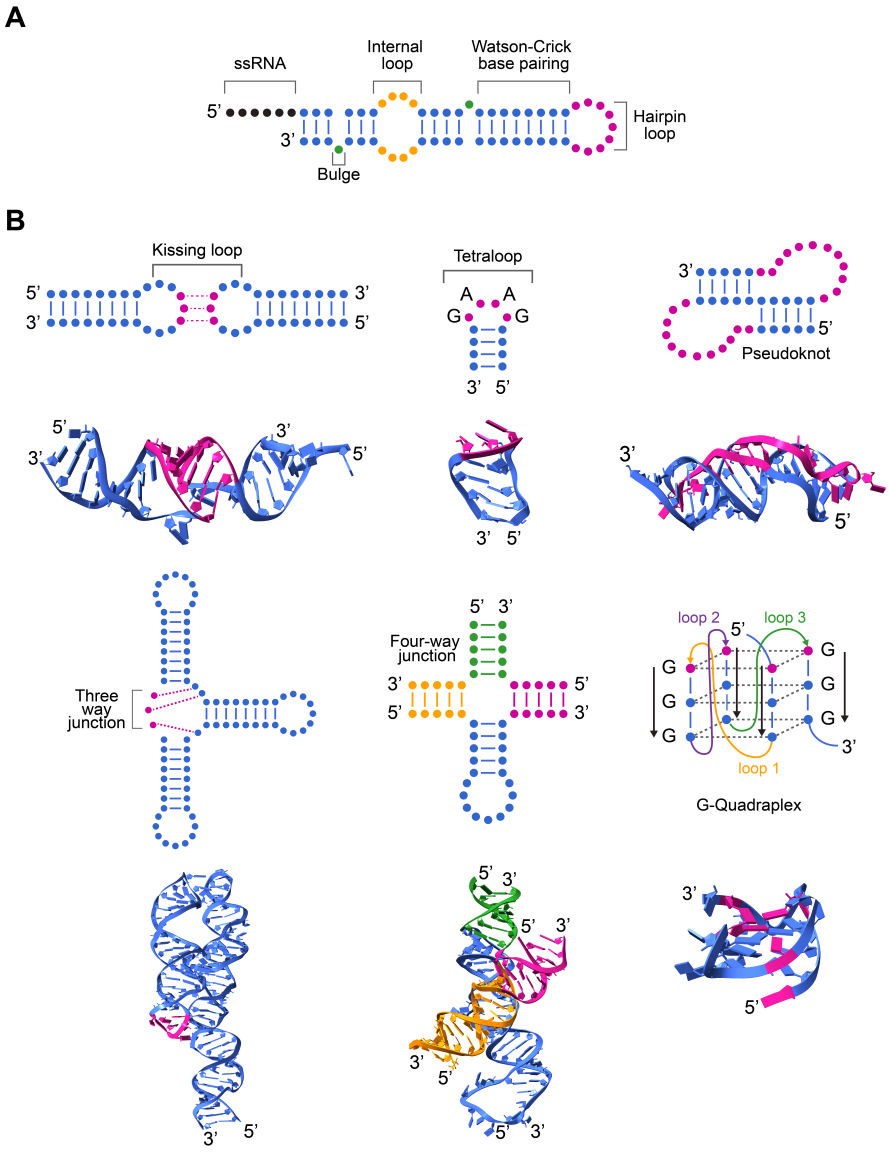

Figure 2.7. Structural motifs found in RNA structure. (A) 2D representation of common RNA secondary motifs; (B) 2D representations of common secondary and tertiary structural motifs found in RNA with corresponding example 3D crystal structures: A kissing loop structure (PDB: 1K9W (*141*)); A tetraloop structure (PDB: 2F87 (*142*)); A pseudoknot structure (PDB: 2K96 (*143*)); A three-way junction (PDB: 1MFQ (*144*)); A four-way junction (PDB: 1M5K (*145*)); and a G-quadruplex (PDB: 31BK (*146*)). The highlighted bases in pink show the characteristic RNA feature except for the four-way junction, where each arm is highlighted with individual colours. All the 3D renderings were made using ChimeraX (*57*, *58*).

(promoter-associated RNA) are utilized in combination with motifs such as bulges, kink-turns, junctions, and kissing loops to fabricate desired shapes, has

provided the basis for the field of RNA nanotechnology (*147–149*). By extrapolating the design principles from DNA nanotechnology and accounting for the structure and composition of RNA [refer to Section 2.1], a wide assortment of complex RNA nanostructures can be fabricated. For example, the design principles laid forth by Goodman *et al.* for the construction of DNA tetrahedron (*97*) were followed by Afonin *et al.* to create cubic RNA wireframe structures (*150*, *151*). Following this paradigm, other design strategies were also employed for RNA nanostructures, such as multiple ssRNA-based assembly of polygons (*152*) and polyhedra (*153*), tile-based assemblies of lattices (*154*) and octameric nanoprisms (*155*), and scaffolded origami-based structures (*156*). These design strategies involve multiple components such as scaffolds and staple strands or several tiles in a concentration-dependent manner to fabricate target structures. However, RNA structures found in Nature are self-folding single strands, that are vital to information transfer in key biological processes. Therefore, nanostructures formed via self-folding single-strand nucleic acids are amplifiable, replicable, and clonable, thereby enabling scaling up in a cost-efficient manner using *in-vitro* or *in-vivo* processes. In addition, unimolecular structures offer higher yields, faster folding, lower errors and high purity compared to multi-component systems.

Strategies for constructing nanostructures from the self-folding of ssDNA have been reported previously (*121*, *157*, *158*). A significant advancement in implementing similar strategies in RNA origami came with the introduction of design principles for folding a long ssRNA directly into the target design (*19*, *20*). The *de-novo* approach described by Geary *et al.* for RNA folding took inspiration from DX tiles and utilized kissing loop motifs to bring different regions of the target structure together. The RNA origami tiles constructed using this approach were up to six helices tall, 660-nt in length, and were folded either by heat annealing or by co-transcriptional folding (Figure 2.8 A). Albeit the size of this ssRNA origami was comparable to that of ssDNA origami, they were at least an order smaller than scaffolded DNA origami structures. To this end, a knot-free novel design strategy that improved the size of both self-folding ssDNA and ssRNA origami structures was introduced by Han *et al.* (*122*). The design principles implemented in their automated design software were readily applicable to both single-stranded DNA and RNA origami structures, since the design was not restricted by RNA kissing-loop interactions. They constructed 18 multi-kb single-stranded origami (ssOrigami) structures, including a ≈10000-nt ssDNA origami and a ≈6000-nt ssRNA origami using partially complemented dsDNA or dsRNA and parallel crossover cohesion. Several improved design strategies have since been reported, including a novel branching kissing loop motif to create trivalently branched nanostructures (*159*) and co-transcriptional folding of larger RNA origami constructs (*160*). The ssRNA nanostructures described above, have been fabricated the same way as ssDNA; using either synthetic or enzymatically synthesized strands or

annealed from strands produced *in-vivo*. Hence, a major challenge in scaling up the field of nucleic acid nanotechnology (DNA/RNA) has been implementing a protocol for the complete *in-vivo* production of these nanostructures. In this respect, Li *et al.* introduced a strategy that allows both *in-vitro* and *in-vivo* production of various 2D RNA structures (*21*). The RNA strands, synthesized *in-vivo* using this strategy, were directly folded into the target shape inside the cells (Figure 2.8 B). A 3D RNA tetrahedron was also constructed *in-vitro* using this method, making it one of the first wireframe RNA nanostructures folded entirely from a single strand. Though the sequence generation and structure validation were performed using online tools in this study, the design of the RNA nanostructures was done manually.

The advances in nucleic acid nanotechnology were largely facilitated by various computational methods, which eased the design process for complex nanostructures. Unlike DNA nanotechnology, dedicated software for the design of RNA nanostructures is sparse: NanoTiler (*161*), Assembly (*162*), and RNAMake (*163*) for 3D structural motifs, and Kwanom (*122*) and ROAD (*160*) for ssOrigami design. And a fully general design scheme and an automated

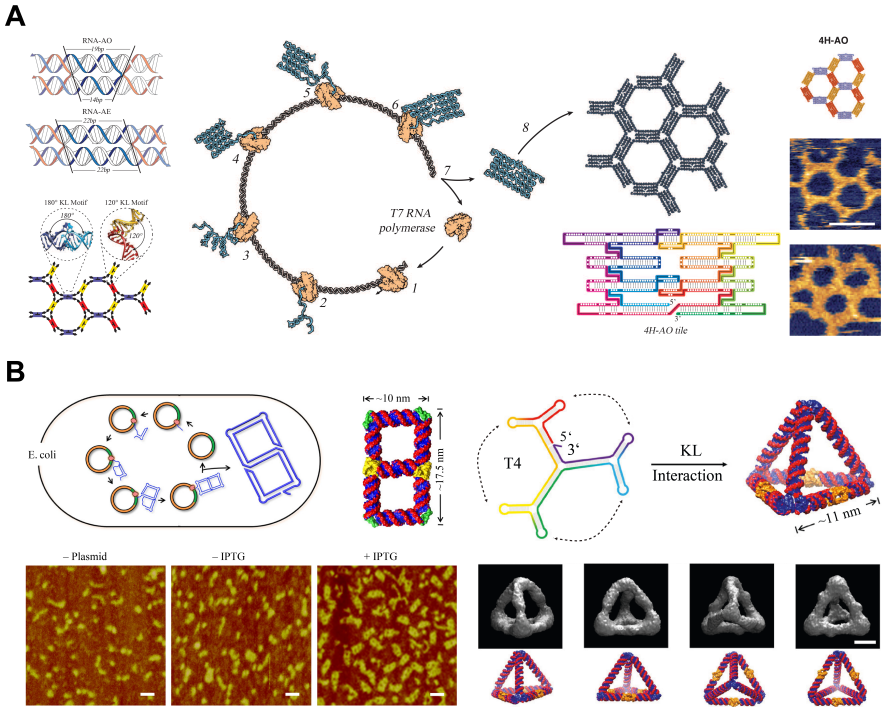

Figure 2.8. Synthesis and folding of ssRNA nanostructures. (A) Design principles of co-transcriptional folding ssRNA origami and representative AFM image of 4H-AO tile; (B) *In-vivo* production and folding of ssRNA into 2D and 3D shapes and single particle reconstructions of an RNA tetrahedron. Part A is adapted with permission from REF. (*20*), AAAS. Part B is adapted from REF. (*21*), Springer Nature Limited.

software pipeline for designing 3D RNA wireframe polyhedra are completely lacking. In Chapter 4.1, we address this gap by experimentally realizing RNA wireframe nanostructures designed using a highly general and automated wireframe design tool.

2.4 Reconfigurable nanostructures

The nucleic acid structures described in the previous sections are mostly static structures bereft of dynamic capabilities. However, to emulate the functions performed by Nature, static nanostructures are inexpedient. Nucleic acids are innately static structures, and to design dynamic structures that can undergo structural reconfiguration upon external stimulation, a general idea would be to incorporate stimuli-responsive elements into these nucleic acid structures. To test this, DNA origami templates have been used predominantly due to the well-established design rules and the relative ease of assembly and purification. DNA origami nanostructures in these dynamic designs undergo nano- to macroscale structural changes caused by the incorporated stimuli-responsive element. The changes can be observed either directly via imaging techniques such as AFM and TEM, or by translating the responses from optical reporters into interpretable outputs. While imaging techniques are invaluable for observing the changes directly, they do not add any functionality to the structures. Whereas, coupling optical reporters by utilizing the functionalization capabilities of DNA can pave the way for structures with well-defined configurations that exhibit tailorable optical and electronic properties. The observed optical response can be fluorescence, optical activity, or scattering-based. Fluorescence-based responses typically arise either from organic fluorophores (*164*) or from the energy transfer between a donor and acceptor fluorophore pair based on their proximity (*165*). They are often used to measure the structural changes in dynamic systems, *e.g.,* fluorescence-based sensors. On the other hand, optical activity (or chiroptical) (*166–168*) and scattering responses (*169*) that are usually generated by the functionalized inorganic nanoparticles, can be used to construct materials with fascinating plasmonic responses. Chiroptical response arises from chiral objects whose mirror images are non-superimposable with themselves, for example, our two hands. Chiral objects can exist in left-handed (LH) or right-handed (RH) enantiomeric forms. In the case of DNA origami constructs, controlled switching between these forms can be achieved using dynamic DNA origami templates. Though DNA has right-handedness, the chiroptical response of individual DNA molecules is rather small. To improve the chiral signal, typically plasmonic metal nanoparticles such as gold and silver are arranged onto DNA origami templates in pairs or multimers. By coupling with one another, the metal particles add to the overall chiral plasmonic response in both static (*170*) and dynamic DNA nanostructures (*171–173*). Chiral

plasmonics in combination with dynamic DNA nanotechnology could open up an avenue of applications including biomolecular sensing, tunable chiral fluids, adaptable nanophotonic circuitry, surface-enhanced Raman and fluorescence-combined chiral spectroscopy, and chiral signal amplification (*171*, *174*, *175*).

Dynamic DNA nanostructures, described above, mainly rely on the incorporated stimuli-responsive elements, which can be driven either by nucleic acid strand chemistry or by chemical or physical stimulation (*176*, *177*). Nucleic acid strand-driven reconfigurability has been achieved largely based on toehold-mediated strand displacement reaction (TMSD). In TMSD, an "original" or "template" ssDNA strand is weakly hybridized with a complementary "leaving" or "protector" strand, which gets replaced by branch migration upon the addition of a "fuel" or "invading" ssDNA strand (*178*). The original strand bound to the protector has an unpaired "toehold" extension (usually about eight nts long) to which the invading strand, which is a complete complement to the original strand, binds. Upon binding, the invading strand displaces the protector strand as it migrates to the other end of the original strand to form a "New" duplex, which is a more stable complex (Figure 2.9 A). The leaving strand in TMSD can in turn invade another complex using a toehold of its own resulting in a strand displacement cascade. Since its introduction by Yurke *et al.* (*164*) in 2000, TMSD has been adapted for use in both DNA and RNA nanotechnology for constructing logic gates, DNA walkers, catalytic amplifiers, autonomous molecular motors, and ribosensors (*50*, *176*, *177*, *179*, *180*). TMSD has also been used in constructing DNA origami-based chiral nanostructures (*166*). In their pioneering work, Kuzyk *et al.* fabricated chiral metamolecules using two 14 helix DNA origami bundles (14-HB) attached at a pivot point in the centre with a tunable angle. Each 14-HB hosts a gold nanorod (AuNR), and by TMSD, the fuel strands were able to switch the DNA origami configuration to desired states and in turn modulate the chiral response from the attached AuNRs. The constructed reconfigurable 3D plasmonic metamolecule was driven to either LH or RH states by adding specific DNA strands as fuels (Figure 2.9 B).

Other DNA strand-based reactions such as strand association/dissociation, strand degradation, Hoogsteen base pairing, motif-based reactions (G-quadruplex, i-motif), base stacking, transformation between conformations (like B-Z transformation), and anti-junctions have also been exploited to construct dynamic DNA origami assemblies. These strand-based reactions operated mostly in tandem with external chemical or physical stimuli such as temperature (*181*), exposure to light (*167*), pH (*168*), electric fields (*182–185*), or concentrations of metal ions (*181*, *186*). Of these, dynamic systems stimulated by light are particularly exciting, as light is a clean, non-invasive, and waste-free energy source. Furthermore, light offers high spatial and temporal resolution, since it can be illuminated at a selected area

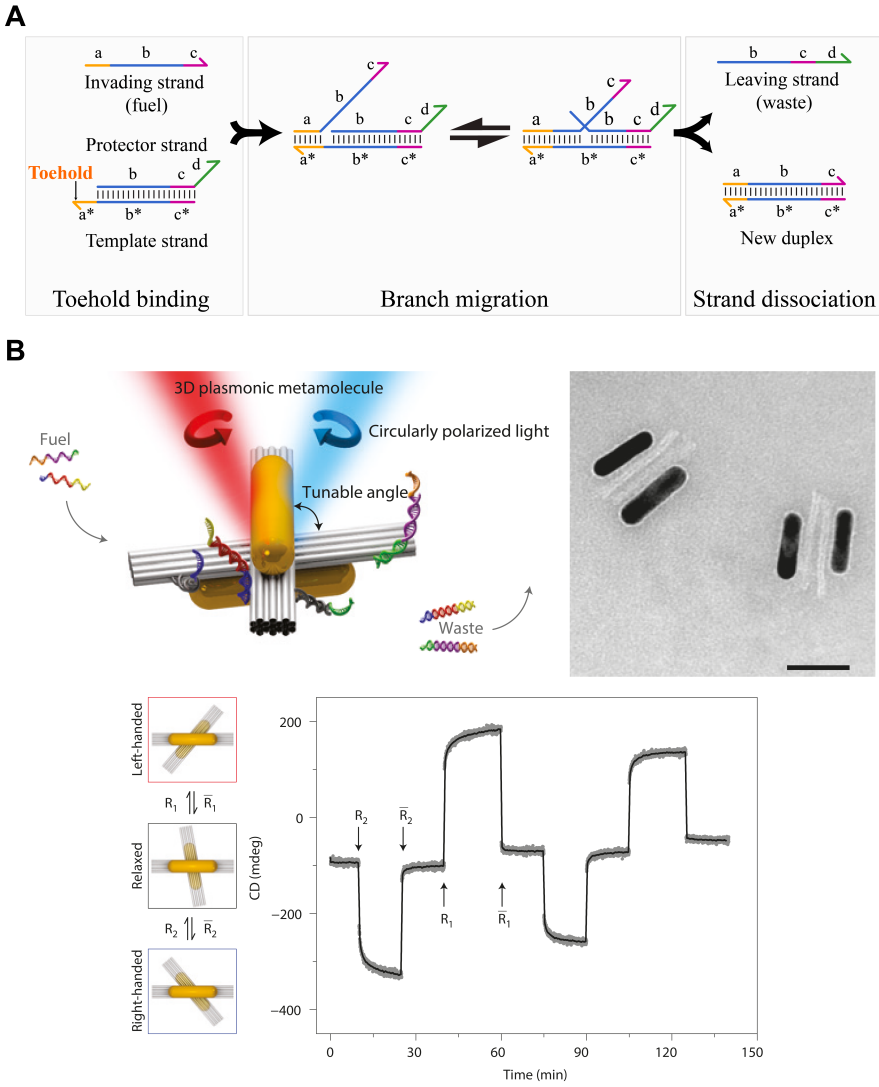

Figure 2.9. Reconfigurable DNA nanostructures. (A) Toe-hold mediated strand displacement mechanism involving toehold binding, branch migration, and strand dissociation. (B) A reconfigurable chiral plasmonic nanostructure based on TMSD, along with a representative TEM image and CD spectrum showing the change in chiroptical response with respect to the structural reconfiguration of DNA origami. Part B is adapted with permission from REF. (*166*), Springer Nature Limited.

with tunable wavelength, focused spot size, and optical power and can be switched on and off with high frequency, respectively. For light-responsive dynamic systems, the azobenzene moieties covalently incorporated into nucleic acid strands have served as the reconfigurable element (*167*, *187*, *188*). However, azobenzene incorporation is time-consuming, expensive, and the light responses are usually relatively slow (typically in the range of tens of

minutes) (*189*, *190*). Inexpensive light-responsive molecules with a rapid response might overcome these drawbacks. To this end, merocyanine-based photoacid, a spiropyran derivative, has been used previously to create dynamic assemblies (*191–193*). The photoacid causes a light-responsive reversible pH change in the medium, which can be utilized to reconfigure pH-responsive dynamic DNA systems. A strategy to fabricate such DNA-based chiral plasmonic structures that rapidly switches upon exposure to light, not via a light-responsive component, but through the pH change caused by merocyanine-based photoacid in the surrounding medium is presented in Chapter 4.2.

2.5 Applications of dynamic nanostructures

Rothemund, in his seminal article, envisioned that DNA origami can serve as a 'nanobreadboard' to host a plethora of components (*14*). DNA templates have since found applications in nanofabrication, nanophotonics and nanoelectronics, catalysis, computation, and molecular machines. For the sake of brevity, this thesis will concentrate on biological applications of dynamic DNA origami in bioimaging, drug delivery, and biophysics; recent reviews on other applications can be found elsewhere (*40*, *50*, *194*). DNA origami templates have a highly heterogeneous surface that affords spatial and sequence addressability, thus enabling the positioning of molecules with nanoscale precision (*195*). For instance, static DNA nanostructures have exploited this positioning capability to elucidate the protein structure by cryo-EM (*196*, *197*), for super-resolution imaging using DNA-PAINT (Points Accumulation for Imaging in Nanoscale Topography) (*198*), to study spatial tolerance and separation of antibodies and aptamers (*199*, *200*), to unravel the forces at single molecule resolution (*201*, *202*), and to study the effects of tethering enzyme cascades (*203–205*). Recently, a system that can sense and capture virus particles has been reported (*206*), showcasing the ingenuity of DNA origami nanostructures.

Dynamic nanostructures with such positioning accuracy, on the other hand, can be exploited to either specifically capture/ release biomolecules of interest or study the biophysical interactions. In the former, the biomolecules either generate a signal upon binding (sensors) or are released upon a certain signal (drug delivery). DNA origami-based sensors are composed of target recognition elements for specific chemical or physical signals and transducers that provide a readout of the structural changes. A wide range of origami-based sensors including those for viral RNA (*207*), adenosine (*175*), aflatoxin (*208*), pH sensing (*209*), and adenosine triphosphate (ATP) and cocaine (*210*) have been reported. The innate biocompatibility, safety, and stability of DNA make them an ideal vector for *in-vivo* drug delivery. Dynamic nanostructures can deliver drugs to the diseased environment in a targeted manner. Additionally, they can be fabricated in a user-defined size and shape with accurate placement of

ligands, all of which contribute to determining the biological fate of the drug molecule delivered (*211*). Various design strategies have been explored over the years to deliver drugs (*211–214*) including *in-vivo* targeting of cancer cells and gene silencing (*215*). These advances pose an exciting promise as these DNA nanostructures can selectively release the cargo in response to a specific overexpressed molecule in the disease environment.

DNA-based dynamic structures have reached the juncture, where they can not only serve as a template to sense or deliver, but also provide a detailed account of biophysical interactions that occur at the nanoscale. These structures can be employed to study the minuscule forces that range between pN and μN (*218*) in biological processes or amplify and help visualize molecular movements that occur (*219*). The former is traditionally performed using single molecule mechanical techniques like optical and magnetic tweezers, or AFM (*220*), that operate in a wide range between 0.1 pN and 100 nM (*218*, *221*). However, achieving sub-nanometer spatial resolutions in the regime of low forces (less than 10 piconewtons (pN)) with these techniques is often hampered by the signal-to-noise limitation. DNA origami coupled with optical tweezers has been exploited in the past with some success to enhance noise suppression in single-molecule force spectroscopy (*222*, *223*). Stand-alone force spectrometers that operate independently of macroscale molecular manipulation tools like AFM and optical traps soon followed. These stand-alone spectrometers relied on the positioning capability of dynamic DNA structures. The primer to stand-alone force spectrometers developed by Dietz lab was based on their earlier work on a molecular positioning device (*195*). The device was capable of controlling the relative positioning between two molecules by adjusting the angle between the two bundles of a hinged DNA origami object using adjuster helices (Figure 2.10 A). They positioned fluorescent molecules and reactive groups with a displacement step as small as 0.4 Å. Concurrently, the group used the positioning device as a force spectrometer to explore the energy landscape of molecular interactions in thermal equilibrium. To this end, they immobilized a single nucleosome on each bundle of the device, and the interactions between nucleosomes shifted the opening angle of the device. From the distribution of angles, observed directly via single-particle TEM imaging, they were able to reveal the energy landscape for nucleosome-nucleosome stacking (*216*) (Figure 2.10 B). Variants of this positioning device were employed to probe the structural and conformational changes that occur over mesoscopic length scales in large macromolecular complexes. For instance, the unwrapping of the nucleosome complex was studied under various conditions via direct observation under TEM (*224*, *225*). The stiffness of the hinge spring and the position of the receptor-ligand pair along the bundle dictates the force bias in these devices. In a seminal work, Nickels *et al.* (*201*) introduced a variation of the force spectrometer, where the force bias was controlled by varying the number of nucleotides in an ssDNA spring that is fixed at the ends of a DNA origami object. The end-to-end distance was held constant, and the contour

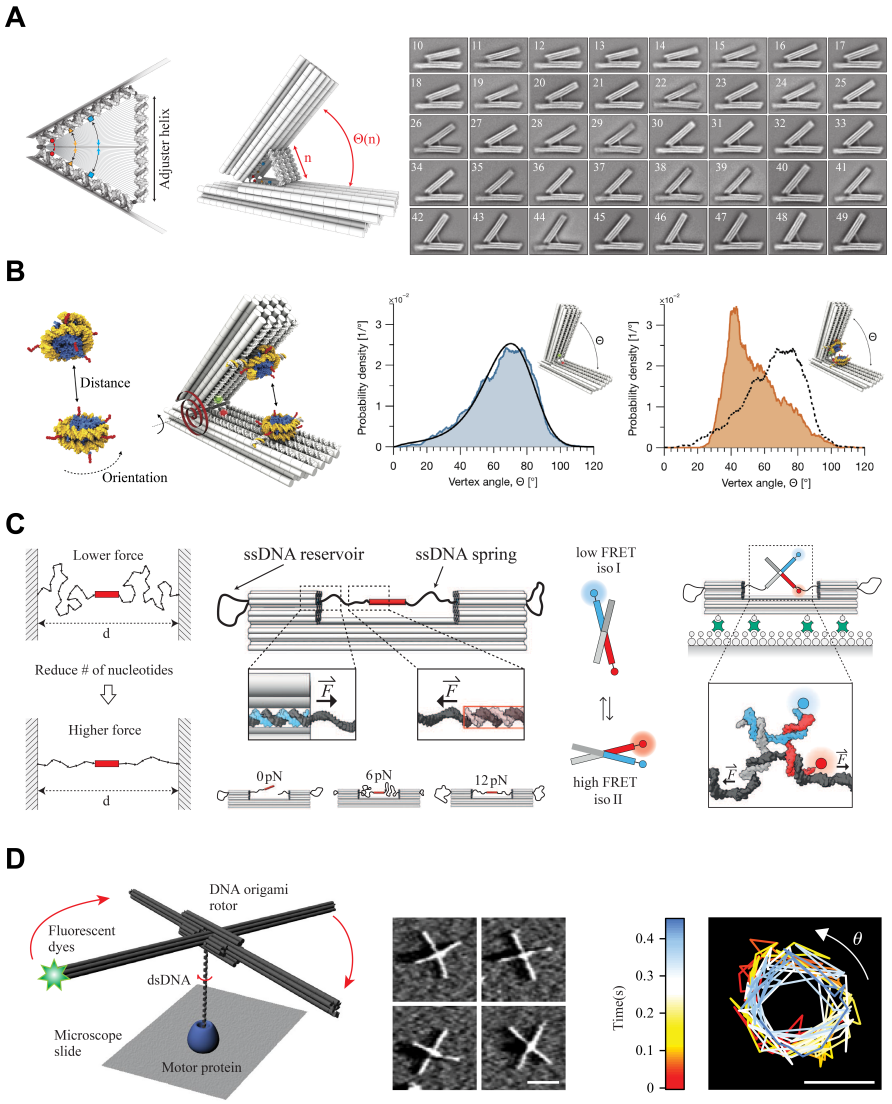

Figure 2.10. Applications of dynamic DNA nanostructures in biophysics. (A) A DNA origami positioning device for relative positioning of two molecules along the arms with sub-nanometer accuracy and representative class averages of devices with different opening angles; (B) A stand-alone DNA origami-based force spectrometer consisting of two arms connected via a hinge that acts as a torsional spring to unravel the interactions between nucleosomes; (C) A DNA origami force clamp that exerts forces by fixing the end-to-end distance of the attached ssDNA spring; (D). A DNA origami device to study the rotary motion of dsDNA upon unwinding by motor proteins with high spatiotemporal resolution. Part A is adapted with permission from REF. (*195*), Springer Nature Limited. Part B is adapted from REF. (*216*), AAAS. Part C is adapted with permission from REF. (*201*), AAAS. Part D is adapted with permission from REF. (*217*), Springer Nature Limited.

length of the spring was varied causing the polymer to be extended (Figure 2.10 C). The Förster resonance energy transfer (FRET) was measured to map the conformational states of Holliday junctions and TATA-Binding protein (TBP), and more recently to investigate the stability of RNA polymerase III preinitiation complex (*202*). Since the structure was pre-stressed, it is not a dynamic structure, however, it demanded a special mention as it enables single-molecule force measurements with much higher throughput than conventional force spectroscopy devices (optical traps or AFM).

Aside from their role as force spectrometers, dynamic DNA constructs are also used to gain insights into molecular movements in biological processes that involve DNA distortion, protein-protein interactions, and DNA-protein interactions. Typically, fluorescence-based optical reporters are used to measure these structural changes. For example, Kosuri *et al.* (*217*) tracked the rotation of dsDNA during biological events such as unwinding by RecBCD helicase and transcription by RNA polymerase by following the dye attached to a DNA origami structure in a fluorescence microscope (Figure 2.10 D). This approach is particularly suitable for measuring rotational movements. Whereas, it would be beneficial to use imaging techniques to directly observe the molecular structural reconfiguration. In particular, the result of DNA bending, looping, and twisting can be translated into the spatial reconfiguration of DNA constructs and be directly imaged. Moreover, due to their large size (in the range of a few MDas), DNA origami structures serve as ideal scaffolds for imaging these movements in AFM (*226*, *227*) and TEM (*195*). Compared to AFM, TEM has a relatively straightforward sample preparation, operation, and fast data acquisition. While scaffolds to interrogate biophysical forces under TEM have been reported (*216*, *224*, *225*), those for studying molecular movements are limited. Hence, Chapter 4.3 concentrates on a dynamic DNA origami-based molecular device, that as a test case was used to measure the DNA distortion induced by a DNA bending protein directly using classical TEM.

3. Methods

This section presents an overview of the methods used in the thesis. The following subsections provide the experimental details for the methods used by the author. Table 3.1 presents the list of methods used in this thesis and the corresponding publications in which they were used.

The design and simulation of structures in Publication (I) were performed by Prof P. Orponen's group and Dr I. Kawamata. The photoacid and the AuNRs used in Publication (II) were synthesized by Dr J. Wang and Dr MK. Nguyen, respectively. The CD characterizations were performed by J.Ryssy. The DNA origami structure used in Publications (II) and (III) was designed by Prof. A. Kuzyk (*166*). Design and experimental details of the above-mentioned methods along with other methods used in the publications can be found in the experimental sections of the respective publications.

3.1 Design and assembly of nanostructures

3.1.1 Amplification and transcription of DNA templates

The DNA templates for tetrahedron (455 bp), triangulated bipyramid (663 bp), and triangulated prism (801 bp) were resuspended in nuclease-free water at a 10 μg/μL concentration for Polymerase Chain Reaction (PCR). The templates were amplified using Phusion High-Fidelity DNA Polymerase with respective forward and reverse primers at 0.5 μM. The samples in 1X Phusion high-fidelity PCR master mix with HF buffer were first denatured at 98 °C for 30 s and then cycled through 8 s of 98 °C, 15 s of 58 °C, and 30 s of 72 °C over 20 cycles, followed by an elongation step for 7 minutes (min) at 72 °C. The amplified PCR products were purified using standard purification kits. The samples were run on a 1.5% (weight/volume (*w/v*)) agarose gel pre-stained with SyBr Safe in 0.5X Tris(hydroxymethyl)aminomethane Borate Ethylenediaminetetraacetic acid (Tris/Borate/EDTA or TBE) buffer and the right-sized product was excised and purified from the gel, The purified templates were transcribed at

Table 3.1. Summary of the main methods and their corresponding publications.

Method	Publication
Design and assembly of nanostructures	
Amplification and transcription of DNA templates	I
Assembly of RNA nanostructures	I
Assembly and purification of DNA origami structures	II, III
Fabrication of AuNRs functionalized DNA origami	II
Design of TATA box and bending experiments	III
Imaging of nucleic acid nanostructures	
AFM imaging	I
Cryo-EM imaging and single-particle reconstruction	I
TEM imaging and measurement of angles	II, III

37 °C for 6 h using ≈1 U/μL T7 RNA polymerase in 1X RNA polymerase buffer containing 12.5 mM $MgCl_2$ and 4 mM of each rNTP. The reaction was stopped by the addition of 2 U/μL DNase I. The transcribed RNA samples were preheated at 95 °C for 5 min and run on an 8% poly acrylamide/bis-acrylamide gel electrophoresis (29:1) (PAGE) (denaturing) containing 8 M Urea and 1X TBE at 58 °C. The PAGE gel was post-stained using 1X SyBr green for 15 min. The bands of interest were excised from the denaturing gels and purified using a standard RNA purification kit. Both agarose and PAGE gels were imaged under blue light for excising the right band.

3.1.2 Assembly of RNA nanostructures

The purified ssRNA of each nanostructure was thermally annealed by heating to 80 °C for 5 min followed by cooling to 20 °C at 0.1 °C/s in a folding buffer containing 0.5X Tris(hydroxymethyl)aminomethane Ethylenediaminetetraacetic acid (Tris/EDTA or TE) buffer with 1 mM $MgCl_2$ and 100 mM NaCl. The folded samples were run in 5% PAGE (native) in an ice bath along with a low-range ssRNA ladder. The gels were post-stained using 1X SyBr green for 15 min and imaged under blue light.

3.1.3 Assembly and purification of DNA origami structures

The DNA origami design was adopted from previous studies (*166–168*). The DNA scaffold strands (p7560) at 10 nM concentration along with core staple strands each at 100 nM concentration were mixed in a 1X TE buffer supplemented with 20 mM $MgCl_2$. The bridging strands for Publication (II) the bridging staples were added at 100 nM concentration, while for

Publication (III) were added at optimized concentration depending on the design (40 nM for design 1 and 80 nM for design 2). The samples were thermally annealed by first heating to 80 °C for 15 min followed by slow cooling to 20 °C over 30 h (*167*). The folding quality was evaluated using a 1% (*w/v*) agarose gels and the excess staples were removed using Amicon Ultra-0.5 centrifugal filter units (Molecular weight cutoff (MWCO)- 100 kDa) by spin-filtering technique (*228*, *229*).

3.1.4 Fabrication of AuNRs functionalized DNA origami

The DNA origami structures consisting of two 14-helix bundles linked in the middle by two ssDNA crossovers were used as templates for the assembly of two AuNRs with an average size of 25 nm × 62 nm. The origami structure was folded with 36 staples (18 on each bundle) modified with additional A10 extensions at the 3′ end for the assembly of AuNRs. The assembly procedure of AuNRs onto origami structures was adopted from a previously established protocol with minor modifications (*175*, *230*). First, the AuNRs were functionalized with complementary T16 DNA strands with thiol modification on the 5′ end. For this, an equivolume of 1 mM T16 strands with thiol modification and tris(carboxyethyl) phosphine hydrochloride (TCEP, 14 mM) were mixed and pre-incubated for 1 h. The strands were then mixed with 10 nM AuNRs (dispersed in water with 0.05% sodium dodecyl sulfate (SDS)) in the molar ratio of 14000:1 and the pH of the solution was adjusted to 2.5-3.0 using 1 M hydrochloric acid. The mixture was placed in a shaker at 400 rpm for 1 h at room temperature. Equivolume of 1 M solutions of sodium chloride (NaCl) was added to the mixture and the sample was placed again in the shaker for an additional 4 h. The solution pH was readjusted to 7.5-8.0 with 10X TBE buffer, followed by overnight incubation. The sample containing AuNRs functionalized with DNA (AuNRs-DNA) was washed by centrifugation (7000 rcf for 30 min) in a 0.5X TBE buffer containing SDS (0.1%) four times, with the supernatant removed after every wash. Ultraviolet-Visible spectroscopy (UV-Vis) was used to estimate the concentration of AuNRs-DNA using Beer-Lambert law and the absorbance value at the longitudinal plasmonic mode resonance (650 nm) and extinction coefficient of $3.8 \cdot 10^9$ $M^{-1}cm^{-1}$. The concentration of $MgCl_2$ in the final solution was adjusted to 10 mM and the AuNRs-DNA was then mixed with the DNA origami templates at a 15:1 ratio. The mixture was annealed overnight in a thermoshaker from 40 °C to 20 °C. The assembled CPM containing DNA origami with two AuNRs was purified using a 0.75% agarose gel with 12 mM $MgCl_2$ run in an ice bath for 3 h. The band of interest was excised and the CPM was extracted using a standard gel extraction filter. The CPMs were washed three times by centrifugation (5 min, 3k rcf) in a buffer-free aqueous solution containing 500 mM NaCl and 0.02% SDS.

3.1.5 Design of TATA box and bending experiments

The bridge sequence containing the TATA box sequence connected the two origami bundles either via i) two complementary individual strands (design 1) or via ii) a single strand running through (design 2). Three bridge sequences were incorporated to study their difference: a) an Adenovirus Major Late Promoter (AdMLP) consensus sequence (CTATAAAAG) (S1), b) a consensus sequence with bases before and after the TATA box mutated to its compliment (GTATAAAAC) (S2), and c) a scramble sequence (ACTTCTCGG) to which TATA binding protein (TBP) does not bind (S3). The bridge-forming strands were incorporated into the DNA origami structures during folding. DNA origami structures of 1 nM concentration with their respective bridge sequences were incubated with various concentrations of TBP, transcription factor II A (TFIIA), and transcription factor II B (TFIIB) in a modified HEPES buffer containing 1X TE, 10 mM NaCl, 10 mM $MgCl_2$, 150 mM KCl, 10 mM HEPES, and 12% Glycerol. The mixture was incubated at 25 °C for 2 h followed by TEM imaging (*231*).

3.2 Imaging of nucleic acid nanostructures

3.2.1 AFM imaging

AFM imaging was performed using a Dimension Icon AFM (Bruker). The sample at ≈1 nM concentration was deposited onto a freshly cleaved mica surface pre-treated with 0.05% 3-aminopropyltriethoxy silane (APTES) (*232*, *233*). In brief, 5 μL of the sample in the folding buffer was incubated on the APTES-treated mica surface for 3 min. The excess liquid was removed using filter paper. Subsequently, the surface was rinsed with 10 μL of the folding buffer and used for imaging. The imaging was performed in the folding buffer by scanning the surface using ScanAsyst-Fluid+ probes (Bruker). The images were collected in ScanAsyst mode and analyzed using AFM scanning software (Nanoscope Analysis 3.0) and ImageJ (`http://imagej.nih.gov/ij/`) software.

3.2.2 Cryo-EM imaging and single-particle reconstruction

The RNA nanostructures in folding buffer were concentrated using 3 kDa MWCO Amicon Ultra centrifugal filters to a final concentration of ≈400 nM. The concentrated sample (5 μL) was applied onto 300 mesh copper (Cu) grids coated with lacey carbon placed in a Leica EM GP2 plunge freezer maintained at 22 °C and 70% relative humidity. The sample was quickly blotted for 3 seconds followed by immediate vitrification using liquid ethane maintained

at -170 °C. The vitrified samples were cryo-transferred to the microscope (JEOL JEM-3200FSC TEM) and imaged while maintaining the specimen temperature of -190 °C. The collected images were processed using EMAN2 (*234*) for contrast transfer function (CTF) correction and reconstruction. In short, the particles were manually picked from the micrographs, CTF corrected, class averaged, and reconstructed. The initial models generated by imposing cyclic C1 (no symmetry) or tetrahedral symmetry (TET) were used for final refinement performed using either C1, C3, or TET symmetry imposition. The reconstructed models were visualized using UCSF Chimera (*235*).

3.2.3 TEM imaging and measurement of angles

The nanostructures at 1 nM concentration (5 μL in volume) were deposited on a freshly glow discharged carbon/fomvar TEM grid and blotted out after 5 min. The grids were stained with 1% uranyl formate solution to get a negative contrast. The grids were then imaged using either Tecnai F12 operating at 120 kV or Tecnai F20 operating at 200 kV. The acute angles between the origami bundles were obtained by manual analysis of the TEM images in Corel Draw (2018) and the histograms were plotted in Origin 2020b.

4. Results and Discussion

This chapter provides a summary of the main results from the three publications included in this thesis.

4.1 Design and assembly of RNA polyhedra (Publication I)

The goal of Publication I was to experimentally realize RNA wireframe structures designed using automated design software. The software tool *Spanning Tree Engineered RNA design* (*Sterna*) (*236*) automates the secondary-structure design of the target polyhedral model created in the open-source *Blender* 3D graphic design software suite (*237*). *Sterna* performs the strand routing and creates the corresponding spatially embedded RNA A-helices, aligns their phases, and adds spacer nucleotides at the vertices for flexibility. The resulting *Simple Nucleic Acid Code* (*snac*) files contain RNA duplexes formed by the RNA strand routed anti-parallel to one another as edges of the polyhedra, and hairpin loops that would later form the kissing loops. The *snac* files are further modified to embed kissing loop sequences, primary structure sequences (designed with the help of NUPACK (*238*, *239*)), and create an additional module *snac2ox* that can be used as input for oxRNA molecular dynamics simulation and visualization package (*240*, *241*). The overall RNA polyhedron design scheme is illustrated in Figure 4.1 A.

We designed a tetrahedron, a triangulated bipyramid, and a triangulated prism using the *Sterna* tool and *snacseq* primary-structure generator to validate our approach. The designed sequences for the aforementioned structures were ordered as DNA templates along with the necessary transcription promoter sequence and primer sequences. The DNA templates were amplified using PCR and purified before being transcribed into RNA. The transcribed RNA strands of the right length were further purified and folded by thermal annealing. The folding was qualitatively verified using native PAGE. Structures where some or all of the kissing loops replaced by non-pairing sequences were used to compare the folding efficiencies of the target models. The structures exhibited distinct bands in native PAGE, indicating a proper folding of the samples.

Additionally, the fully folded structures migrated faster than their counterpart (structures without some or all kissing loops). Additional bands in native PAGE were presumed to be formed as a result of aggregation. The tetrahedron and bipyramid folded with high yields, whereas the prism structures had low yield possibly due to the large number of kissing loops (7 in prism vs 5 and 3 in bipyramid and tetrahedron, respectively) that leads to aggregation (Figure 4.1 B).

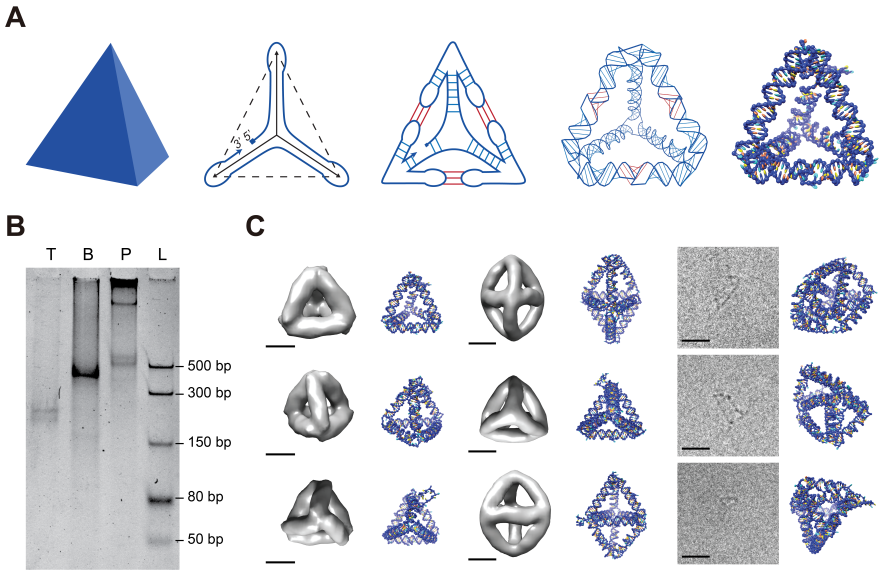

Figure 4.1. Design and validation of RNA polyhedral models (A) Design workflow of an RNA wireframe mesh in *Sterna* tool; (B) Native PAGE for tetrahedron (T), bipyramid (B), and prism (P) along with the low-range ssRNA ladder (L); (C) Cryo-EM reconstruction images of T and B along with representative cryo-EM images of P. The oxRNA/Chimera renderings from ChimeraX are presented alongside the images. Scale bars for reconstructed maps: 5 nm; Scale bars for cryo-EM images: 20 nm. The figure is adapted from REF. (*242*), American Chemical Society. Licensed under Creative Commons CC BY.

To verify the folding, the structures were imaged using cryo-EM. Using the single-particle reconstruction technique, the tetrahedron and the bipyramid structures were reconstructed without imposing any symmetry on the data. The prism structure had severe aggregation, corroborating the PAGE results. However, individual particles resembling the structure of a prism can still be seen in cryo-EM images (Figure 4.1 C). The results showcase a highly generalizable and fully automated design pipeline for rendering 3D wireframe polyhedra as native confirmations of ssRNA molecules. The design principles introduced here are not restricted by the size or complexity of the target polyhedra. The RNA structures can serve as templates for functionalizing nucleic acids, small molecules, and proteins and perform a plethora of functions from imaging to drug delivery (*130*, *131*, *243*). Moreover, the ssRNA wireframe

design approach described here can not only be applied to polyhedral models but also be extended to arbitrary straight-line 3D meshes.

4.2 Reconfigurable chiral plasmonic nanostructures (Publication II)

Publication II aimed at the fabrication of a chiral plasmonic nanostructure that reconfigures upon external stimuli. In lieu of incorporating a stimuli-responsive reconfigurable element into the origami, we employed a photo-responsive medium that changes pH in response to visible light. To this end, we utilized an aqueous solution of merocyanine-based photoacid (MCH^+), wherein the release of H^+ from a ring-closing reaction of MCH^+ occurs when illuminated with blue light (*245*, *246*) (Figure 4.2 A). The pH change is reversible, *i.e.*, MCH^+ is regenerated by a ring-opening reaction when the light irradiation is ceased. The pH change triggers the formation of DNA triplex "locks", that switch the configuration of the DNA-based chiral plasmonic assembly (*168*). The DNA triplexes were composed of 20 bp dsDNA and 20 nt ssDNA. The latter undergoes a protonation at the cytosine bases upon pH change leading to the formation of the sequence-specific parallel Hoogsteen interactions that

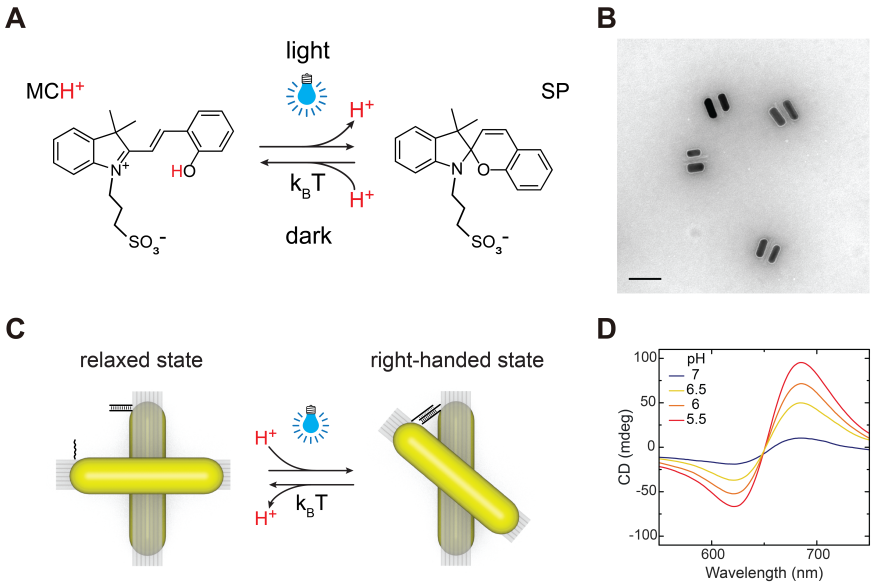

Figure 4.2. Schematic illustration of stimuli-responsive plasmonic structures and their characterization. (A) Release of protons by MCH^+ under blue light illumination and recapture of protons upon turning off the light source; (B) TEM image of CPMs (not representative of solution structures). Scale bar: 100 nm; (C) Illustration of CPMs and triplex locks. The DNA triplex formation renders the CPMs with an RH configuration that can be reversibly switched to an open relaxed state; (D) CD spectra of CPMs at different pH conditions (solution pH adjusted manually). The figure is adapted from REF. (*244*), Wiley. Licensed under Creative Commons CC BY.

are tunable based on their sequence (*247*, *248*). To be compatible with the photoacid that typically modulates the pH to values below 6.0 (*245*, *249*), DNA triplexes with 40% T-A·T content were used, as they operated in the pH range between pH 5.5 and pH 7.0. The triplex DNA strands, incorporated into reconfigurable DNA origami templates consisting of two AuNRs (without a fixed angle between the rods), upon formation, locks the structure in a right-handed spatial configuration by design (at ≈50° fixed angle between the AuNRs). A representative TEM image of the CPM is shown in Figure 4.2 B, where the CPMs appear as pairs of AuNRs lying side by side due to the affinity of AuNRs to the TEM grid. The closed configuration of the triplex locks corresponding to the metastable state adopts an open relaxed state spontaneously when the irradiation is turned off (*168*, *248*). Figure 4.2 C illustrates the switching between the relaxed and RH states of the CPMs as the DNA triplex locks are formed. The CPMs exhibited a strong chiroptical response to the change in solution pH (Figure 4.2 D).

The CPMs were dispersed in a buffer-free aqueous solution of MCH^+ containing DMSO to increase MCH^+ solubility in water, NaCl for stable triplex formation, sodium bicarbonate to adjust the solution pH, and SDS to stabilize the CPM structures. The photo-responsive MCH^+-containing solution had a pH drop of ≈1.2 units from the initial ≈6.7 pH within 5 minutes of irradiation with blue light (emission wavelength of 415 nm). The

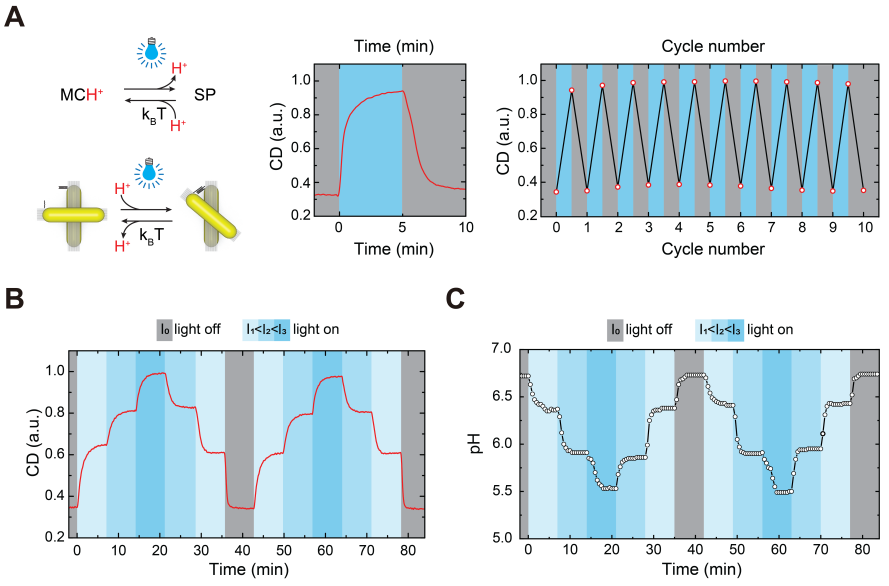

Figure 4.3. Light intensity-dependent controlled switching of photoresponsive medium and CPMs. (A) CD response of the CPM under subsequent light illumination and dark exposure; (B) Distinct steady states of the CD level of the CPMs depending on the intensity of incident light; (C) Modulation of pH of the photoresponsive medium based on the light intensity. The figure is adapted from REF. (*244*), Wiley. Licensed under Creative Commons CC BY.

pH returned to its initial value after ≈5 minutes in dark, as the released protons were recaptured. In response to the pH modulation induced by light, the CPMs in the photo-responsive medium expressed a change in chirality. The chiral response from the AuNRs (absorbance in the visible red region) was studied using a CD spectrometer fitted with a long pass filter that eliminates the possible interference of the blue light stimulus. A strong chiral response was observed from the closed, RH configuration of the CPMs upon irradiation with blue light. The switch between open and closed confirmations followed similar kinetics as pH modulation without severe lag, as the typical time constants for opening/closing of triplex locks and the DNA-origami-based CPMs are in the milliseconds (*248*) and seconds (*168*) range, respectively. The pH switching and the subsequent chirality modulation could be repeated for at least ten cycles. The change in the amplitude of CD response when the blue light was turned on and off validates the reversibility of the system without any signs of fatigue (Figure 4.3 A). Further, the amplitude of CD response was found to be dependent on the intensity of the incident light. The system reached a distinct steady state within ≈5 minutes under each light intensity studied (Figure 4.3 B). This dynamic control over the structural and optical properties of DNA-origami-based plasmonic assemblies partly relies on the ability of the photo-responsive medium to modulate pH to distinct states under different light intensities (Figure 4.3 C).

Our system required a certain threshold light intensity for adopting an out-of-equilibrium state. With continuous light illumination at the required threshold, the CPMs maintained the steady out-of-equilibrium state and quickly returned to equilibrium (relaxed) configuration only when the light was turned off. These results indicate that the structural and optical properties of the DNA-origami-based chiral plasmonic assemblies can be manipulated with a great degree of control. Our non-contact light-driven plasmonic assemblies can be integrated into microelectrical/optical devices, thereby promoting the application of DNA nanodevices.

4.3 DNA origami-based device to study DNA bending proteins (Publication III)

Publication III demonstrated a potential application for dynamic DNA origami structures. The reconfigurable DNA origami design from Publication II was modified to study DNA bending caused by DNA bending proteins. For the proof-of-concept of our approach, we utilized TBP, that upon binding to the TATA box sequence, causes the DNA to bend ≈90° (*250–252*). DNA bending by TBP is a key transcription initiation process, as it is required by all three eukaryotic RNA polymerases (*253*). The TATA box sequence was inserted in the middle of the dsDNA bridge that locks the origami bundles at an ≈80° angle. The bending caused by the bound TBP in the TATA box sequentially changes

the angle of the DNA origami structure (Figure 4.4 A). The angle change can be directly observed using TEM imaging. The histogram of relative frequencies of the angle between the origami bundles was calculated by manually measuring at least 200 origami structures. The histograms were binned at 5° intervals to effectively represent the fluctuations in the angle formed between the origami bundles since the origami has a wide distribution.

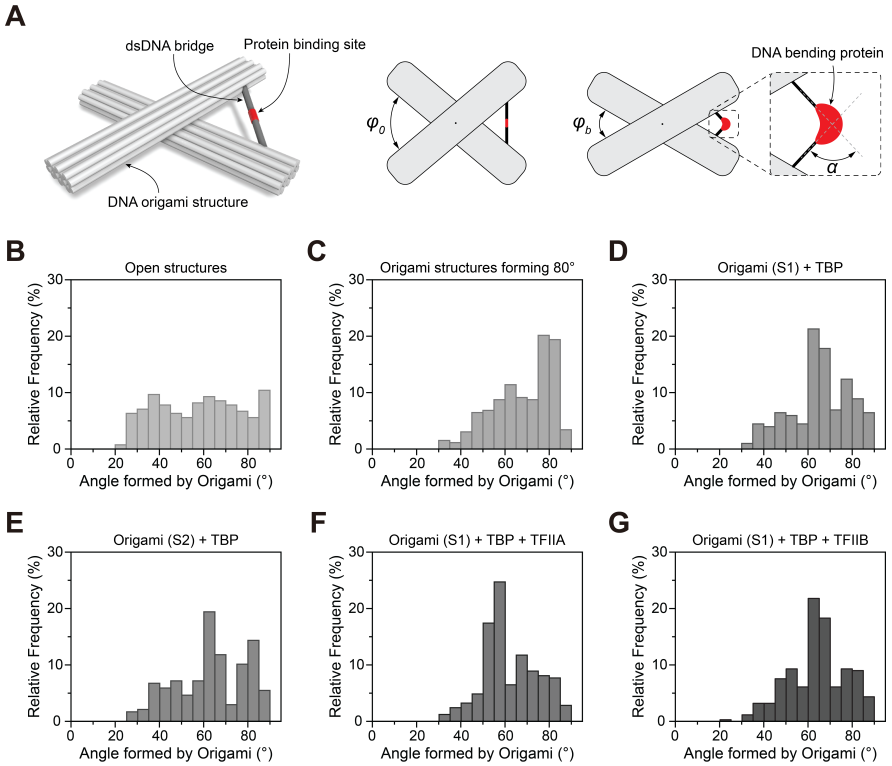

Figure 4.4. TBP-induced DNA bending of TATA box. (A) Schematic of TATA box bending by TBP and the subsequent angle change in DNA origami device; Relative frequency histograms of (B) Open structures; (C) Origami structures forming 80° angle between the two 14HBs; (D) Origami structures with S1 sequence in bridge incubated with 100 nM TBP; (E) Origami structures with S2 sequence in bridge incubated with 100 nM TBP; (F) Origami structures with S1 sequence in bridge incubated with 100 nM TBP and 100 nM TFIIA; (G) Origami structures with S1 sequence in bridge incubated with 100 nM TBP and 100 nM TFIIB. The figure is adapted from REF. (*254*), Royal Society of Chemistry. Licensed under Creative Commons CC BY.

While the open structures without the bridge had a broad distribution (Figure 4.4 B), the locked devices had an angle distribution peak at ≈80° (Figure 4.4 C). At first, the DNA origami bridge design and concentration were optimized to achieve the maximum yield of locked structures (≈40%). The optimized structures were used for evaluating the bending of the TATA box by TBP. The bending was evaluated in devices containing a) consensus TATA box sequence CTATAAAAG (S1) from AdMLP, b) mutated TATA box sequence

GTATAAAAC (S2) where the bases at the start and end of the consensus TATA box was inverted to its complement, and c) control scramble sequence (S3) to which TATA box does not bind. The devices containing the S1 sequence were incubated with increasing concentrations of TBP. The occurrence of structures with ≈65° angle increased as the concentration of TBP was increased from 25 nM to 100 nM (Figure 4.4 D). This corroborated well with the decrease in relative frequency at around 80°. The peak at φ=65° corresponds to α=83°, which was in good agreement with the bending angle of the consensus TATA box (S1) by TBP. The distribution of devices containing S2 was also similar to that of devices containing S1, implying that the base pairs before and after the TATA box sequence do not influence the bending angle (Figure 4.4 E). The devices with control sequence S3 exhibited a negligible change in relative frequency distribution as expected.

In addition to TBP, the transcription factors associated with TBP, in particular, TFIIA and TFIIB were studied for their role in bending. Although the crystal structures of TFIIA-TBP-DNA and TFIIB-TBP-DNA complexes have been available since 1990ties (*255*, *256*), biophysical studies to validate the influence of these transcription factors on TBP-DNA interaction have been sparse. Furthermore, the results of these biophysical studies were contradictory at times, especially in the case of TFIIA. TFIIA binding to the TBP-TATA box complex has been reported to stabilize the complex (*257*) without altering the structure (*256*). Furthermore, it has been reported that the stability of the TFIIA-TBP-DNA complex is sequence dependent (*258*). Another report, however, suggested in addition to the increase in kinetic stability in the TBP-DNA complex, TFIIA most likely also causes conformational changes to the DNA (*259*). In our experiments, we observed that in the devices containing the S1 sequence incubated with the equimolar concentrations of TBP and TFIIA, the angle distribution peak shifted from ≈65° to ≈55° (Figure 4.4 F). To verify this, we kept the TBP concentration constant at 50 nM, and the TFIIA concentration was varied from 0 to 100 nM. The distribution shifted from having an angle distribution maximum at ≈65° for 0 nM TFIIA to having a broad distribution at 25 nM TFIIA to having a peak at ≈55° for 50 nM TFIIA. Increasing the concentration of TFIIA further did not increase the amplitude of the peak, as TFIIA alone does not alter the bend angle. The results indicate that TFIIA alters the structure of the TBP-TATA box complex since an increase in stability would only influence the amplitude of the angle distribution peak and not the peak position.

TFIIB, on the other hand, has been reported to either help the formation of a fully bent state or decrease the bend angle upon binding to the TBP-DNA complex (*260–262*). TFIIB did not alter the distribution of either the TBP-TATA box complex (Figure 4.4 G) or TBP-TATA box-TFIIA complex when incubated with devices containing the consensus S1 sequence. The results imply that TFIIB does not cause any structural changes to the TBP-TATA box or TBP-TFIIA-TATA box complexes.

The toolbox translated the bending caused by TBP and transcription factors into observable change under TEM. By measuring the angle between the origami bundles, we were able to construct a histogram of relative frequencies that provided us with information on DNA bending by DNA bending proteins. We observed that TFIIA caused noticeable changes to the conformation of TBP-DNA complex, whereas TFIIB did not alter the structure of the complex. In addition, the base pairs before and after the TATA box sequence (S2 sequence) do not have a noticeable influence on TBP bending the TATA box. The approach can also be used to study DNA bending by other DNA bending proteins such as IHF (*Escherichia coli*), HU (*Bacillus stearothermophilus*), and TF1 (*Bacillus subtilis*) and can be further expanded to study DNA distortions such as looping and twisting with careful design considerations.

5. Conclusions and Outlook

Nucleic acids have become a viable bottom-up self-assembly system owing to their programmability and predictability. The field of nucleic acid nanotechnology has been burgeoning in recent years and enabled the creation of reconfigurable nanostructures with complex functionalities. In reality, the growth of nucleic acid nanotechnology is a result of assiduous and collaborative efforts from researchers in diverse fields. These efforts have not only lowered the entry barrier to the field with improvements in automated design and in-silico structure validation tools (oxDNA, caDNAno, magicDNA) (*75*, *240*, *263*) but also pushed the technological landscape of potential applications (plasmonics, molecular circuitry, nanorobotics, bioimaging, biophysics) (*50*, *194*, *219*). A tiny fraction of such efforts made toward the advancement of nucleic acid nanotechnology field is presented in this thesis.

Predominantly, the design and assembly of DNA-based nanostructures have been explored, leaving the pursuit of RNA origami a challenging but exciting opportunity. To address the scarcity of RNA design tools, Publication I presents a general high-level and fully automated design approach for the assembly of 3D RNA wireframe meshes implemented in the design tool *Sterna*. The generality of the design scheme was experimentally demonstrated with the assembly and visualization of three wireframe polyhedra structures, *i.e.,* a tetrahedron, a triangular bipyramid, and a triangular prism. In principle, the design approach has no limit on the size or complexity of the target meshes. However, in practice, the assembly of complex meshes can often be hindered by aggregation and/or poor folding yields. To mitigate the issues in folding complex meshes and improve their future yield, design choices such as different spanning trees for a given mesh, binding strength of kissing loop pairs, the rigidity of mesh vertices, and experimental choices such as step-wise annealing, different salt conditions, and strand conditions should be considered. Although the folding of the complex prism structure wasn't particularly astounding, the automated design pipeline presented here can catalyze further developments in RNA-based wireframe structures that can eventually make them as robust and functional as their DNA counterpart.

RNA-based nanostructures create a sanguine expectation for the future of

nucleic acid nanotechnology due to the versatility they bring via RNA motifs. Whereas in the present, the transformation of DNA nanotechnology from creating static objects to creating functional dynamic structures has introduced new inspirations and challenges. The ability to control the configuration in relation to external stimuli is particularly interesting as it can perform certain mechanical operations, such as rotational motion (*182*), or manipulation of optical and plasmonic responses (*166–168*). To this end, we fabricated chiral plasmonic metamolecules in Publication II that, through the formation of triplexes, reconfigure to produce a strong chiral response from the functionalized AuNRs on the origami template. The triplex formation occurs as a response to the change in pH and pushes the system to a steady out-of-equilibrium state. While the CPMs themselves are non-responsive to light, a photoresponsive medium, *i.e.,* MCH^+, dictates the pH range of the solution and in turn the chiral response through the intensity of incident light. Our approach offers a reversible, fatigue-free, and incident light intensity dependent pH-responsive switching of plasmonic optical properties that can be adapted to cascaded DNA circuitry, biosensing, DNA nanomachines, and smart nanomaterials with tailored functionalities.

Dynamic nanostructures can also be employed to study biological phenomena that occur at the nanoscale. Such devices have already been explored for performing force spectroscopy (*201*, *216*, *225*) and understanding DNA unwinding by helicase (*217*). Direct observation of molecular structural reconfiguration, especially concerning proteins that distort DNA could help gain an in-depth understanding of the function of these proteins. In this respect, we introduced a DNA device in publication III to study the amount of bending caused by DNA bending proteins directly by imaging under conventional and generally accessible TEM. We used TBP that bends the DNA ≈90° upon binding to evaluate our device. Additionally, transcription factors II A and II B were studied for their role in DNA bending using our device. The device offers insights into structural changes caused by TBP, as it provides directly observable TEM images, and can be expanded to other DNA-bending proteins. Our DNA origami-based device can also be expanded to study other DNA-distorting proteins with some design alterations, such as changing the symmetry of the structure. Furthermore, the data analysis can be semi-automated (*264*). However, the current design for the DNA origami-based device suffers from sub-optimal yield of structures with prescribed design angle and low resolution, *i.e.,* the amount of bending cannot be resolved to exact values. Recent advances in scaffold production (*83*, *84*) might improve the overall yield of devices with the desired angle between the bundles by engineering the TATA-box sequence into the scaffold strand and routing it to form the bridge. Further, the improved yield might result in a normal histogram distribution rather than a partial bimodal distribution. The low resolution, on the other hand, requires careful redesigning of the origami structure, for example, modifying the hinge-based structures from literature

(*216*, *264*) or functionalizing gold markers ≈5 nm in opposite ends of the origami bundles to improve the angle measurement during image processing. Our approach is more suitable as an initial screening procedure for optimizing experimental conditions, which might especially be useful for multi-component systems such as those involving DNA, proteins, and other co-factors. Furthermore, the device can help provide useful preliminary insight into DNA-protein interaction before proceeding to advanced structural biology techniques, such as cryo-EM.

In conclusion, this thesis presented how versatile nucleic acid nanostructures are, and how they could pave the way toward more exciting and interesting complex structures with tailored functionalities. The thesis consisting of three publications that present a general design pipeline for RNA wireframe structures (Publication I), a reconfigurable system, where the stimuli-responsive element was not directly incorporated into the origami system, but rather encoded into the photoswitchable medium (Publication II), and a potential application of DNA-origami-based device to study the molecular structural reconfiguration induced by DNA bending proteins (Publication III). This thesis illustrates that nucleic acid nanotechnology still has a large unexplored design space, novel switching mechanisms, and under-explored applications. In hindsight, this thesis was a culmination of different projects from design to reconfigurability to applications. Although the work presented in this thesis at times seemed disjoint, the individual conclusions from each section of the thesis highlight the advances made and showcase the limitations. On a general level, several design and experimental factors can be considered to improve the shortcomings and increase the utility of nucleic acid nanostructures.

In the long term, a real challenge would be to create completely predictable and almost defect-free structures that can perform complex functionalities, such as characterising minuscule molecular movements with higher precision, determining structures of mechanosensitive proteins under tension, emulating active sites of enzymes to catalyze reactions or help construct these sites with chemical functionalities, and delivering drugs in a targeted fashion or even altering cellular and inter-cellular mechanisms. One could only dare to imagine using precise nucleic acid structures to create artificial biomolecular machines that can transport external load autonomously on a molecular scale with functionalities such as sensing, processing signals, and catalyzing chemical reactions. While current nucleic acid nanostructures are still very far from achieving the intricacy and complexity of molecular machines that are found in Nature, it is certainly not that far from finding applications on an industrial scale, especially with start-ups blooming in fields such as data storage (DNA data storage alliance, `www.dnastoragealliance.org`), programmable antiviral agents (Capsitec, `www.capsitec.com`), biosensing (Palamedrix, now acquired by SomaLogic `www.somalogic.com`), diagnostic assays (Smartprobes, `www.smartprobes.de`), DNA sequencing and proteomics (Nanogami, `www.nanogami.bio`), cancer immunotherapy agents (Plectonic

Biotech www.plectonic.com), and gene therapy (Kano Therapeutics, www.kanotherapeutics.com). The extent to which nucleic acid nanotechnology will influence the way we fabricate nanostructures in the future might be obscure, but it has certainly laid the groundwork to build exciting and functional materials.

References

(*1*) Hoffmann, R. (1994). DNA as clay. *Am. Sci 82*, 308–311 (cit. on p. 27).

(*2*) Case, L. B., Baird, M. A., Shtengel, G., Campbell, S. L., Hess, H. F., Davidson, M. W., and Waterman, C. M. (2015). Molecular mechanism of vinculin activation and nanoscale spatial organization in focal adhesions. *Nature Cell Biology 17*, 880–892 (cit. on p. 27).

(*3*) Fabre, P. J., Benke, A., Joye, E., Nguyen Huynh, T. H., Manley, S., and Duboule, D. (2015). Nanoscale spatial organization of the HoxD gene cluster in distinct transcriptional states. *Proceedings of the National Academy of Sciences 112*, 13964–13969 (cit. on p. 27).

(*4*) Ariotti, N., Fernández-Rojo, M. A., Zhou, Y., Hill, M. M., Rodkey, T. L., Inder, K. L., Tanner, L. B., Wenk, M. R., Hancock, J. F., and Parton, R. G. (2014). Caveolae regulate the nanoscale organization of the plasma membrane to remotely control Ras signaling. *Journal of Cell Biology 204*, 777–792 (cit. on p. 27).

(*5*) Goswami, D., Gowrishankar, K., Bilgrami, S., Ghosh, S., Raghupathy, R., Chadda, R., Vishwakarma, R., Rao, M., and Mayor, S. (2008). Nanoclusters of GPI-Anchored Proteins Are Formed by Cortical Actin-Driven Activity. *Cell 135*, 1085–1097 (cit. on p. 27).

(*6*) Roco, M. C. (2007). National nanotechnology initiative-past, present, future. *Handbook on nanoscience, engineering and technology 2* (cit. on p. 27).

(*7*) Sattler, K. D., *Handbook of nanophysics: nanoparticles and quantum dots*; CRC press: 2016 (cit. on p. 27).

(*8*) Feynman, R. P. (1960). There's Plenty of Room at the Bottom. *Engineering and Science 23*, 22–36 (cit. on p. 27).

(*9*) Whitesides, G. M., and Grzybowski, B. (2002). Self-Assembly at All Scales. *Science 295*, 2418–2421 (cit. on p. 28).

(*10*) Seeman, N. C. (1982). Nucleic acid junctions and lattices. *Journal of Theoretical Biology 99*, 237–247 (cit. on pp. 28, 34, 35).

(*11*) Chen, J., and Seeman, N. C. (1991). Synthesis from DNA of a molecule with the connectivity of a cube. *Nature 350*, 631–633 (cit. on pp. 28, 35, 43).

(*12*) Winfree, E., Liu, F., Wenzler, L. A., and Seeman, N. C. (1998). Design and self-assembly of two-dimensional DNA crystals. *Nature 394*, 539–544 (cit. on pp. 28, 35, 36).

(*13*) Shih, W. M., Quispe, J. D., and Joyce, G. F. (2004). A 1.7-kilobase single-stranded DNA that folds into a nanoscale octahedron. *Nature 427*, 618 (cit. on pp. 28, 37, 43).

(*14*) Rothemund, P. W. K. (2006). Folding DNA to create nanoscale shapes and patterns. *Nature 440*, 297–302 (cit. on pp. 28, 37–39, 52).

(*15*) Douglas, S. M., Dietz, H., Liedl, T., Högberg, B., Graf, F., and Shih, W. M. (2009). Self-assembly of DNA into nanoscale three-dimensional shapes. *Nature 459*, 414–418 (cit. on pp. 28, 39, 40).

(*16*) Wang, P., Meyer, T. A., Pan, V., Dutta, P. K., and Ke, Y. (2017). The Beauty and Utility of DNA Origami. *Chem 2*, 359–382 (cit. on p. 28).

(*17*) Xu, X., and Chen, S.-J. (2020). Topological constraints of RNA pseudoknotted and loop-kissing motifs: applications to three-dimensional structure prediction. *Nucleic Acids Research 48*, 6503–6512 (cit. on pp. 29, 44).

(*18*) Guo, P., Zhang, C., Chen, C., Garver, K., and Trottier, M. (1998). Inter-RNA interaction of phage phi29 pRNA to form a hexameric complex for viral DNA transportation. *Molecular Cell 2*, 149–155 (cit. on pp. 29, 44).

(*19*) Geary, C. W., and Andersen, E. S. In *DNA Computing and Molecular Programming*, ed. by Murata, S., and Kobayashi, S., Springer International Publishing: Cham, 2014, pp 1–19 (cit. on pp. 29, 47).

(*20*) Geary, C., Rothemund, P. W. K., and Andersen, E. S. (2014). A single-stranded architecture for cotranscriptional folding of RNA nanostructures. *Science 345*, 799–804 (cit. on pp. 29, 47, 48).

(*21*) Li, M., Zheng, M., Wu, S., Tian, C., Liu, D., Weizmann, Y., Jiang, W., Wang, G., and Mao, C. (2018). In vivo production of RNA nanostructures via programmed folding of single-stranded RNAs. *Nature Communications 9*, 2196 (cit. on pp. 29, 48).

(*22*) Dahm, R. (2005). Friedrich Miescher and the discovery of DNA. *Developmental Biology 278*, 274–288 (cit. on p. 31).

(*23*) Miescher, F. (1869). Letter i; to wilhelm his; tübingen, february 26th, 1869. *Die histochemischen und physiologischen arbeiten von Friedrich Miescher-aus dem wissenschaftlichen Briefwechsel von F. Miescher 1*, 33–38 (cit. on p. 31).

(*24*) Miescher-Rüsch, F., *Ueber die chemische Zusammensetzung der Eiterzellen*, 1871 (cit. on p. 31).

(*25*) Piccard, J. (1874). Ueber Protamin, Guanin und Sarkin, als Bestandtheile des Lachssperma. *Berichte der deutschen chemischen Gesellschaft 7*, 1714–1719 (cit. on p. 31).

(*26*) Kossel, A. (1879). Ueber das Nucleïn der Hefe. (cit. on p. 31).

(*27*) Kossel, A. (1891). Ueber die chemische Zusammensetzung der Zelle. *Du Bois-Reymond's Archiv/Arch Anat Physiol Physiol Abt 278*, 181–186 (cit. on p. 31).

(*28*) Bergstretser, E. (1895). Nuclein. *The American journal of dental science 29*, 164–174 (cit. on p. 31).

(*29*) Levene, P. A. (1919). The Structure of Yeast Nucleic Acid : IV. Ammonia hydrolysis. *Journal of Biological Chemistry 40*, 415–424 (cit. on p. 31).

(*30*) Avery, O. T., Macleod, C. M., and McCarty, M. (1944). Studies on the chemical nature of the substance inducing transformation of Pneumococcal Types: Induction of transformation by a desoxyribonucleic acid fraction isolated from Pneumococcus type III. *The Journal of Experimental Medicine 79*, 137–158 (cit. on p. 32).

(*31*) Chargaff, E. (1950). Chemical specificity of nucleic acids and mechanism of their enzymatic degradation. *Experientia 6*, 201–209 (cit. on p. 32).

(*32*) Zamenhof, S., Brawerman, G., and Chargaff, E. (1952). On the desoxypentose nucleic acids from several microorganisms. *Biochimica et Biophysica Acta 9*, 402–405 (cit. on p. 32).

(*33*) Franklin, R. E., and Gosling, R. G. (1953). Molecular Configuration in Sodium Thymonucleate. *Nature 171*, 740–741 (cit. on p. 32).

(*34*) Wilkins, M. H. F., and Randall, J. T. (1953). Crystallinity in sperm heads: Molecular structure of nucleoprotein in vivo. *Biochimica et Biophysica Acta 10*, 192–193 (cit. on p. 32).

(*35*) Watson, J. D., and Crick, F. H. (1953). Molecular structure of nucleic acids; a structure for deoxyribose nucleic acid. *Nature 171*, 737–738 (cit. on p. 32).

(*36*) BIOVIA, Discovery Studio Visualizer, (2021), version 21.1.0.20298, San Diego: Dassault Systèmes (cit. on p. 33).

(*37*) Ball, M. P. (2022). DNA. *Wikipedia, https://en.wikipedia.org/wiki/DNA* (cit. on p. 33).

(*38*) Saenger, W., *Principles of Nucleic Acid Structure*, 1st ed.; Springer Advanced Texts in Chemistry; Springer New York, NY: 1984; XX, 556 (cit. on p. 33).

(*39*) Seeman, N. C. (2003). DNA in a material world. *Nature 421*, 427–431 (cit. on pp. 33, 34).

(*40*) Ramezani, H., and Dietz, H. (2020). Building machines with DNA molecules. *Nature Reviews Genetics 21*, 5–26 (cit. on pp. 33, 52).

(*41*) Robertus, J. D., Ladner, J. E., Finch, J. T., Rhodes, D., Brown, R. S., Clark, B. F., and Klug, A. (1974). Structure of yeast phenylalanine tRNA at 3 A resolution. *Nature 250*, 546–551 (cit. on p. 33).

(*42*) Masliah, G., Barraud, P., and Allain, F. H.-T. (2013). RNA recognition by double-stranded RNA binding domains: a matter of shape and sequence. *Cellular and molecular life sciences: CMLS 70*, 1875–1895 (cit. on p. 34).

(*43*) Kebbekus, P., Draper, D. E., and Hagerman, P. (1995). Persistence length of RNA. *Biochemistry 34*, 4354–4357 (cit. on p. 34).

(*44*) Petersheim, M., and Turner, D. H. (1983). Base-stacking and base-pairing contributions to helix stability: thermodynamics of double-helix formation with CCGG, CCGGp, CCGGAp, ACCGGp, CCGGUp, and ACCGGUp. *Biochemistry 22*, 256–263 (cit. on p. 34).

(*45*) Yakovchuk, P., Protozanova, E., and Frank-Kamenetskii, M. D. (2006). Base-stacking and base-pairing contributions into thermal stability of the DNA double helix. *Nucleic Acids Research 34*, 564–574 (cit. on p. 34).

(*46*) Marek, P. H., Szatylowicz, H., and Krygowski, T. M. (2019). Stacking of nucleic acid bases: optimization of the computational approach—the case of adenine dimers. *Structural Chemistry 30*, 351–359 (cit. on p. 34).

(*47*) Creeth, J. M., Gulland, J. M., and Jordan, D. O. (1947). Deoxypentose nucleic acids. Part III. Viscosity and streaming birefringence of solutions of the sodium salt of the deoxypentose nucleic acid of calf thymus. *Journal of the Chemical Society (Resumed)*, 1141–1145 (cit. on p. 34).

(*48*) Pauling, L., and Corey, R. B. (1956). Specific hydrogen-bond formation between pyrimidines and purines in deoxyribonucleic acids. *Archives of Biochemistry and Biophysics 65*, 164–181 (cit. on p. 34).

(*49*) Donohue, J. (1956). Hydrogen-bonded helical configurations of polynucleotides*. *Proceedings of the National Academy of Sciences 42*, 60–65 (cit. on p. 34).

(*50*) Seeman, N. C., and Sleiman, H. F. (2018). DNA nanotechnology. *Nature Reviews Materials 3*, 1–23 (cit. on pp. 35, 37, 50, 52, 71).

(*51*) McBride, L. J., and Caruthers, M. H. (1983). An investigation of several deoxynucleoside phosphoramidites useful for synthesizing deoxyoligonucleotides. *Tetrahedron Letters 24*, 245–248 (cit. on p. 35).

(*52*) Seeman, N. C., and Kallenbach, N. R. (1983). Design of immobile nucleic acid junctions. *Biophysical Journal 44*, 201–209 (cit. on p. 35).

(*53*) Kallenbach, N. R., Ma, R.-I., and Seeman, N. C. (1983). An immobile nucleic acid junction constructed from oligonucleotides. *Nature 305*, 829–831 (cit. on p. 35).

(*54*) Gopaul, D. N., Guo, F., and Van Duyne, G. D. (1998). Structure of the Holliday junction intermediate in Cre-loxP site-specific recombination. *The EMBO Journal 17*, 4175–4187 (cit. on p. 36).

(*55*) Eichman, B. F., Vargason, J. M., Mooers, B. H. M., and Ho, P. S. (2000). The Holliday junction in an inverted repeat DNA sequence: Sequence effects on the structure of four-way junctions. *Proceedings of the National Academy of Sciences 97*, 3971–3976 (cit. on p. 36).

(*56*) NanoEngineer-1, (2008). Version 1.1.1, 2008 (cit. on p. 36).

(*57*) Goddard, T. D., Huang, C. C., Meng, E. C., Pettersen, E. F., Couch, G. S., Morris, J. H., and Ferrin, T. E. (2018). UCSF ChimeraX: Meeting modern challenges in visualization and analysis. *Protein Science: A Publication of the Protein Society 27*, 14–25 (cit. on pp. 36, 46).

(*58*) Pettersen, E. F., Goddard, T. D., Huang, C. C., Meng, E. C., Couch, G. S., Croll, T. I., Morris, J. H., and Ferrin, T. E. (2021). UCSF ChimeraX: Structure visualization for researchers, educators, and developers. *Protein Science: A Publication of the Protein Society 30*, 70–82 (cit. on pp. 36, 46).

(*59*) Petrillo, M. L., Newton, C. J., Cunningham, R. P., Ma, R. I., Kallenbach, N. R., and Seeman, N. C. (1988). The ligation and flexibility of four-arm DNA junctions. *Biopolymers 27*, 1337–1352 (cit. on p. 35).

(*60*) Fu, T. J., and Seeman, N. C. (1993). DNA double-crossover molecules. *Biochemistry 32*, 3211–3220 (cit. on p. 35).

(*61*) Yan, H., Park, S. H., Finkelstein, G., Reif, J. H., and LaBean, T. H. (2003). DNA-Templated Self-Assembly of Protein Arrays and Highly Conductive Nanowires. *Science 301*, 1882–1884 (cit. on p. 37).

(*62*) He, Y., Chen, Y., Liu, H., Ribbe, A. E., and Mao, C. (2005). Self-Assembly of Hexagonal DNA Two-Dimensional (2D) Arrays. *Journal of the American Chemical Society 127*, 12202–12203 (cit. on p. 37).

(*63*) Zhang, C., Su, M., He, Y., Zhao, X., Fang, P.-a., Ribbe, A. E., Jiang, W., and Mao, C. (2008). Conformational flexibility facilitates self-assembly of complex DNA nanostructures. *Proceedings of the National Academy of Sciences 105*, 10665–10669 (cit. on pp. 37, 44).

(*64*) Ohayon, Y. P., Sha, R., Flint, O., Chandrasekaran, A. R., Abdallah, H. O., Wang, T., Wang, X., Zhang, X., and Seeman, N. C. (2015). Topological Linkage of DNA Tiles Bonded by Paranemic Cohesion. *ACS Nano 9*, 10296–10303 (cit. on p. 37).

(*65*) Liu, D., Park, S. H., Reif, J. H., and LaBean, T. H. (2004). DNA nanotubes self-assembled from triple-crossover tiles as templates for conductive nanowires. *Proceedings of the National Academy of Sciences 101*, 717–722 (cit. on p. 37).

(*66*) Rothemund, P. W. K., Papadakis, N., and Winfree, E. (2004). Algorithmic Self-Assembly of DNA Sierpinski Triangles. *PLoS Biology 2*, e424 (cit. on p. 37).

(*67*) Liu, D., Wang, M., Deng, Z., Walulu, R., and Mao, C. (2004). Tensegrity: Construction of Rigid DNA Triangles with Flexible Four-Arm DNA Junctions. *Journal of the American Chemical Society 126*, 2324–2325 (cit. on p. 37).

(*68*) Zheng, J., Birktoft, J. J., Chen, Y., Wang, T., Sha, R., Constantinou, P. E., Ginell, S. L., Mao, C., and Seeman, N. C. (2009). From molecular to macroscopic via the rational design of a self-assembled 3D DNA crystal. *Nature 461*, 74–77 (cit. on p. 37).

(*69*) Woods, D., Doty, D., Myhrvold, C., Hui, J., Zhou, F., Yin, P., and Winfree, E. (2019). Diverse and robust molecular algorithms using reprogrammable DNA self-assembly. *Nature 567*, 366 (cit. on p. 37).

(*70*) Dietz, H., Douglas, S. M., and Shih, W. M. (2009). Folding DNA into Twisted and Curved Nanoscale Shapes. *Science 325*, 725–730 (cit. on pp. 39, 40).

(*71*) Andersen, E. S., Dong, M., Nielsen, M. M., Jahn, K., Subramani, R., Mamdouh, W., Golas, M. M., Sander, B., Stark, H., Oliveira, C. L. P., Pedersen, J. S., Birkedal, V., Besenbacher, F., Gothelf, K. V., and Kjems, J. (2009). Self-assembly of a nanoscale DNA box with a controllable lid. *Nature 459*, 73–76 (cit. on p. 39).

(*72*) Ke, Y., Sharma, J., Liu, M., Jahn, K., Liu, Y., and Yan, H. (2009). Scaffolded DNA Origami of a DNA Tetrahedron Molecular Container. *Nano Letters 9*, 2445–2447 (cit. on p. 39).

(*73*) Kuzuya, A., and Komiyama, M. (2009). Design and construction of a box-shaped 3D-DNA origami. *Chemical Communications*, 4182–4184 (cit. on p. 39).

(*74*) Douglas, S. M., Chou, J. J., and Shih, W. M. (2007). DNA-nanotube-induced alignment of membrane proteins for NMR structure determination. *Proceedings of the National Academy of Sciences 104*, 6644–6648 (cit. on p. 39).

(*75*) Douglas, S. M., Marblestone, A. H., Teerapittayanon, S., Vazquez, A., Church, G. M., and Shih, W. M. (2009). Rapid prototyping of 3D DNA-origami shapes with caDNAno. *Nucleic Acids Research 37*, 5001–5006 (cit. on pp. 39, 71).

(*76*) Tikhomirov, G., Petersen, P., and Qian, L. (2017). Fractal assembly of micrometre-scale DNA origami arrays with arbitrary patterns. *Nature 552*, 67–71 (cit. on pp. 39, 41).

(*77*) Zhang, T., Hartl, C., Frank, K., Heuer-Jungemann, A., Fischer, S., Nickels, P. C., Nickel, B., and Liedl, T. (2018). 3D DNA Origami Crystals. *Advanced Materials 30*, 1800273 (cit. on pp. 40, 41).

(*78*) Wagenbauer, K. F., Sigl, C., and Dietz, H. (2017). Gigadalton-scale shape-programmable DNA assemblies. *Nature 552*, 78–83 (cit. on p. 41).

(*79*) Tikhomirov, G., Petersen, P., and Qian, L. (2017). Programmable disorder in random DNA tilings. *Nature Nanotechnology 12*, 251–259 (cit. on p. 39).

(*80*) Minev, D., Wintersinger, C. M., Ershova, A., and Shih, W. M. (2021). Robust nucleation control via crisscross polymerization of highly coordinated DNA slats. *Nature Communications 12*, 1741 (cit. on p. 42).

(*81*) Wintersinger, C. M., Minev, D., Ershova, A., Sasaki, H. M., Gowri, G., Berengut, J. F., Corea-Dilbert, F. E., Yin, P., and Shih, W. M. (2022). Multi-micron crisscross structures from combinatorially assembled DNA-origami slats. *bioRxiv* (cit. on p. 42).

(*82*) Kick, B., Praetorius, F., Dietz, H., and Weuster-Botz, D. (2015). Efficient Production of Single-Stranded Phage DNA as Scaffolds for DNA Origami. *Nano Letters 15*, 4672–4676 (cit. on p. 42).

(*83*) Nafisi, P. M., Aksel, T., and Douglas, S. M. (2018). Construction of a novel phagemid to produce custom DNA origami scaffolds. *Synthetic Biology 3*, ysy015 (cit. on pp. 42, 72).

(*84*) Engelhardt, F. A. S., Praetorius, F., Wachauf, C. H., Brüggenthies, G., Kohler, F., Kick, B., Kadletz, K. L., Pham, P. N., Behler, K. L., Gerling, T., and Dietz, H. (2019). Custom-Size, Functional, and Durable DNA Origami with Design-Specific Scaffolds. *ACS Nano 13*, 5015–5027 (cit. on pp. 42, 72).

(*85*) Reese, C. B. (2005). Oligo- and poly-nucleotides: 50 years of chemical synthesis. *Organic & Biomolecular Chemistry 3*, 3851–3868 (cit. on p. 42).

(*86*) Ducani, C., Kaul, C., Moche, M., Shih, W. M., and Högberg, B. (2013). Enzymatic production of 'monoclonal stoichiometric' single-stranded DNA oligonucleotides. *Nature Methods 10*, 647–652 (cit. on p. 42).

(*87*) Praetorius, F., Kick, B., Behler, K. L., Honemann, M. N., Weuster-Botz, D., and Dietz, H. (2017). Biotechnological mass production of DNA origami. *Nature 552*, 84–87 (cit. on p. 42).

(*88*) Perrault, S. D., and Shih, W. M. (2014). Virus-Inspired Membrane Encapsulation of DNA Nanostructures To Achieve In Vivo Stability. *ACS Nano 8*, 5132–5140 (cit. on p. 42).

(*89*) Chopra, A., Krishnan, S., and Simmel, F. C. (2016). Electrotransfection of Polyamine Folded DNA Origami Structures. *Nano Letters 16*, 6683–6690 (cit. on p. 42).

(*90*) Ponnuswamy, N., Bastings, M. M. C., Nathwani, B., Ryu, J. H., Chou, L. Y. T., Vinther, M., Li, W. A., Anastassacos, F. M., Mooney, D. J., and Shih, W. M. (2017). Oligolysine-based coating protects DNA nanostructures from low-salt denaturation and nuclease degradation. *Nature Communications 8*, 15654 (cit. on p. 42).

(*91*) Agarwal, N. P., Matthies, M., Gür, F. N., Osada, K., and Schmidt, T. L. (2017). Block Copolymer Micellization as a Protection Strategy for DNA Origami. *Angewandte Chemie International Edition 56*, 5460–5464 (cit. on p. 42).

(*92*) Nguyen, M.-K., Nguyen, V. H., Natarajan, A. K., Huang, Y., Ryssy, J., Shen, B., and Kuzyk, A. (2020). Ultrathin Silica Coating of DNA Origami Nanostructures. *Chemistry of Materials 32*, 6657–6665 (cit. on p. 42).

(*93*) Martin, T. G., and Dietz, H. (2012). Magnesium-free self-assembly of multi-layer DNA objects. *Nature Communications 3*, 1103 (cit. on p. 42).

(*94*) Kielar, C., Xin, Y., Shen, B., Kostiainen, M. A., Grundmeier, G., Linko, V., and Keller, A. (2018). On the Stability of DNA Origami Nanostructures in Low-Magnesium Buffers. *Angewandte Chemie International Edition 57*, 9470–9474 (cit. on p. 42).

(*95*) Zhang, Y., and Seeman, N. C. (1994). Construction of a DNA-Truncated Octahedron. *Journal of the American Chemical Society 116*, 1661–1669 (cit. on p. 43).

(*96*) Goodman, R. P., Berry, R. M., and Turberfield, A. J. (2004). The single-step synthesis of a DNA tetrahedron. *Chemical Communications (Cambridge, England)*, 1372–1373 (cit. on p. 43).

(*97*) Goodman, R. P., Schaap, I. a. T., Tardin, C. F., Erben, C. M., Berry, R. M., Schmidt, C. F., and Turberfield, A. J. (2005). Rapid Chiral Assembly of Rigid DNA Building Blocks for Molecular Nanofabrication. *Science 310*, 1661–1665 (cit. on pp. 43, 47).

(*98*) Orponen, P. (2018). Design methods for 3D wireframe DNA nanostructures. *Natural Computing 17*, 147–160 (cit. on p. 43).

(*99*) Han, D., Pal, S., Yang, Y., Jiang, S., Nangreave, J., Liu, Y., and Yan, H. (2013). DNA gridiron nanostructures based on four-arm junctions. *Science (New York, N.Y.) 339*, 1412–1415 (cit. on pp. 43, 45).

(*100*) Benson, E., Mohammed, A., Gardell, J., Masich, S., Czeizler, E., Orponen, P., and Högberg, B. (2015). DNA rendering of polyhedral meshes at the nanoscale. *Nature 523*, 441–444 (cit. on pp. 43, 45).

(*101*) Veneziano, R., Ratanalert, S., Zhang, K., Zhang, F., Yan, H., Chiu, W., and Bathe, M. (2016). Designer nanoscale DNA assemblies programmed from the top down. *Science* (cit. on pp. 43, 45).

(*102*) Zhang, F., Jiang, S., Wu, S., Li, Y., Mao, C., Liu, Y., and Yan, H. (2015). Complex wireframe DNA origami nanostructures with multi-arm junction vertices. *Nature Nanotechnology 10*, 779–784 (cit. on p. 43).

(*103*) Jun, H., Zhang, F., Shepherd, T., Ratanalert, S., Qi, X., Yan, H., and Bathe, M. (2019). Autonomously designed free-form 2D DNA origami. *Science Advances 5*, eaav0655 (cit. on p. 44).

(*104*) Matthies, M., Agarwal, N. P., and Schmidt, T. L. (2016). Design and Synthesis of Triangulated DNA Origami Trusses. *Nano Letters 16*, 2108–2113 (cit. on p. 44).

(*105*) Sa-Ardyen, P., Vologodskii, A. V., and Seeman, N. C. (2003). The Flexibility of DNA Double Crossover Molecules. *Biophysical Journal 84*, 3829–3837 (cit. on p. 44).

(*106*) Wang, T., Schiffels, D., Martinez Cuesta, S., Kuchnir Fygenson, D., and Seeman, N. C. (2012). Design and Characterization of 1D Nanotubes and 2D Periodic Arrays Self-Assembled from DNA Multi-Helix Bundles. *Journal of the American Chemical Society 134*, 1606–1616 (cit. on p. 44).

(*107*) Jun, H., Wang, X., Bricker, W. P., and Bathe, M. (2019). Automated sequence design of 2D wireframe DNA origami with honeycomb edges. *Nature Communications 10*, 5419 (cit. on p. 44).

(*108*) Wang, X., Li, S., Jun, H., John, T., Zhang, K., Fowler, H., Doye, J. P., Chiu, W., and Bathe, M. (2022). Planar 2D wireframe DNA origami. *Science Advances 8*, eabn0039 (cit. on p. 44).

(*109*) Jun, H., Shepherd, T. R., Zhang, K., Bricker, W. P., Li, S., Chiu, W., and Bathe, M. (2019). Automated Sequence Design of 3D Polyhedral Wireframe DNA Origami with Honeycomb Edges. *ACS Nano 13*, 2083–2093 (cit. on p. 44).

(*110*) Jun, H., Wang, X., Parsons, M. F., Bricker, W. P., John, T., Li, S., Jackson, S., Chiu, W., and Bathe, M. (2021). Rapid prototyping of arbitrary 2D and 3D wireframe DNA origami. *Nucleic Acids Research 49*, 10265–10274 (cit. on p. 44).

(*111*) de Llano, E., Miao, H., Ahmadi, Y., Wilson, A. J., Beeby, M., Viola, I., and Barisic, I. (2020). Adenita: interactive 3D modelling and visualization of DNA nanostructures. *Nucleic Acids Research 48*, 8269–8275 (cit. on p. 44).

(*112*) Shi, J., and Bergstrom, D. E. (1997). Assembly of Novel DNA Cycles with Rigid Tetrahedral Linkers. *Angewandte Chemie International Edition in English 36*, 111–113 (cit. on p. 44).

(*113*) Shchepinov, M. S., Mir, K. U., Elder, J. K., Frank-Kamenetskii, M. D., and Southern, E. M. (1999). Oligonucleotide dendrimers: stable nanostructures. *Nucleic Acids Research 27*, 3035–3041 (cit. on p. 44).

(*114*) Wang, W., Wan, W., Zhou, H.-H., Niu, S., and Li, A. D. Q. (2003). Alternating DNA and π-Conjugated Sequences. Thermophilic Foldable Polymers. *Journal of the American Chemical Society 125*, 5248–5249 (cit. on p. 44).

(*115*) Yang, H., McLaughlin, C. K., Aldaye, F. A., Hamblin, G. D., Rys, A. Z., Rouiller, I., and Sleiman, H. F. (2009). Metal–nucleic acid cages. *Nature Chemistry 1*, 390–396 (cit. on p. 44).

(*116*) Chien, M.-P., Rush, A. M., Thompson, M. P., and Gianneschi, N. C. (2010). Programmable Shape-Shifting Micelles. *Angewandte Chemie International Edition 49*, 5076–5080 (cit. on p. 44).

(*117*) Edwardson, T. G. W., Carneiro, K. M. M., McLaughlin, C. K., Serpell, C. J., and Sleiman, H. F. (2013). Site-specific positioning of dendritic alkyl chains on DNA cages enables their geometry-dependent self-assembly. *Nature Chemistry 5*, 868–875 (cit. on p. 44).

(*118*) Dong, Y., Yang, Y. R., Zhang, Y., Wang, D., Wei, X., Banerjee, S., Liu, Y., Yang, Z., Yan, H., and Liu, D. (2017). Cuboid Vesicles Formed by Frame-Guided Assembly on DNA Origami Scaffolds. *Angewandte Chemie International Edition 56*, 1586–1589 (cit. on p. 44).

(*119*) Ke, Y., Ong, L. L., Shih, W. M., and Yin, P. (2012). Three-Dimensional Structures Self-Assembled from DNA Bricks. *Science 338*, 1177–1183 (cit. on p. 44).

(*120*) Ong, L. L. et al. (2017). Programmable self-assembly of three-dimensional nanostructures from 10,000 unique components. *Nature 552*, 72–77 (cit. on p. 44).

(*121*) Li, Z., Wei, B., Nangreave, J., Lin, C., Liu, Y., Mi, Y., and Yan, H. (2009). A Replicable Tetrahedral Nanostructure Self-Assembled from a Single DNA Strand. *Journal of the American Chemical Society 131*, 13093–13098 (cit. on pp. 44, 47).

(*122*) Han, D., Qi, X., Myhrvold, C., Wang, B., Dai, M., Jiang, S., Bates, M., Liu, Y., An, B., Zhang, F., Yan, H., and Yin, P. (2017). Single-stranded DNA and RNA origami. *Science 358*, eaao2648 (cit. on pp. 44, 47, 48).

(*123*) He, Y., Ye, T., Su, M., Zhang, C., Ribbe, A. E., Jiang, W., and Mao, C. (2008). Hierarchical self-assembly of DNA into symmetric supramolecular polyhedra. *Nature 452*, 198–201 (cit. on p. 44).

(*124*) Wang, W., Chen, S., An, B., Huang, K., Bai, T., Xu, M., Bellot, G., Ke, Y., Xiang, Y., and Wei, B. (2019). Complex wireframe DNA nanostructures from simple building blocks. *Nature Communications 10*, 1067 (cit. on p. 44).

(*125*) Huang, K., Yang, D., Tan, Z., Chen, S., Xiang, Y., Mi, Y., Mao, C., and Wei, B. (2019). Self-Assembly of Wireframe DNA Nanostructures from Junction Motifs. *Angewandte Chemie International Edition 58*, 12123–12127 (cit. on p. 44).

(*126*) Praetorius, F., and Dietz, H. (2017). Self-assembly of genetically encoded DNA-protein hybrid nanoscale shapes. *Science 355*, eaam5488 (cit. on p. 44).

(*127*) Guo, P. (2010). The emerging field of RNA nanotechnology. *Nature Nanotechnology 5*, 833–842 (cit. on p. 44).

(*128*) Leontis, N. B., and Westhof, E. (2014). Self-assembled RNA nanostructures. *Science 345*, 732–733 (cit. on p. 44).

(*129*) Afonin, K. A., Lindsay, B., and Shapiro, B. A. (2015). Engineered RNA Nanodesigns for Applications in RNA Nanotechnology. *DNA and RNA nanotechnology 1*, 1–15 (cit. on p. 44).

(*130*) Jasinski, D., Haque, F., Binzel, D. W., and Guo, P. (2017). Advancement of the Emerging Field of RNA Nanotechnology. *ACS nano 11*, 1142–1164 (cit. on pp. 44, 64).

(*131*) Ohno, H., Akamine, S., and Saito, H. (2019). RNA nanostructures and scaffolds for biotechnology applications. *Current Opinion in Biotechnology 58*, 53–61 (cit. on pp. 44, 64).

(*132*) Chang, K. Y., and Tinoco, I. (1994). Characterization of a "kissing" hairpin complex derived from the human immunodeficiency virus genome. *Proceedings of the National Academy of Sciences of the United States of America 91*, 8705–8709 (cit. on p. 44).

(*133*) Bindewald, E., Hayes, R., Yingling, Y. G., Kasprzak, W., and Shapiro, B. A. (2008). RNAJunction: a database of RNA junctions and kissing loops for three-dimensional structural analysis and nanodesign. *Nucleic Acids Research 36*, D392–397 (cit. on p. 44).

(*134*) Leontis, N. B., and Westhof, E. (2001). Geometric nomenclature and classification of RNA base pairs. *RNA (New York, N.Y.) 7*, 499–512 (cit. on p. 44).

(*135*) Lemieux, S., and Major, F. (2002). RNA canonical and non-canonical base pairing types: a recognition method and complete repertoire. *Nucleic Acids Research 30*, 4250–4263 (cit. on p. 44).

(*136*) Leontis, N. B., Stombaugh, J., and Westhof, E. (2002). The non-Watson-Crick base pairs and their associated isostericity matrices. *Nucleic Acids Research 30*, 3497–3531 (cit. on p. 44).

(*137*) Leontis, N. B., and Westhof, E. (2003). Analysis of RNA motifs. *Current Opinion in Structural Biology 13*, 300–308 (cit. on p. 44).

(*138*) Leontis, N. B., Lescoute, A., and Westhof, E. (2006). The building blocks and motifs of RNA architecture. *Current Opinion in Structural Biology 16*, 279–287 (cit. on p. 44).

(*139*) Searle, M. S., and Williams, D. H. (1993). On the stability of nucleic acid structures in solution: enthalpy-entropy compensations, internal rotations and reversibility. *Nucleic Acids Research 21*, 2051–2056 (cit. on p. 45).

(*140*) Sugimoto, N., Nakano, S., Katoh, M., Matsumura, A., Nakamuta, H., Ohmichi, T., Yoneyama, M., and Sasaki, M. (1995). Thermodynamic parameters to predict stability of RNA/DNA hybrid duplexes. *Biochemistry 34*, 11211–11216 (cit. on p. 45).

(*141*) Ennifar, E., Walter, P., Ehresmann, B., Ehresmann, C., and Dumas, P. (2001). Crystal structures of coaxially stacked kissing complexes of the HIV-1 RNA dimerization initiation site. *Nature Structural Biology 8*, 1064–1068 (cit. on p. 46).

(*142*) Okada, K., Takahashi, M., Sakamoto, T., Kawai, G., Nakamura, K., and Kanai, A. (2006). Solution Structure of a GAAG Tetraloop in Helix 6 of SRP RNA from Pyrococcus furiosus. *Nucleosides, Nucleotides & Nucleic Acids 25*, 383–395 (cit. on p. 46).

(*143*) Kim, N.-K., Zhang, Q., Zhou, J., Theimer, C. A., Peterson, R. D., and Feigon, J. (2008). Solution Structure and Dynamics of the Wild-type Pseudoknot of Human Telomerase RNA. *Journal of Molecular Biology 384*, 1249–1261 (cit. on p. 46).

(*144*) Kuglstatter, A., Oubridge, C., and Nagai, K. (2002). Induced structural changes of 7SL RNA during the assembly of human signal recognition particle. *Nature Structural Biology 9*, 740–744 (cit. on p. 46).

(*145*) Rupert, P. B., and Ferré-D'Amaré, A. R. (2001). Crystal structure of a hairpin ribozyme–inhibitor complex with implications for catalysis. *Nature 410*, 780–786 (cit. on p. 46).

(*146*) Collie, G. W., Haider, S. M., Neidle, S., and Parkinson, G. N. (2010). A crystallographic and modelling study of a human telomeric RNA (TERRA) quadruplex. *Nucleic Acids Research 38*, 5569–5580 (cit. on p. 46).

(*147*) Jaeger, L., and Chworos, A. (2006). The architectonics of programmable RNA and DNA nanostructures. *Current Opinion in Structural Biology 16*, 531–543 (cit. on p. 47).

(*148*) Grabow, W. W., and Jaeger, L. (2014). RNA Self-Assembly and RNA Nanotechnology. *Accounts of Chemical Research 47*, 1871–1880 (cit. on p. 47).

(*149*) Geary, C., Chworos, A., Verzemnieks, E., Voss, N. R., and Jaeger, L. (2017). Composing RNA Nanostructures from a Syntax of RNA Structural Modules. *Nano Letters 17*, 7095–7101 (cit. on p. 47).

(*150*) Afonin, K. A., Bindewald, E., Yaghoubian, A. J., Voss, N., Jacovetty, E., Shapiro, B. A., and Jaeger, L. (2010). In vitro assembly of cubic RNA-based scaffolds designed in silico. *Nature Nanotechnology 5*, 676–682 (cit. on p. 47).

(*151*) Afonin, K. A., Kasprzak, W., Bindewald, E., Puppala, P. S., Diehl, A. R., Hall, K. T., Kim, T. J., Zimmermann, M. T., Jernigan, R. L., Jaeger, L., and Shapiro, B. A. (2014). Computational and experimental characterization of RNA cubic nanoscaffolds. *Methods 67*, 256–265 (cit. on p. 47).

(*152*) Bui, M. N., Brittany Johnson, M., Viard, M., Satterwhite, E., Martins, A. N., Li, Z., Marriott, I., Afonin, K. A., and Khisamutdinov, E. F. (2017). Versatile RNA tetra-U helix linking motif as a toolkit for nucleic acid nanotechnology. *Nanomedicine: Nanotechnology, Biology and Medicine 13*, 1137–1146 (cit. on p. 47).

(*153*) Høiberg, H. C., Sparvath, S. M., Andersen, V. L., Kjems, J., and Andersen, E. S. (2019). An RNA Origami Octahedron with Intrinsic siRNAs for Potent Gene Knockdown. *Biotechnology Journal 14*, 1700634 (cit. on p. 47).

(*154*) Stewart, J. M., Subramanian, H. K. K., and Franco, E. (2017). Self-assembly of multi-stranded RNA motifs into lattices and tubular structures. *Nucleic Acids Research 45*, 5449–5457 (cit. on p. 47).

(*155*) Yu, J., Liu, Z., Jiang, W., Wang, G., and Mao, C. (2015). De novo design of an RNA tile that self-assembles into a homo-octameric nanoprism. *Nature Communications 6*, 5724 (cit. on p. 47).

(*156*) Endo, M., Takeuchi, Y., Emura, T., Hidaka, K., and Sugiyama, H. (2014). Preparation of Chemically Modified RNA Origami Nanostructures. *Chemistry – A European Journal 20*, 15330–15333 (cit. on p. 47).

(*157*) Lin, C., Xie, M., Chen, J. J. L., Liu, Y., and Yan, H. (2006). Rolling-Circle Amplification of a DNA Nanojunction. *Angewandte Chemie International Edition 45*, 7537–7539 (cit. on p. 47).

(*158*) Lin, C., Wang, X., Liu, Y., Seeman, N. C., and Yan, H. (2007). Rolling Circle Enzymatic Replication of a Complex Multi-Crossover DNA Nanostructure. *Journal of the American Chemical Society 129*, 14475–14481 (cit. on p. 47).

(*159*) Liu, D., Geary, C. W., Chen, G., Shao, Y., Li, M., Mao, C., Andersen, E. S., Piccirilli, J. A., Rothemund, P. W. K., and Weizmann, Y. (2020). Branched kissing loops for the construction of diverse RNA homooligomeric nanostructures. *Nature Chemistry 12*, 249–259 (cit. on p. 47).

(*160*) Geary, C., Grossi, G., McRae, E. K. S., Rothemund, P. W. K., and Andersen, E. S. (2021). RNA origami design tools enable cotranscriptional folding of kilobase-sized nanoscaffolds. *Nature Chemistry*, 1–10 (cit. on pp. 47, 48).

(*161*) Bindewald, E., Grunewald, C., Boyle, B., O'Connor, M., and Shapiro, B. A. (2008). Computational strategies for the automated design of RNA nanoscale structures from building blocks using NanoTiler. *Journal of Molecular Graphics & Modelling 27*, 299–308 (cit. on p. 48).

(*162*) Jossinet, F., Ludwig, T. E., and Westhof, E. (2010). Assemble: an interactive graphical tool to analyze and build RNA architectures at the 2D and 3D levels. *Bioinformatics 26*, 2057–2059 (cit. on p. 48).

(*163*) Yesselman, J. D., Eiler, D., Carlson, E. D., Gotrik, M. R., d'Aquino, A. E., Ooms, A. N., Kladwang, W., Carlson, P. D., Shi, X., Costantino, D. A., Herschlag, D., Lucks, J. B., Jewett, M. C., Kieft, J. S., and Das, R. (2019). Computational design of three-dimensional RNA structure and function. *Nature Nanotechnology 14*, 866–873 (cit. on p. 48).

(*164*) Yurke, B., Turberfield, A. J., Mills, A. P., Simmel, F. C., and Neumann, J. L. (2000). A DNA-fuelled molecular machine made of DNA. *Nature 406*, 605–608 (cit. on pp. 49, 50).

(*165*) Liu, M., Fu, J., Hejesen, C., Yang, Y., Woodbury, N. W., Gothelf, K., Liu, Y., and Yan, H. (2013). A DNA tweezer-actuated enzyme nanoreactor. *Nature Communications 4*, 2127 (cit. on p. 49).

(*166*) Kuzyk, A., Schreiber, R., Zhang, H., Govorov, A. O., Liedl, T., and Liu, N. (2014). Reconfigurable 3D plasmonic metamolecules. *Nature Materials 13*, 862–866 (cit. on pp. 49–51, 57, 58, 72).

(*167*) Kuzyk, A., Yang, Y., Duan, X., Stoll, S., Govorov, A. O., Sugiyama, H., Endo, M., and Liu, N. (2016). A light-driven three-dimensional plasmonic nanosystem that translates molecular motion into reversible chiroptical function. *Nature Communications 7*, 10591 (cit. on pp. 49–51, 58, 59, 72).

(*168*) Kuzyk, A., Urban, M. J., Idili, A., Ricci, F., and Liu, N. (2017). Selective control of reconfigurable chiral plasmonic metamolecules. *Science Advances 3*, e1602803 (cit. on pp. 49, 50, 58, 65–67, 72).

(*169*) Zhan, P., Dutta, P. K., Wang, P., Song, G., Dai, M., Zhao, S.-X., Wang, Z.-G., Yin, P., Zhang, W., Ding, B., and Ke, Y. (2017). Reconfigurable Three-Dimensional Gold Nanorod Plasmonic Nanostructures Organized on DNA Origami Tripod. *ACS Nano 11*, 1172–1179 (cit. on p. 49).

(*170*) Kuzyk, A., Schreiber, R., Fan, Z., Pardatscher, G., Roller, E.-M., Högele, A., Simmel, F. C., Govorov, A. O., and Liedl, T. (2012). DNA-based self-assembly of chiral plasmonic nanostructures with tailored optical response. *Nature 483*, 311–314 (cit. on p. 49).

(*171*) Zhou, C., Duan, X., and Liu, N. (2017). DNA-Nanotechnology-Enabled Chiral Plasmonics: From Static to Dynamic. *Accounts of Chemical Research 50*, 2906–2914 (cit. on pp. 49, 50).

(*172*) Kuzyk, A., Jungmann, R., Acuna, G. P., and Liu, N. (2018). DNA Origami Route for Nanophotonics. *ACS Photonics 5*, 1151–1163 (cit. on p. 49).

(*173*) Nguyen, M.-K., and Kuzyk, A. (2019). Reconfigurable Chiral Plasmonics beyond Single Chiral Centers. *ACS Nano 13*, 13615–13619 (cit. on p. 49).

(*174*) Liu, N., and Liedl, T. (2018). DNA-Assembled Advanced Plasmonic Architectures. *Chemical Reviews 118*, 3032–3053 (cit. on p. 50).

(*175*) Huang, Y., Nguyen, M.-K., Natarajan, A. K., Nguyen, V. H., and Kuzyk, A. (2018). A DNA Origami-Based Chiral Plasmonic Sensing Device. *ACS Applied Materials & Interfaces* (cit. on pp. 50, 52, 59).

(*176*) Zhang, Y., Pan, V., Li, X., Yang, X., Li, H., Wang, P., and Ke, Y. (2019). Dynamic DNA Structures. *Small 15*, 1900228 (cit. on p. 50).

(*177*) Pitikultham, P., Wang, Z., Wang, Y., Shang, Y., Jiang, Q., and Ding, B. (2022). Stimuli-Responsive DNA Origami Nanodevices and Their Biological Applications. *ChemMedChem 17*, e202100635 (cit. on p. 50).

(*178*) Zhang, D. Y., and Seelig, G. (2011). Dynamic DNA nanotechnology using strand-displacement reactions. *Nature Chemistry 3*, 103–113 (cit. on p. 50).

(*179*) Simmel, F. C., Yurke, B., and Singh, H. R. (2019). Principles and Applications of Nucleic Acid Strand Displacement Reactions. *Chemical Reviews 119*, 6326–6369 (cit. on p. 50).

(*180*) Hong, F., and Šulc, P. (2019). An emergent understanding of strand displacement in RNA biology. *Journal of Structural Biology 207*, 241–249 (cit. on p. 50).

(*181*) Gerling, T., Wagenbauer, K. F., Neuner, A. M., and Dietz, H. (2015). Dynamic DNA devices and assemblies formed by shape-complementary, non–base pairing 3D components. *Science 347*, 1446–1452 (cit. on p. 50).

(*182*) Kopperger, E., List, J., Madhira, S., Rothfischer, F., Lamb, D. C., and Simmel, F. C. (2018). A self-assembled nanoscale robotic arm controlled by electric fields. *Science 359*, 296–301 (cit. on pp. 50, 72).

(*183*) Kroener, F., Heerwig, A., Kaiser, W., Mertig, M., and Rant, U. (2017). Electrical Actuation of a DNA Origami Nanolever on an Electrode. *Journal of the American Chemical Society 139*, 16510–16513 (cit. on p. 50).

(*184*) Kroener, F., Traxler, L., Heerwig, A., Rant, U., and Mertig, M. (2019). Magnesium-Dependent Electrical Actuation and Stability of DNA Origami Rods. *ACS Applied Materials & Interfaces 11*, 2295–2301 (cit. on p. 50).

(*185*) Pumm, A.-K., Engelen, W., Kopperger, E., Isensee, J., Vogt, M., Kozina, V., Kube, M., Honemann, M. N., Bertosin, E., Langecker, M., Golestanian, R., Simmel, F. C., and Dietz, H. (2022). A DNA origami rotary ratchet motor. *Nature 607*, 492–498 (cit. on p. 50).

(*186*) Sannohe, Y., Endo, M., Katsuda, Y., Hidaka, K., and Sugiyama, H. (2010). Visualization of Dynamic Conformational Switching of the G-Quadruplex in a DNA Nanostructure. *Journal of the American Chemical Society 132*, 16311–16313 (cit. on p. 50).

(*187*) Willner, E. M., Kamada, Y., Suzuki, Y., Emura, T., Hidaka, K., Dietz, H., Sugiyama, H., and Endo, M. (2017). Single-Molecule Observation of the Photoregulated Conformational Dynamics of DNA Origami Nanoscissors. *Angewandte Chemie International Edition 56*, 15324–15328 (cit. on p. 51).

(*188*) Liu, Q., Kuzyk, A., Endo, M., and Smalyukh, I. I. (2019). Colloidal plasmonic DNA-origami with photo-switchable chirality in liquid crystals. *Optics Letters 44*, 2831–2834 (cit. on p. 51).

(*189*) Asanuma, H., Liang, X., Nishioka, H., Matsunaga, D., Liu, M., and Komiyama, M. (2007). Synthesis of azobenzene-tethered DNA for reversible photo-regulation of DNA functions: hybridization and transcription. *Nature Protocols 2*, 203–212 (cit. on p. 52).

(*190*) Liang, X., Mochizuki, T., and Asanuma, H. (2009). A Supra-photoswitch Involving Sandwiched DNA Base Pairs and Azobenzenes for Light-Driven Nanostructures and Nanodevices. *Small 5*, 1761–1768 (cit. on p. 52).

(*191*) Kundu, P. K., Samanta, D., Leizrowice, R., Margulis, B., Zhao, H., Börner, M., Udayabhaskararao, T., Manna, D., and Klajn, R. (2015). Light-controlled self-assembly of non-photoresponsive nanoparticles. *Nature Chemistry 7*, 646–652 (cit. on p. 52).

(*192*) Zhang, H., Junaid, M., Liu, K., A. Ras, R. H., and Ikkala, O. (2019). Light-induced reversible hydrophobization of cationic gold nanoparticles via electrostatic adsorption of a photoacid. *Nanoscale 11*, 14118–14122 (cit. on p. 52).

(*193*) M. Jansze, S., Cecot, G., and Severin, K. (2018). Reversible disassembly of metallasupramolecular structures mediated by a metastable-state photoacid. *Chemical Science 9*, 4253–4257 (cit. on p. 52).

(*194*) Dey, S., Fan, C., Gothelf, K. V., Li, J., Lin, C., Liu, L., Liu, N., Nijenhuis, M. A. D., Saccà, B., Simmel, F. C., Yan, H., and Zhan, P. (2021). DNA origami. *Nature Reviews Methods Primers 1*, 1–24 (cit. on pp. 52, 71).

(*195*) Funke, J. J., and Dietz, H. (2016). Placing molecules with Bohr radius resolution using DNA origami. *Nature Nanotechnology 11*, 47–52 (cit. on pp. 52–55).

(*196*) Martin, T. G., Bharat, T. A. M., Joerger, A. C., Bai, X.-C., Praetorius, F., Fersht, A. R., Dietz, H., and Scheres, S. H. W. (2016). Design of a molecular support for cryo-EM structure determination. *Proceedings of the National Academy of Sciences of the United States of America 113*, E7456–E7463 (cit. on p. 52).

(*197*) Aksel, T., Yu, Z., Cheng, Y., and Douglas, S. M. (2021). Molecular goniometers for single-particle cryo-electron microscopy of DNA-binding proteins. *Nature Biotechnology 39*, 378–386 (cit. on p. 52).

(*198*) Jungmann, R., Steinhauer, C., Scheible, M., Kuzyk, A., Tinnefeld, P., and Simmel, F. C. (2010). Single-Molecule Kinetics and Super-Resolution Microscopy by Fluorescence Imaging of Transient Binding on DNA Origami. *Nano Letters 10*, 4756–4761 (cit. on p. 52).

(*199*) Shaw, A., Hoffecker, I. T., Smyrlaki, I., Rosa, J., Grevys, A., Bratlie, D., Sandlie, I., Michaelsen, T. E., Andersen, J. T., and Högberg, B. (2019). Binding to nanopatterned antigens is dominated by the spatial tolerance of antibodies. *Nature Nanotechnology 14*, 184 (cit. on p. 52).

(*200*) Aghebat Rafat, A., Sagredo, S., Thalhammer, M., and Simmel, F. C. (2020). Barcoded DNA origami structures for multiplexed optimization and enrichment of DNA-based protein-binding cavities. *Nature Chemistry 12*, 852–859 (cit. on p. 52).

(*201*) Nickels, P. C., Wünsch, B., Holzmeister, P., Bae, W., Kneer, L. M., Grohmann, D., Tinnefeld, P., and Liedl, T. (2016). Molecular force spectroscopy with a DNA origami–based nanoscopic force clamp. *Science 354*, 305–307 (cit. on pp. 52–54, 72).

(*202*) Kramm, K., Schröder, T., Gouge, J., Vera, A. M., Gupta, K., Heiss, F. B., Liedl, T., Engel, C., Berger, I., Vannini, A., Tinnefeld, P., and Grohmann, D. (2020). DNA origami-based single-molecule force spectroscopy elucidates RNA Polymerase III pre-initiation complex stability. *Nature Communications 11*, 2828 (cit. on pp. 52, 55).

(*203*) Wilner, O. I., Weizmann, Y., Gill, R., Lioubashevski, O., Freeman, R., and Willner, I. (2009). Enzyme cascades activated on topologically programmed DNA scaffolds. *Nature Nanotechnology 4*, 249–254 (cit. on p. 52).

(*204*) Linko, V., Eerikäinen, M., and Kostiainen, M. A. (2015). A modular DNA origami-based enzyme cascade nanoreactor. *Chemical Communications 51*, 5351–5354 (cit. on p. 52).

(*205*) Rosier, B. J. H. M., Markvoort, A. J., Gumí Audenis, B., Roodhuizen, J. A. L., den Hamer, A., Brunsveld, L., and de Greef, T. F. A. (2020). Proximity-induced caspase-9 activation on a DNA origami-based synthetic apoptosome. *Nature Catalysis 3*, 295–306 (cit. on p. 52).

(*206*) Sigl, C., Willner, E. M., Engelen, W., Kretzmann, J. A., Sachenbacher, K., Liedl, A., Kolbe, F., Wilsch, F., Aghvami, S. A., Protzer, U., Hagan, M. F., Fraden, S., and Dietz, H. (2021). Programmable icosahedral shell system for virus trapping. *Nature Materials 20*, 1281–1289 (cit. on p. 52).

(*207*) Funck, T., Nicoli, F., Kuzyk, A., and Liedl, T. (2018). Sensing Picomolar Concentrations of RNA Using Switchable Plasmonic Chirality. *Angewandte Chemie International Edition 57*, 13495–13498 (cit. on p. 52).

(*208*) Lu, Z., Wang, Y., Xu, D., and Pang, L. (2017). Aptamer-tagged DNA origami for spatially addressable detection of aflatoxin B1. *Chemical Communications 53*, 941–944 (cit. on p. 52).

(*209*) Kuzuya, A., Watanabe, R., Yamanaka, Y., Tamaki, T., Kaino, M., and Ohya, Y. (2014). Nanomechanical DNA Origami pH Sensors. *Sensors 14*, 19329–19335 (cit. on p. 52).

(*210*) Zhou, C., Xin, L., Duan, X., Urban, M. J., and Liu, N. (2018). Dynamic Plasmonic System That Responds to Thermal and Aptamer-Target Regulations. *Nano Letters 18*, 7395–7399 (cit. on p. 52).

(*211*) Williford, J.-M., Santos, J. L., Shyam, R., and Mao, H.-Q. (2015). Shape Control in Engineering of Polymeric Nanoparticles for Therapeutic Delivery. *Biomaterials science 3*, 894–907 (cit. on p. 53).

(*212*) Douglas, S. M., Bachelet, I., and Church, G. M. (2012). A Logic-Gated Nanorobot for Targeted Transport of Molecular Payloads. *Science 335*, 831–834 (cit. on p. 53).

(*213*) Bujold, K. E., Hsu, J. C. C., and Sleiman, H. F. (2016). Optimized DNA "Nanosuitcases" for Encapsulation and Conditional Release of siRNA. *Journal of the American Chemical Society 138*, 14030–14038 (cit. on p. 53).

(*214*) Ijäs, H., Shen, B., Heuer-Jungemann, A., Keller, A., Kostiainen, M. A., Liedl, T., Ihalainen, J. A., and Linko, V. (2021). Unraveling the interaction between doxorubicin and DNA origami nanostructures for customizable chemotherapeutic drug release. *Nucleic Acids Research 49*, 3048–3062 (cit. on p. 53).

(*215*) Lee, H. et al. (2012). Molecularly self-assembled nucleic acid nanoparticles for targeted in vivo siRNA delivery. *Nature Nanotechnology 7*, 389–393 (cit. on p. 53).

(*216*) Funke, J. J., Ketterer, P., Lieleg, C., Schunter, S., Korber, P., and Dietz, H. (2016). Uncovering the forces between nucleosomes using DNA origami. *Science Advances 2*, e1600974 (cit. on pp. 53–55, 72, 73).

(*217*) Kosuri, P., Altheimer, B. D., Dai, M., Yin, P., and Zhuang, X. (2019). Rotation tracking of genome-processing enzymes using DNA origami rotors. *Nature 572*, 136–140 (cit. on pp. 54, 55, 72).

(*218*) Müller, D. J., Helenius, J., Alsteens, D., and Dufrêne, Y. F. (2009). Force probing surfaces of living cells to molecular resolution. *Nature Chemical Biology 5*, 383–390 (cit. on p. 53).

(*219*) Engelen, W., and Dietz, H. (2021). Advancing Biophysics Using DNA Origami. *Annual Review of Biophysics 50*, null (cit. on pp. 53, 71).

(*220*) Scholl, Z. N., Li, Q., and Marszalek, P. E. (2014). Single molecule mechanical manipulation for studying biological properties of proteins, DNA, and sugars. *WIREs Nanomedicine and Nanobiotechnology 6*, 211–229 (cit. on p. 53).

(*221*) Neuman, K. C., and Nagy, A. (2008). Single-molecule force spectroscopy: optical tweezers, magnetic tweezers and atomic force microscopy. *Nature Methods 5*, 491–505 (cit. on p. 53).

(*222*) Pfitzner, E., Wachauf, C., Kilchherr, F., Pelz, B., Shih, W. M., Rief, M., and Dietz, H. (2013). Rigid DNA Beams for High-Resolution Single-Molecule Mechanics. *Angewandte Chemie International Edition 52*, 7766–7771 (cit. on p. 53).

(*223*) Kilchherr, F., Wachauf, C., Pelz, B., Rief, M., Zacharias, M., and Dietz, H. (2016). Single-molecule dissection of stacking forces in DNA. *Science 353*, aaf5508 (cit. on p. 53).

(*224*) Le, J. V., Luo, Y., Darcy, M. A., Lucas, C. R., Goodwin, M. F., Poirier, M. G., and Castro, C. E. (2016). Probing Nucleosome Stability with a DNA Origami Nanocaliper. *ACS Nano 10*, 7073–7084 (cit. on pp. 53, 55).

(*225*) Funke, J. J., Ketterer, P., Lieleg, C., Korber, P., and Dietz, H. (2016). Exploring Nucleosome Unwrapping Using DNA Origami. *Nano Letters 16*, 7891–7898 (cit. on pp. 53, 55, 72).

(*226*) Endo, M., and Sugiyama, H. (2014). Single-Molecule Imaging of Dynamic Motions of Biomolecules in DNA Origami Nanostructures Using High-Speed Atomic Force Microscopy. *Accounts of Chemical Research 47*, 1645–1653 (cit. on p. 55).

(*227*) Rajendran, A., Endo, M., and Sugiyama, H. (2014). State-of-the-Art High-Speed Atomic Force Microscopy for Investigation of Single-Molecular Dynamics of Proteins. *Chemical Reviews 114*, 1493–1520 (cit. on p. 55).

(*228*) Shaw, A., Benson, E., and Högberg, B. (2015). Purification of Functionalized DNA Origami Nanostructures. *ACS Nano 9*, 4968–4975 (cit. on p. 59).

(*229*) Linko, V., Shen, B., Tapio, K., Toppari, J. J., Kostiainen, M. A., and Tuukkanen, S. (2015). One-step large-scale deposition of salt-free DNA origami nanostructures. *Scientific Reports 5*, 15634 (cit. on p. 59).

(*230*) Huang, Y., Nguyen, M.-K., and Kuzyk, A. (2019). Assembly of Gold Nanorods into Chiral Plasmonic Metamolecules Using DNA Origami Templates. *JoVE (Journal of Visualized Experiments)*, e59280 (cit. on p. 59).

(*231*) Blair, R. H., Goodrich, J. A., and Kugel, J. F. (2012). Single-Molecule Fluorescence Resonance Energy Transfer Shows Uniformity in TATA Binding Protein-Induced DNA Bending and Heterogeneity in Bending Kinetics. *Biochemistry 51*, 7444–7455 (cit. on p. 60).

(*232*) Suzuki, Y., Sakai, N., Yoshida, A., Uekusa, Y., Yagi, A., Imaoka, Y., Ito, S., Karaki, K., and Takeyasu, K. (2013). High-speed atomic force microscopy combined with inverted optical microscopy for studying cellular events. *Scientific Reports 3*, 2131 (cit. on p. 60).

(*233*) Yoshida, A., Sakai, N., Uekusa, Y., Imaoka, Y., Itagaki, Y., Suzuki, Y., and Yoshimura, S. H. (2018). Morphological changes of plasma membrane and protein assembly during clathrin-mediated endocytosis. *PLOS Biology 16*, e2004786 (cit. on p. 60).

(*234*) Tang, G., Peng, L., Baldwin, P. R., Mann, D. S., Jiang, W., Rees, I., and Ludtke, S. J. (2007). EMAN2: An extensible image processing suite for electron microscopy. *Journal of Structural Biology 157*, 38–46 (cit. on p. 61).

(*235*) Pettersen, E. F., Goddard, T. D., Huang, C. C., Couch, G. S., Greenblatt, D. M., Meng, E. C., and Ferrin, T. E. (2004). UCSF Chimera–a visualization system for exploratory research and analysis. *Journal of Computational Chemistry 25*, 1605–1612 (cit. on p. 61).

(*236*) Elonen, A. Sterna: A software tool for designing 3D wireframe RNA polyhedra, 2020 (cit. on p. 63).

(*237*) Community, B. Blender - a 3D modelling and rendering package. Stichting Blender Foundation, Amsterdam. 2018 (cit. on p. 63).

(*238*) Zadeh, J. N., Steenberg, C. D., Bois, J. S., Wolfe, B. R., Pierce, M. B., Khan, A. R., Dirks, R. M., and Pierce, N. A. (2011). NUPACK: Analysis and design of nucleic acid systems. *Journal of Computational Chemistry 32*, 170–173 (cit. on p. 63).

(*239*) Zadeh, J. N., Wolfe, B. R., and Pierce, N. A. (2011). Nucleic acid sequence design via efficient ensemble defect optimization. *Journal of Computational Chemistry 32*, 439–452 (cit. on p. 63).

(*240*) Šulc, P., Romano, F., Ouldridge, T. E., Rovigatti, L., Doye, J. P. K., and Louis, A. A. (2012). Sequence-dependent thermodynamics of a coarse-grained DNA model. *The Journal of Chemical Physics 137*, 135101 (cit. on pp. 63, 71).

(*241*) Šulc, P., Romano, F., Ouldridge, T. E., Doye, J. P. K., and Louis, A. A. (2014). A nucleotide-level coarse-grained model of RNA. *The Journal of Chemical Physics 140*, 235102 (cit. on p. 63).

(*242*) Elonen, A., Natarajan, A. K., Kawamata, I., Oesinghaus, L., Mohammed, A., Seitsonen, J., Suzuki, Y., Simmel, F. C., Kuzyk, A., and Orponen, P. (2022). Algorithmic Design of 3D Wireframe RNA Polyhedra. *ACS Nano 16*, 16608–16616 (cit. on p. 64).

(*243*) Kim, J., and Franco, E. (2020). RNA nanotechnology in synthetic biology. *Current Opinion in Biotechnology 63*, 135–141 (cit. on p. 64).

(*244*) Ryssy, J., Natarajan, A. K., Wang, J., Lehtonen, A. J., Nguyen, M.-K., Klajn, R., and Kuzyk, A. (2021). Light-Responsive Dynamic DNA-Origami-Based Plasmonic Assemblies. *Angewandte Chemie International Edition 60*, 5859–5863 (cit. on pp. 65, 66).

(*245*) Shi, Z., Peng, P., Strohecker, D., and Liao, Y. (2011). Long-Lived Photoacid Based upon a Photochromic Reaction. *Journal of the American Chemical Society 133*, 14699–14703 (cit. on pp. 65, 66).

(*246*) Liao, Y. (2017). Design and Applications of Metastable-State Photoacids. *Accounts of Chemical Research 50*, 1956–1964 (cit. on p. 65).

(*247*) Hu, Y., Cecconello, A., Idili, A., Ricci, F., and Willner, I. (2017). Triplex-DNA-Nanostrukturen: von grundlegenden Eigenschaften zu Anwendungen. *Angewandte Chemie 129*, 15410–15434 (cit. on p. 66).

(*248*) Idili, A., Vallée-Bélisle, A., and Ricci, F. (2014). Programmable pH-Triggered DNA Nanoswitches. *Journal of the American Chemical Society 136*, 5836–5839 (cit. on pp. 66, 67).

(*249*) Samanta, D., and Klajn, R. (2016). Aqueous Light-Controlled Self-Assembly of Nanoparticles. *Advanced Optical Materials 4*, 1373–1377 (cit. on p. 66).

(*250*) Kim, J. L., Nikolov, D. B., and Burley, S. K. (1993). Co-crystal structure of TBP recognizing the minor groove of a TATA element. *Nature 365*, 520–527 (cit. on p. 67).

(*251*) Kim, Y., Geiger, J. H., Hahn, S., and Sigler, P. B. (1993). Crystal structure of a yeast TBP/TATA-box complex. *Nature 365*, 512–520 (cit. on p. 67).

(*252*) Kosa, P. F., Ghosh, G., DeDecker, B. S., and Sigler, P. B. (1997). The 2.1-Å crystal structure of an archaeal preinitiation complex: TATA-box-binding protein/transcription factor (II)B core/TATA-box. *Proceedings of the National Academy of Sciences 94*, 6042–6047 (cit. on p. 67).

(*253*) Mishal, R., and Luna-Arias, J. P. (2022). Role of the TATA-box binding protein (TBP) and associated family members in transcription regulation. *Gene 833*, 146581 (cit. on p. 67).

(*254*) Natarajan, A. K., Ryssy, J., and Kuzyk, A. (2023). A DNA origami-based device for investigating DNA bending proteins by transmission electron microscopy. *Nanoscale* (cit. on p. 68).

(*255*) Nikolov, D. B., Chen, H., Halay, E. D., Usheva, A. A., Hisatake, K., Lee, D. K., Roeder, R. G., and Burley, S. K. (1995). Crystal structure of a TFIIB–TBP–TATA-element ternary complex. *Nature 377*, 119–128 (cit. on p. 69).

(*256*) Geiger, J. H., Hahn, S., Lee, S., and Sigler, P. B. (1996). Crystal Structure of the Yeast TFIIA/TBP/DNA Complex. *Science 272*, 830–836 (cit. on p. 69).

(*257*) Imbalzano, A. N., Zaret, K. S., and Kingston, R. E. (1994). Transcription factor (TF) IIB and TFIIA can independently increase the affinity of the TATA-binding protein for DNA. *Journal of Biological Chemistry 269*, 8280–8286 (cit. on p. 69).

(*258*) Stewart, J. J., and Stargell, L. A. (2001). The Stability of the TFIIA-TBP-DNA Complex Is Dependent on the Sequence of the TATAAA Element *. *Journal of Biological Chemistry 276*, 30078–30084 (cit. on p. 69).

(*259*) Hieb, A. R., Halsey, W. A., Betterton, M. D., Perkins, T. T., Kugel, J. F., and Goodrich, J. A. (2007). TFIIA Changes the Conformation of the DNA in TBP/TATA Complexes and Increases their Kinetic Stability. *Journal of Molecular Biology 372*, 619–632 (cit. on p. 69).

(*260*) Gietl, A., Holzmeister, P., Blombach, F., Schulz, S., von Voithenberg, L. V., Lamb, D. C., Werner, F., Tinnefeld, P., and Grohmann, D. (2014). Eukaryotic and archaeal TBP and TFB/TF(II)B follow different promoter DNA bending pathways. *Nucleic Acids Research 42*, 6219–6231 (cit. on p. 69).

(*261*) Buratowski, R. M., Downs, J., and Buratowski, S. (2002). Interdependent Interactions between TFIIB, TATA Binding Protein, and DNA. *Molecular and Cellular Biology 22*, 8735–8743 (cit. on p. 69).

(*262*) Zhao, X., and Herr, W. (2002). A Regulated Two-Step Mechanism of TBP Binding to DNA: A Solvent-Exposed Surface of TBP Inhibits TATA Box Recognition. *Cell 108*, 615–627 (cit. on p. 69).

(*263*) Huang, C.-M., Kucinic, A., Johnson, J. A., Su, H.-J., and Castro, C. E. (2021). Integrated computer-aided engineering and design for DNA assemblies. *Nature Materials 20*, 1264–1271 (cit. on p. 71).

(*264*) Johnson, J. A., Dehankar, A., Winter, J. O., and Castro, C. E. (2019). Reciprocal Control of Hierarchical DNA Origami-Nanoparticle Assemblies. *Nano Letters 19*, 8469–8475 (cit. on pp. 72, 73).

Errata

Publication II

Fig. 3A. The proton arrows go in the wrong direction.

Why restrict the role of nucleic acids to store and express genomic information? Why not use it to build something- something unnatural and useful. The predictability and programmability of nucleic acids make them an almost ideal candidate for self-assembly of nanoscale structures. These properties have been explored over the past few decades for the design and fabrication of complex and reconfigurable nucleic acid nanostructures, thus creating a new paradigm that is the field of nucleic acid nanotechnology. In this doctoral thesis, the author presents the design, reconfigurability, and applications of nucleic acid nanostructures. Through the use of RNA wireframe polyhedral nanostructures and DNA origami, the author demonstrates the potential of these structures for use in various fields, including plasmonics, bioimaging, and biophysics. The findings in this thesis highlight the vast unexplored design space, novel switching mechanisms, and exciting potential applications of nucleic acid nanotechnology.

Aalto-DT 20/2023

ISBN 978-952-64-1152-1 (printed)
ISBN 978-952-64-1153-8 (pdf)
ISSN 1799-4934 (printed)
ISSN 1799-4942 (pdf)

Aalto University
School of Science
Department of Neuroscience and Biomedical Engineering
www.aalto.fi

BUSINESS + ECONOMY

ART + DESIGN + ARCHITECTURE

SCIENCE + TECHNOLOGY

CROSSOVER

DOCTORAL THESES